

CONSTRAINING COMPETING MODELS OF DARK ENERGY WITH
COSMOLOGICAL OBSERVATIONS

by

ANATOLY PAVLOV

B.S., Saint Petersburg State Polytechnic University, Russia 2005

M.S., Saint Petersburg State Polytechnic University, Russia 2007

AN ABSTRACT OF A DISSERTATION

submitted in partial fulfillment of the
requirements for the degree

DOCTOR OF PHILOSOPHY

Department of Physics
College of Arts and Sciences

KANSAS STATE UNIVERSITY
Manhattan, Kansas

2015

Abstract

The last decade of the 20th century was marked by the discovery of the accelerated expansion of the universe. This discovery puzzles physicists and has yet to be fully understood. It contradicts the conventional theory of gravity, i.e. Einstein's General Relativity (GR). According to GR, a universe filled with dark matter and ordinary matter, i.e. baryons, leptons, and photons, can only expand with deceleration.

Two approaches have been developed to study this phenomenon. One attempt is to assume that GR might not be the correct description of gravity, hence a modified theory of gravity has to be developed to account for the observed acceleration of the universe's expansion. This approach is known as the "Modified Gravity Theory". The other way is to assume that the energy budget of the universe has one more component which causes expansion of space with acceleration on large scales. Dark Energy (DE) was introduced as a hypothetical type of energy homogeneously filling the entire universe and very weakly or not at all interacting with ordinary and dark matter.

Observational data suggest that if DE is assumed then its contribution to the energy budget of the universe at the current epoch should be about 70% of the total energy density of the universe. In the standard cosmological model a DE term is introduced into the Einstein GR equations through the cosmological constant, a constant in time and space, and proportional to the metric tensor $g_{\mu\nu}$. While this model so far fits most available observational data, it has some significant conceptual shortcomings. Hence there are a number of alternative cosmological models of DE in which the dark energy density is allowed to vary in time and space.

CONSTRAINING COMPETING MODELS OF DARK ENERGY WITH
COSMOLOGICAL OBSERVATIONS

by

ANATOLY PAVLOV

B.S., Saint Petersburg State Polytechnic University, Russia 2005

M.S., Saint Petersburg State Polytechnic University, Russia 2007

A DISSERTATION

submitted in partial fulfillment of the
requirements for the degree

DOCTOR OF PHILOSOPHY

Department of Physics
College of Arts and Sciences

KANSAS STATE UNIVERSITY
Manhattan, Kansas

2015

Approved by:

Major Professor
Bharat Ratra

Copyright

ANATOLY PAVLOV

2015

Abstract

The last decade of the 20th century was marked by the discovery of the accelerated expansion of the universe. This discovery puzzles physicists and has yet to be fully understood. It contradicts the conventional theory of gravity, i.e. Einstein's General Relativity (GR). According to GR, a universe filled with dark matter and ordinary matter, i.e. baryons, leptons, and photons, can only expand with deceleration.

Two approaches have been developed to study this phenomenon. One attempt is to assume that GR might not be the correct description of gravity, hence a modified theory of gravity has to be developed to account for the observed acceleration of the universe's expansion. This approach is known as the "Modified Gravity Theory". The other way is to assume that the energy budget of the universe has one more component which causes expansion of space with acceleration on large scales. Dark Energy (DE) was introduced as a hypothetical type of energy homogeneously filling the entire universe and very weakly or not at all interacting with ordinary and dark matter.

Observational data suggest that if DE is assumed then its contribution to the energy budget of the universe at the current epoch should be about 70% of the total energy density of the universe. In the standard cosmological model a DE term is introduced into the Einstein GR equations through the cosmological constant, a constant in time and space, and proportional to the metric tensor $g_{\mu\nu}$. While this model so far fits most available observational data, it has some significant conceptual shortcomings. Hence there are a number of alternative cosmological models of DE in which the dark energy density is allowed to vary in time and space.

Table of Contents

List of Figures	ix
List of Tables	xiv
Acknowledgements	xiv
1 Introduction	1
1.1 Theoretical Cosmology	1
1.1.1 Short overview of General Relativity	1
1.1.2 Friedmann Equations	4
1.1.3 Solutions of Friedmann Equations	8
1.1.4 Cosmological Constant	13
1.1.5 Standard Cosmological Model	16
1.2 Observational Cosmology	17
1.2.1 Redshift	17
1.2.2 Hubble parameter	18
1.2.3 Luminosity Distance	19
2 Forecasting cosmological parameter constraints from near-future space-	
based galaxy surveys	23
2.1 Introduction	23
2.2 Measured power spectrum of galaxies	28
2.3 Cosmological models	32

2.3.1	Λ CDM, XCDM and ω CDM parameterizations	32
2.3.2	ϕ CDM model	33
2.4	Fisher matrix formalism	34
2.5	Results	36
2.5.1	Constraints on growth rate	36
2.5.2	Constraints on dark energy model parameters	37
3	Nonflat time-variable dark energy cosmology	47
3.1	Introduction	47
3.2	The Model	49
3.2.1	Solution for the curvature-dominated epoch	51
3.3	Some observational predictions	54
3.3.1	The time parameter $H_0 t_0$	55
3.3.2	The distance modulus difference $\Delta m(z)$	57
3.3.3	Number counts	59
3.3.4	The growth of structure	59
4	Cosmological constraints from large-scale structure growth rate measurements	63
4.1	Introduction	63
4.2	Data and analysis	65
4.2.1	Growth rate of LSS	65
4.2.2	SNIa distance modulus	68
4.2.3	Hubble parameter	68
4.2.4	Computation of joint $\chi^2(\mathbf{p})$	69
4.3	Results and discussion	70

5 Conclusion	74
Bibliography	85
A Appendix for Chapter 2	86
B Appendix for Chapter 3	90

List of Figures

1.1	Light cone diagram.	3
1.2	Cosmic Microwave Background radiation map of the last scattering epoch. Data of 2012 WMAP mission, Source: http://map.gsfc.nasa.gov/media/060913/index.html	5
1.3	Two dimensional analogies of hyperbolic, flat, and spherical manifolds. . . .	7
1.4	Solutions of Friedmann equations for a single component universes with flat, closed, and open geometries. The time and the scale factor in arbitrary units.	12
1.5	Numerical solution of Eq. (1.30) for standard cosmology. Time and the scale factor presented in arbitrary units, where $a = 1$ corresponds to the current epoch.	15
1.6	The plot of $\log_{10}(\rho_i/\rho_{cr})$ vs the log of the scale factor $\log_{10}(a)$ for each component. One can see that the early universe was dominated by radiation, however since energy density of radiation dissipates as a^{-4} while energy density of ordinary matter decreases as a^{-3} , the radiation dominated epoch switches to matter dominated. Eventually, the universe becomes dominated by the cosmological constant, since its energy density does not evolve in time. . . .	16
1.7	Hubble diagram for the Union2.1 compilation. The solid line represents the best-fit cosmology for a flat Λ CDM universe for supernovae alone. Source: Fig.(4) of [12]	22

2.1	Predicted relative error on the measurements of growth rate as a function of redshift z in redshift bins of $\Delta z = 0.1$ for different models of dark energy. The upper solid black line shows predictions for the case when no assumption is made about the nature of dark energy.	40
2.2	Predicted one standard deviation confidence level contour constraints on the current renormalized Hubble constant h and the parameter γ that describes deviations from general relativity for different dark energy models.	41
2.3	Upper panel shows one standard deviation confidence level contours constraints on parameters ω_a and ω_0 of the ω CDM parametrization, while lower panel shows these for parameters Ω_k and Ω_m	42
2.4	One standard deviation confidence level contour constraints on parameters of the XCDM parametrization.	43
2.5	One standard deviation confidence level contour constraints on parameters α and Ω_m of the ϕ CDM model. Lower panel shows a magnification of the tightest two contours in the lower left corner of the upper panel.	44
2.6	One standard deviation confidence level contour constraints on parameters Ω_k and Ω_m of the ϕ CDM model. The lower panel shows a magnification of the two tightest contours in the center of the upper panel.	45
2.7	One standard deviation confidence level contour constraints on parameters Ω_k and Ω_m of the Λ CDM model.	46

- 3.1 Contours of fixed time parameter $H_0 t_0$, as a function of the present value of the nonrelativistic matter density parameter Ω_{m0} and scalar field potential power-law index α , at various values of the current value of the space-curvature density parameter Ω_{k0} (as listed in the inset legend boxes). The upper panel shows a larger part of (Ω_{m0}, α) space for a larger range of Ω_{k0} values [for $H_0 t_0 = 0.7, 0.75, 0.8, 0.85, 0.95, 1.05$ and 1.15 , from right to left], while the lower panel focuses on a smaller range of the three parameters [for $H_0 t_0$ from 0.8 to 1.15 in steps of 0.05 , from right to left]. 56
- 3.2 Contours of fixed bolometric distance modulus relative to the Einstein–de Sitter model, $\Delta m(z = 1.5)$, as a function of the matter density parameter Ω_{m0} and scalar field potential power-law index α , and various values of the space curvature density parameter Ω_{k0} (as listed in the inset legend boxes). The upper panel shows a larger part of (Ω_{m0}, α) space for a larger range of Ω_{k0} values [for $\Delta m(z = 1.5) = 0.1, 0.2, 0.3, 0.4, 0.5, 0.6$, and 0.8 from right to left], while the lower panel focuses on a smaller range of the three parameters [for $\Delta m(z = 1.5)$ from 0.3 to 0.8 in steps of 0.1 , from right to left]. In the upper panel there is no $\Omega_{k0} = 0.2$ contour for $\Delta m(z = 1.5) = 0.1$ since in this case the model is too open for such a small distance modulus difference. 58
- 3.3 Contours of fixed $A(z = 0.7)$ as a function of Ω_{m0} and α at various values of Ω_{k0} (as listed in the inset legend boxes). The upper panel shows a larger part of the parameter space for $A(z = 0.7) = 0.25, 0.3, 0.35$ and 0.45 from right to left. The lower panel shows a smaller range of the three parameters for $A(z = 0.7) = 0.3, 0.35, 0.4$ and 0.45 from right to left. 60

3.4 Contours of the factor by which the growth of ordinary matter perturbations falls below that of the Einstein–de Sitter model, $\Delta(\Omega_{m0}, \Omega_{k0}, \alpha)$, as a function of the matter density parameter Ω_{m0} and scalar field potential power-law index α , and various values of the space curvature density parameter Ω_{k0} (as listed in the inset legend boxes). The upper panel shows a larger part of (Ω_{m0}, α) space for a larger range of Ω_{k0} values [for $\Delta(\Omega_{m0}, \Omega_{k0}, \alpha) = 0.3, 0.5, 0.7$ and 0.9 from left to right], while the right panel focuses on a smaller range of the three parameters [for $\Delta(\Omega_{m0}, \Omega_{k0}, \alpha)$ from 0.2 to 0.8 in steps of 0.1 , from left to right]. In the lower panel there is no $\Omega_{k0} = 0.2$ contour for $\Delta = 0.9$ since in this case the model is too open to allow such a large growth factor. 61

4.1 $1, 2,$ and 3σ constraint contours for the Λ CDM model from: growth factor measurements [blue dashed lines with blue filled circle at best-fit $(\Omega_m, \Omega_\Lambda) = (0.41, 0.87)$ with $\chi^2_{\min}/\text{dof} = 7.65/12$]; SNIa+ $H(z)$ apparent magnitude data [red dot-dashed lines with red filled circle at best-fit $(\Omega_m, \Omega_\Lambda) = (0.23, 0.59)$ with $\chi^2_{\min}/\text{dof} = 562/598$]; and a combination of all data sets [black solid lines and black filled circle at best-fit $(\Omega_m, \Omega_\Lambda) = (0.28, 0.69)$ with $\chi^2_{\min}/\text{dof} = 571/612$]. The dashed straight line corresponds to spatially-flat models, the dotted line demarcates zero acceleration models, and the area in the upper left-hand corner is the region for which there is no big bang. 71

- 4.2 1, 2, and 3σ constraint contours for the XCDM model from: growth factor measurements [blue dashed lines with blue filled circle at best-fit $(\Omega_m, w_X) = (0.36, -1.34)$ with $\chi^2_{\min}/\text{dof} = 7.70/12$]; SNIa+ $H(z)$ apparent magnitude data [red dot-dashed lines with red filled circle at best-fit $(\Omega_m, w_X) = (0.27, -0.90)$ with $\chi^2_{\min}/\text{dof} = 562/598$]; and a combination of all data sets [black solid lines and black filled circle at best-fit $(\Omega_m, w_X) = (0.28, -0.94)$ with $\chi^2_{\min}/\text{dof} = 571/612$]. The dashed straight line corresponds to spatially-flat Λ CDM models and the dotted curved line demarcates zero acceleration models. . . . 72
- 4.3 1, 2, and 3σ constraint contours for the ϕ CDM model from: growth factor measurements [blue dashed lines with blue filled circle at best-fit $(\Omega_m, \alpha) = (0.28, 0.052)$ with $\chi^2_{\min}/\text{dof} = 8.62/12$]; SNIa+ $H(z)$ apparent magnitude data [red dot-dashed lines with red filled circle at best-fit $(\Omega_m, \alpha) = (0.26, 0.302)$ with $\chi^2_{\min}/\text{dof} = 562/598$]; and a combination of all data sets [black solid lines and black filled circle at best-fit $(\Omega_m, \alpha) = (0.27, 0.300)$ with $\chi^2_{\min}/\text{dof} = 570/612$]. The dotted curved line demarcates zero acceleration models and the horizontal $\alpha = 0$ axis corresponds to spatially-flat Λ CDM models. . . . 73

List of Tables

2.1	Values of the parameters of the fiducial Λ CDM model and the survey.	39
2.2	Predicted deviations of parameter γ from its fiducial value, at one standard deviation confidence level, for different assumptions about dark energy.	39
4.1	Growth parameter measurements and 1σ uncertainties. Reference number shown in the last column: 1. [133], 2. [134], 3. [135], 4. [64], 5. [65], 6. [136], 7. [66], 8. [63], 9. [137].	66
A.1	Values of the k_{max} , bias $b(z)$ from [87], and the number densities $n(z)$ taken from [88].	89

Acknowledgments

I greatly appreciate the help and support of so many people among my colleagues and friends while writing this dissertation. I would like to thank specially my research adviser Professor Bharat Vishnu Ratra who was advising me through my research and studies at Kansas State University. Thank you for your help and patience in educating me in the most complicated areas of physical cosmology and data analysis. I am grateful to Lado Samushia for his priceless help while I was working on my research as well as on projects we have worked in collaboration. Lado has helped me a lot in the most complicated technical caveats of the research activities of our field. I am indebted to Mikhail Makouski and Data Mania for their help with programming which was the main technical skill required to successfully conduct my research. I am very thankful to Professor Tim Bolton for thoughtful conversations and tricky questions during High Energy Physics seminars, which helped me to reveal many details in areas of experimental as well as theoretical physics. I am also grateful to Professor Tim Bolton for his guidance while I was teaching for Engineering Physics I and II studios. Special thanks to Professors Yurii Maravin and Tina Kanhiashvili; its mainly due to their suggestion and help that I joined Kansas State University as a graduate student. I am endlessly thankful to Professor Larry Weaver for discussions we had about various subjects of theoretical physics. Thank you very much for listening to my ideas and giving me suggestions on how to bring them to life by using mathematics to develop a framework of a physical model. I also would like to thank Professor Sanjoy Das for his help in understanding of how modern Machine Learning techniques work and how can it be applied to problems of data analysis in physical cosmology. Thank you very much.

Chapter 1

Introduction

1.1 Theoretical Cosmology

Cosmology is the study of the universe as a whole. Since ancient times people across the globe have tried to understand the origins of the universe and predict its future. However, it was not until the beginning of the 20th century when cosmology emerged as a quantitative scientific field rather than a philosophical attempt to make sense of the universe in a mythological manner. The theoretical basis of cosmology lies mainly on Einstein's description of gravity, i.e. General Relativity, a theory in which gravity is described as the geometry of space-time, rather than a force, where the geometry is determined by the matter content and its distribution. On the other hand, the geometry of space-time governs the motion of matter.

1.1.1 Short overview of General Relativity

Differential geometry provides a mathematical framework for general relativity. The differential of distance between two near by points in space-time, x^μ and $x^\mu + dx^\mu$, is given by

the line element which is defined via the following quadratic form

$$ds^2 = g_{\mu\nu} dx^\mu dx^\nu \tag{1.1}$$

where $g_{\mu\nu}$ is the metric tensor and x^μ are coordinates. In general relativity coordinates describe 4-dimensional space-time with one-time dimension and three-dimensions of space. The coordinate $x^\mu = (x^0, x^1, x^2, x^3)$ where $x^0 = ct$ with c being the speed of light and t is time, while x^1, x^2, x^3 label spatial part of the space-time. The metric tensor $g_{\mu\nu}$ is a fundamental object in general relativity. It may loosely be thought of as gravitational potentials in Newtonian gravitation terms. It has a total of 16 components but due to its symmetry $g_{\mu\nu} = g_{\nu\mu}$ there are only 10 independent components. The line element ds^2 describes the casual structure of space-time. If $ds^2 > 0$, the interval is time-like and the line element is the proper time interval between the events in space-time traversed by massive particles. When $ds^2 = 0$, the interval is light-like and the line element is the proper time interval between events in space-time which can only be traversed by mass-less particles. In the case when $ds^2 < 0$, the interval is space-like and the absolute value of the line element describes the proper length between events in space-time that cannot be in casual connection with one another. The structure of space-time can be represented through the light-cone diagram which is shown on Fig. (1.1).

We now discuss how the geometry of space-time interacts with its matter content and how geometry governs dynamics of motion of matter. The mechanism of interaction between geometry and matter is what general relativity is all about, and the Einstein equations give a quantitative description of this interaction. The Einstein equations are

$$R_{\mu\nu} - \frac{1}{2}Rg_{\mu\nu} = \frac{8\pi G}{c^4}T_{\mu\nu}, \tag{1.2}$$

where G is Newton's gravitational constant, $R = g^{\mu\nu}R_{\mu\nu}$ the scalar curvature, and $R_{\mu\nu}$ is

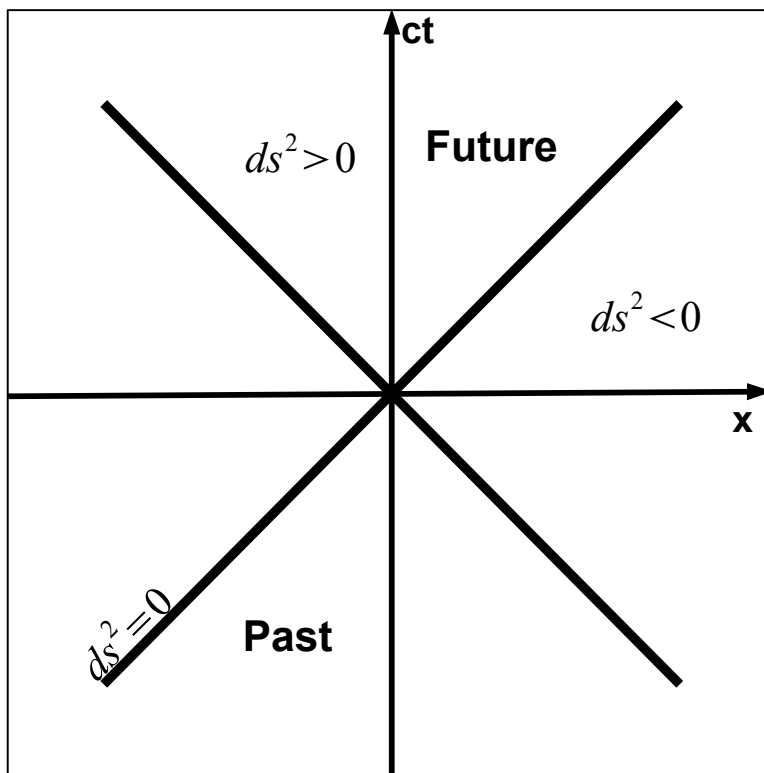


Figure 1.1: *Light cone diagram.*

the Ricci tensor

$$R_{\mu\nu} = \frac{\partial \Gamma_{\mu\nu}^{\lambda}}{\partial x^{\lambda}} - \frac{\partial \Gamma_{\lambda\mu}^{\nu}}{\partial x^{\nu}} + \Gamma_{\lambda\kappa}^{\lambda} \Gamma_{\mu\nu}^{\kappa} - \Gamma_{\mu\kappa}^{\lambda} \Gamma_{\lambda\nu}^{\kappa}. \quad (1.3)$$

Here $\Gamma_{\mu\nu}^{\lambda}$ are the Christoffel symbols defined as

$$\Gamma_{\mu\nu}^{\lambda} = \frac{1}{2} g^{\lambda\kappa} \left(\frac{\partial g_{\kappa\mu}}{\partial x^{\nu}} + \frac{\partial g_{\kappa\nu}}{\partial x^{\mu}} - \frac{\partial g_{\mu\nu}}{\partial x^{\kappa}} \right). \quad (1.4)$$

The Ricci tensor is symmetric $R_{\mu\nu} = R_{\nu\mu}$ as can be seen from the definition above, thus

there are only 10 independent components. The term on the right hand side of Eq. (1.2) is the energy-momentum tensor $T_{\mu\nu}$ that describes matter. Einstein's equations of general relativity form a system of 10 non-linear equations of second order with respect to metric tensor $g_{\mu\nu}$. They reduce to Newton's gravity law in the weak gravity limit. The energy-momentum tensor $T_{\mu\nu}$ must satisfy a conservation equation of the following form in general relativity $T^\mu{}_{\nu;\mu} = 0$ and it expresses energy and momentum conservation laws. Semicolon in the equation of energy-momentum conservation refers to co-variant differentiation which is the appropriate way of computing derivatives in differential geometry. The conservation equation played a major role when Einstein was trying to guess the right form of the equations that describe how matter curves space. The very first equation which Einstein wrote was simply $R_{\mu\nu} \sim T_{\mu\nu}$ but he quickly discovered that the Ricci tensor alone does not satisfy the conservation equation. However, the tensor $2R_{\mu\nu} - Rg_{\mu\nu}$ does satisfy the conservation condition and is what Einstein stated as the equations of general relativity. The tensor on the left hand side of Eqs. (1.2) $R_{\mu\nu} - Rg_{\mu\nu}/2$ is called the Einstein tensor and labeled $G_{\mu\nu}$ in the literature.

1.1.2 Friedmann Equations

Observational data of Cosmic Microwave Background (CMB) radiation anisotropy, see Fig. (1.2), and other measurements [1] indicate that the universe is homogeneous on scales beyond 100 Mpc while the observable part of the universe is about 4000 Mpc, which makes it reasonable to chose spatially homogeneous and isotropic metrics to describe the space-time of the universe. The appropriate form of metrics for the universe was introduced by Alexander Friedmann in 1922 where he allowed them to be time-variable. Friedmann showed that the universe would be dynamic and would expand six years before the expansion was observed by Edwin Hubble in 1928. The line element in Friedmann's metric is

$$ds^2 = -dt^2 + a^2(t)\gamma_{ij}dx^i dx^j \tag{1.5}$$

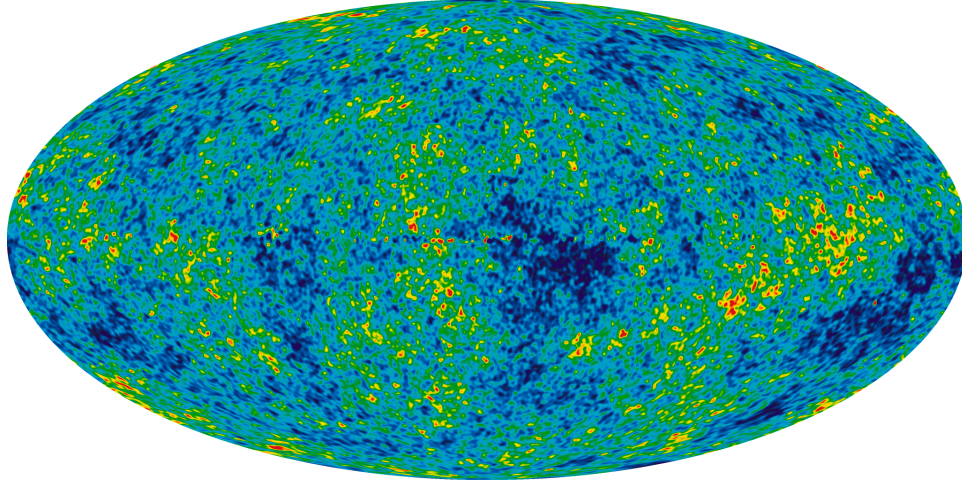


Figure 1.2: *Cosmic Microwave Background radiation map of the last scattering epoch. Data of 2012 WMAP mission, Source: <http://map.gsfc.nasa.gov/media/060913/index.html>*

where we chose units in which $c = 1$ and metric tensor sign convention $(-+++)$. The indexes are labeled with Greek letters when they run in 4-dimensional space-time, i.e. from 0 to 3, and when they run in the 3-dimensional spatial part of space-time labeling is done with Latin letters that go from 1 through 3. The function $a(t)$ is called the scale factor and it describes how the distance between two points in space evolves with time. The term $a^2(t)\gamma_{ij} = g_{ij}$ is the spatial part of the metric tensor. Because of the assumption of isotropy and homogeneity, adopted based on observational evidence, the metric tensor has to be diagonal, hence, g_{ij} is also diagonal.

The Friedmann equations are a special case of Einstein's equations of general relativity Eq. (1.2) for metrics of Eq. (1.5). These reduce the Einsteinian system of 10 equations to a system of two equations for one unknown function, the scale factor $a(t)$,

$$\left(\frac{\dot{a}}{a}\right)^2 + \frac{k}{a^2} = \frac{8\pi G}{3}\rho, \quad (1.6)$$

$$\frac{\ddot{a}}{a} = -\frac{4\pi G}{3}(\rho + 3p). \quad (1.7)$$

Here ρ is the matter density and p is pressure. The left hand side of Eqs. (1.6)-(1.7) are

derived from the left hand side of Einstein's equations (1.2) which describe the geometry of space-time, while the right hand side of equations (1.6)-(1.7) are components of the energy-momentum tensor $T_{\mu\nu}$. In particular Eq. (1.6) corresponds to equality between the time components of Einstein and energy-momentum tensors $G_{00} = 8\pi GT_{00}$ and Eq. (1.7) corresponds to equality between diagonal elements of the spatial part of Einstein and energy-momentum tensors $G_{ii} = 8\pi GT_{ii}$ and is derived with the use of Eq. (1.6). For more detailed derivation see paragraph 2.1.3 of [2].

Eqs. (1.6)-(1.7) are written for a universe that has only one form of matter that fills it. If there are multiple constituents present, then Eqs. (1.6)-(1.7) have to be generalized by replacing mass density ρ and pressure p with sums over all types of matter i.e. $\Sigma\rho_i \rightarrow \rho$ and $\Sigma p_i \rightarrow p$. In order to solve the Friedmannian equations one has to know how density and pressure depend on time. In some cases pressure and density can be related by an equation of state whose exact form depends on the particular form of fluid. For example, in the case of barotropic fluids pressure is a function of mass density only i.e., $p = p(\rho)$, hence one needs to know only how mass density varies with time.

There are three possible spatial geometries that meet requirements of homogeneity and isotropy of the universe. These are: flat, spherical, and hyperbolic geometries. Flat or non-curve space, is a space which obeys all properties of Euclidean geometry, and in general relativity it can be dynamic. Spherical and hyperbolic spaces do not obey the axioms of Euclidean geometry; these types of spaces are curved. Euclidean relationships of elemental figures and objects of geometry are not satisfied in curved spaces. For example, the sum of all angles of a triangle need not equal π and the ratio of circumference of a circle to its radius r need not equal $2\pi r$. In Fig. (1.3) two dimensional analogies of hyperbolic, flat, and spherical spaces are shown.

Mathematical description of spaces presented in Fig. (1.3) are given by the following

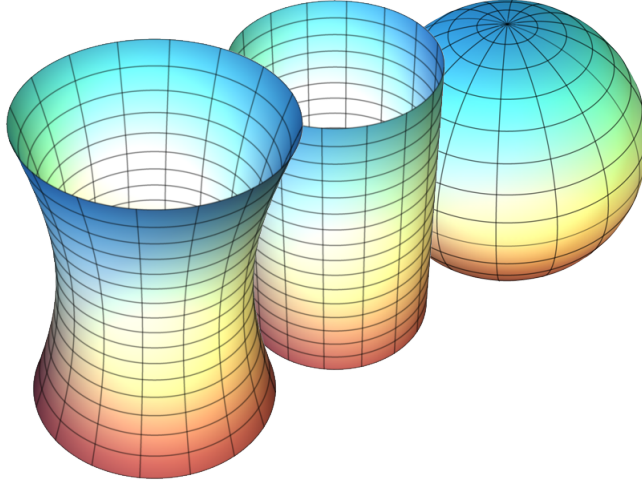


Figure 1.3: *Two dimensional analogies of hyperbolic, flat, and spherical manifolds.*

metrics, written in Cartesian coordinates

$$g_{ij} = \frac{a^2(t)}{1 - k\mathbf{r}^2} \delta_{ij}, \quad (1.8)$$

where $\mathbf{r}^2 = \delta_{ij}x^i x^j$ is square of distance between two points in space, δ_{ij} is the Kronecker delta symbol and k is the curvature parameter which takes values $k = 0$ for flat space, $k = 1$ for spherically curved space, and $k = -1$ in case of hyperbolic geometry. The normalization of the absolute value of curvature parameter $|k| = 1$ is chosen for convenience.

Geometry of space determines significant two properties of the universe. One property is whether our universe is finite or infinite and the other characteristic is if the universe is eternal or has a finite life span from the Big Bang to what is proposed as the opposite of the Big Bang, the Big Crunch. The universe is finite in case of spherical geometry of space as it is shown in Fig. (1.3). Such a universe has a limited volume and because of that is called a “closed” universe. A closed universe, filled with ordinary and dark matter alone, has a finite life span, but if it contains dark energy there is a set of solutions which allow for an eternal universe with and without the Big Bang. A non-eternal closed universe expands from the Big Bang, reaches its maximum volume, and then contracts until it reaches the Big Crunch.

In the other two cases of geometry i.e. flat or hyperbolic the universe is infinite and will expand forever after the Big Bang. These two scenarios of infinite and eternal universes are also called “open” universes. In order to determine which universe we live in, its curvature parameter has to be measured.

1.1.3 Solutions of Friedmann Equations

Flat Matter and Radiation Dominated Universes, $k = 0$: Since the second Friedmann equation (1.7) does not contain curvature parameter explicitly, reviewing different scenarios of the universe’s dynamics with respect to its curvature will involve only the first Friedmann equation (1.6), which for the flat universe is

$$\left(\frac{\dot{a}_m}{a_m}\right)^2 = \frac{8\pi G}{3}\rho_m \quad (1.9)$$

here the subscript m denotes the universe is filled with non-relativistic dust-like fluid and called a matter dominated universe. It is important to emphasize that the Eq. (1.9) expresses a condition for matter density to yield flat universe and for this reason the density defined as

$$\rho_{cr} = \frac{3}{8\pi G} \left(\frac{\dot{a}}{a}\right)^2 \quad (1.10)$$

is called critical density of the universe. Substituting the equation of state $p_m(\rho_m) = 0$ of non-relativistic matter in the second Friedman equation (1.7) and rewriting it with the use of Eq. (1.9) yields the conservation equation

$$\dot{\rho}_m + 3\rho_m \frac{\dot{a}_m}{a_m} = 0, \quad (1.11)$$

from which one recovers $a_m^3(t)\rho_m(t) = const.$ In what follow, I will use the following conditions: the Big Bang time $t_{BB} = 0$, the present time will be labeled t_0 and it also will be the age of the universe, the scale factor for the Big Bang and current epoch satisfies

$a(t_{BB}) = a_{BB} = 0$, $a(t_0) = a_0 = 1$, and $\rho_i(t_0) = \rho_{i0}$ is the present value of matter density of the type “ i ”. With the conditions adopted above the solution of the Eq. (1.9) is

$$a_m(t) = (6\pi G\rho_{m0})^{1/3} t^{2/3}. \quad (1.12)$$

This solution is known as the Einstein-De Sitter model.

In case when the universe dominated by relativistic type of fluid, i.e. particles that move with speeds close to the speed of light (neutrinos for example) or mass-less particles (photons), the equation of state is the same as for radiation $p_r = \rho_r/3$, where subscript r denotes radiation and thus this type of universe is called radiation dominated. Substitution of this equation of state in the second Friedmann Eq. (1.7) results in the conservation relation $a_r^4(t)\rho_r(t) = const$, which provides the following solution of Eq. (1.9),

$$a_r(t) = \left(\frac{2}{3}\pi G\rho_{r0}\right)^{1/4} t^{1/2}. \quad (1.13)$$

Closed Matter and Radiation Dominated Universes, $k = 1$: Now, let us derive solutions for the previous two matter constituents but in presence of positive curvature parameter $k = 1$ which corresponds to closed spherically curved universe. First I will solve Friedmann equations for non-relativistic matter dominated case i.e.

$$\left(\frac{\dot{a}_m}{a_m}\right)^2 + \frac{1}{a_m^2} = \frac{8\pi G}{3}\rho_m, \quad (1.14)$$

where $\rho_m \sim a^{-3}$. The solution in this case cannot be obtained as an explicit function of time however, parameterization through conformal time, defined as $d\eta = dt/a(t)$, yields the

cycloidal solution

$$a_m(\eta) = \frac{q_0}{2q_0 - 1} [1 - \cos(\eta)], \quad (1.15)$$

$$t(\eta) = \frac{q_0}{2q_0 - 1} [\eta - \sin(\eta)]. \quad (1.16)$$

Here q_0 is the value of the deceleration parameter at the current epoch $q_0 = q(t_0)$ where the deceleration parameter is defined as

$$q = -\frac{\ddot{a}a}{\dot{a}^2}, \quad (1.17)$$

and its physical meaning is that it gives a quantitative measure of the deceleration rate of the universe's expansion. It can be rewritten with the use of Friedmann equations (1.6)-(1.7) as

$$q = \frac{\rho}{2\rho_{cr}} \quad (1.18)$$

from which one can notice that the deceleration parameter can also be thought of as a measure of how much the universe deviates from being flat in case when it has curvature and deceleration parameter $q \neq 1/2$. In order to quantify more strictly how the deceleration parameter q depends upon the curvature parameter k one has to substitute the expression for the matter density ρ from the first Friedmann equation (1.6) into the Eq. (1.18) from which one can retrieve the following

$$k = 1 \quad \text{then} \quad q > \frac{1}{2} \quad (1.19)$$

$$k = -1 \quad \text{then} \quad q < \frac{1}{2}. \quad (1.20)$$

Relations (1.19)-(1.20) show that when matter density is higher than critical density the universe is closed while when the matter density is less than critical density the universe is open. If one introduces the dimensionless density as the ratio $\Omega = \rho/\rho_{cr}$ then the deceleration

parameter can be simply written as $q = \Omega/2$. In this particular example of a matter dominated universe one has ρ_m , hence $q = \Omega_m/2$, where $\Omega_m = \rho_m/\rho_{cr}$.

In case of a radiation dominated universe one has

$$\left(\frac{\dot{a}_r}{a_r}\right)^2 + \frac{1}{a_r^2} = \frac{8\pi G}{3}\rho_r, \quad (1.21)$$

where $\rho_r \sim a^{-4}$. The solution is

$$a_r(\eta) = \sqrt{\frac{2q_0}{2q_0 - 1}} \sin(\eta), \quad (1.22)$$

$$t(\eta) = \sqrt{\frac{2q_0}{2q_0 - 1}} [1 - \cos(\eta)], \quad (1.23)$$

where $q_0 = \Omega_{r0}/2$.

Open Matter and Radiation Dominated Universes, $k = -1$: The Friedmann equation for an open universe is

$$\left(\frac{\dot{a}_i}{a_i}\right)^2 - \frac{1}{a_i^2} = \frac{8\pi G}{3}\rho_i, \quad (1.24)$$

where i takes the values m for a matter dominated universe and the value r for a radiation dominated universe. The solution for the matter dominated universe is

$$a_m(\eta) = \frac{q_0}{1 - 2q_0} [\cosh(\eta) - 1], \quad (1.25)$$

$$t(\eta) = \frac{q_0}{1 - 2q_0} [\sinh(\eta) - \eta]. \quad (1.26)$$

And for radiation dominated case the solution is

$$a_r(\eta) = \sqrt{\frac{2q_0}{1-2q_0}} \sinh(\eta), \quad (1.27)$$

$$t(\eta) = \sqrt{\frac{2q_0}{1-2q_0}} [\cosh(\eta) - 1]. \quad (1.28)$$

The solutions we derived are shown below in Fig. (1.4).

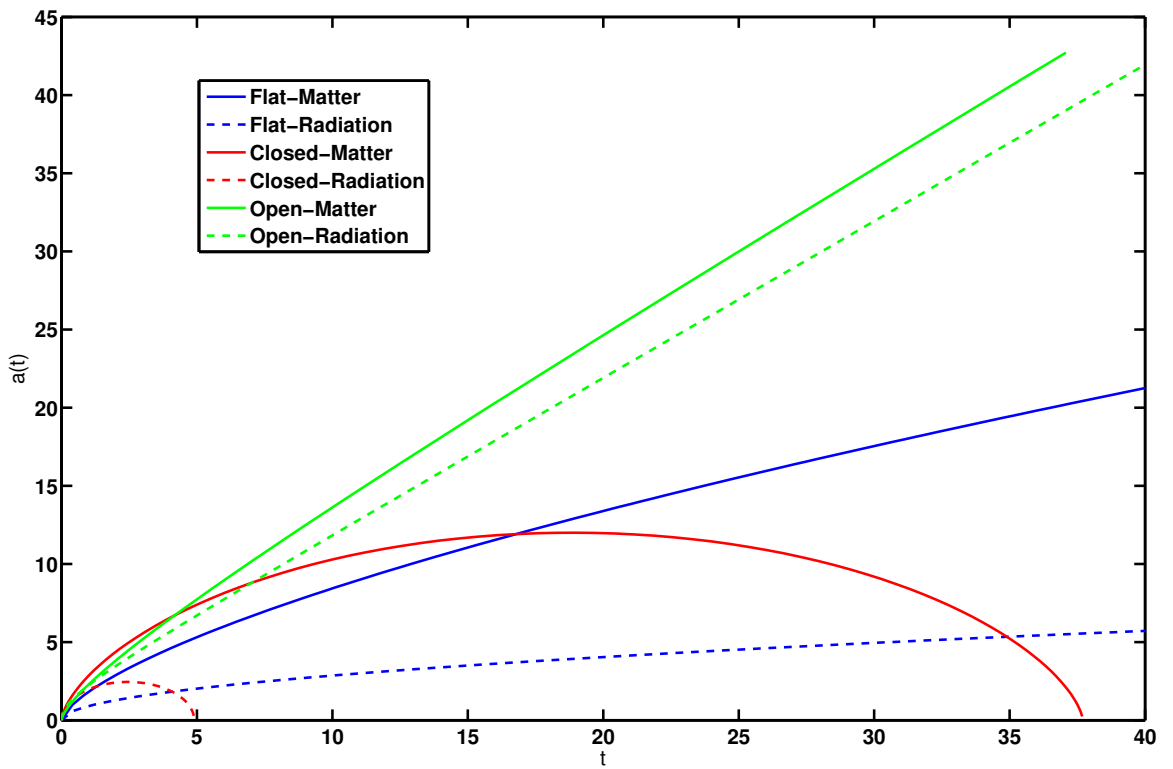


Figure 1.4: *Solutions of Friedmann equations for a single component universes with flat, closed, and open geometries. The time and the scale factor in arbitrary units.*

In the above we reviewed examples of ideal universes which contain one type of matter i.e. non-relativistic dust or radiation. The real universe consists of both types of matter and possibly dark energy. In the section below I investigate more realistic solutions of the

Friedmann equations for a universe with multiple types of matter content.

1.1.4 Cosmological Constant

The cosmological constant was first introduced by Albert Einstein when he was attempting to apply his theory of general relativity to the entire universe. It was commonly assumed in the early 20th century that the universe was static. However, since gravity is an attractive force with bottomless potential to find a static solution Einstein introduced the cosmological constant labeled by Greek letter Λ , in his equations

$$R_{\mu\nu} - \frac{1}{2}Rg_{\mu\nu} + \Lambda g_{\mu\nu} = 8\pi GT_{\mu\nu}. \quad (1.29)$$

The effect of the cosmological constant is to causes space to expand as if there were a repulsive gravitational force. Einstein's idea was to use the effect of repulsion from the cosmological constant to cancel out ordinary matter's attraction and so have a static solution for the universe. However, it was shown that even with a cosmological constant a static solution is not stable with respect to small perturbations in matter density and eventually the idea of a static universe was abandoned after Hubble's discovery of the expansion of the universe. Einstein called his invention of a cosmological constant as his biggest blunder. However, since Einstein's times scientists keep coming back to the idea of a cosmological constant over and over again because of theoretical physics considerations such as the quantum vacuum and cosmic inflation. However, it was not until the discovery of the accelerated expansion of the universe in the late 1990's which provided the first observational evidence for a cosmological constant.

The way Einstein thought of the cosmological constant was that it was a fundamental constant of nature and was part of the gravity law, thus Einstein was the first who developed a "Modified Gravity Theory" with Λ placed on the left hand side of Eq. (1.29), i.e. geometrical part of the Einstein equations. The modified gravity as an alternative explanation

of the accelerated cosmological expansion is highly discussed topic in modern cosmology, however I do not address this approach in a great details. For recent reviews of modified gravity see [3] and [4].

When cosmological constant is written on the right hand side of Einstein's equations it introduces a type of energy that fills the universe homogeneously and causes repulsion on the scales determined by the cosmological constant. This view gives the first Friedmann equation as

$$\left(\frac{\dot{a}}{a}\right)^2 = \frac{8\pi G}{3} \left(\frac{\rho_{r0}}{a^4} + \frac{\rho_{m0}}{a^3} + \frac{\rho_{k0}}{a^2} + \rho_{\Lambda}\right), \quad (1.30)$$

where $\rho_{k0} = -3k/8\pi G$ is the present value of “curvature density” chosen to represent curvature as if it were a type of matter and the meaning of this representation is that it shows amount of matter density deficit in the universe to make it flat when it has hyperbolic geometry while in case of spherically curved universe ρ_k represents how much extra matter density in the universe over critical density. Here ρ_{Λ} is the energy density associated with the cosmological constant

$$\rho_{\Lambda} = \frac{\Lambda}{8\pi G}, \quad (1.31)$$

which is constant in time with equation of state

$$p_{\Lambda} = -\rho_{\Lambda}. \quad (1.32)$$

Energy density associated with a cosmological constant is called Dark Energy, where “dark” refers to the fact that it does not shine like ordinary Byronic matter i.e. protons, nuclei, ions, atoms, and electrons. The Eq. (1.30) does not have analytic solution in general case. Numerical solutions for standard cosmological model are presented in Fig. (1.5). It is worth to emphasize how different constituencies that fill the universe evolve with time after the Big Bang. For that purpose I plot $\log_{10}(\rho_i/\rho_{cr})$ vs the log of the scale factor $\log_{10}(a)$ for each component in a single graph shown in Fig. (1.6).

Motivation for a cosmological constant as a type of energy comes from quantum field

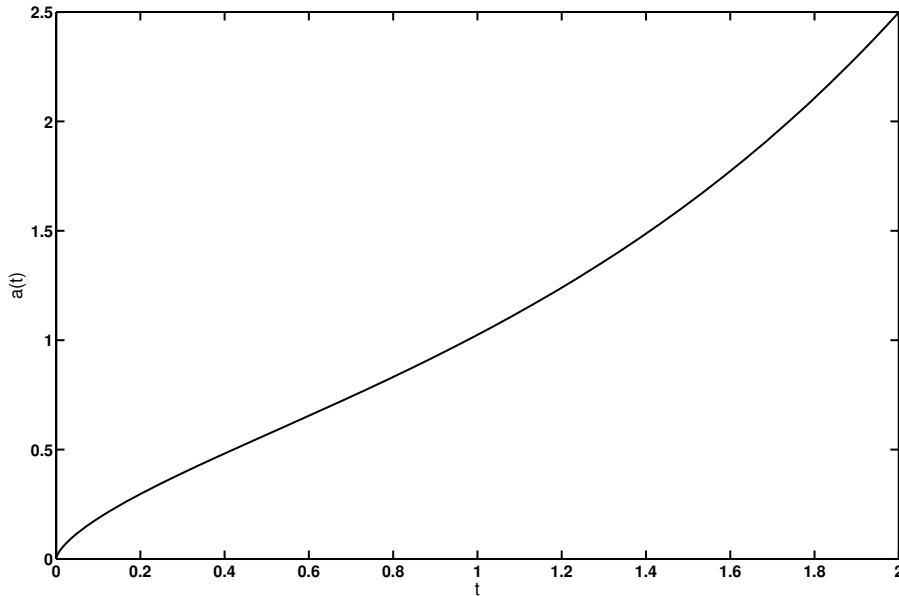


Figure 1.5: Numerical solution of Eq. (1.30) for standard cosmology. Time and the scale factor presented in arbitrary units, where $a = 1$ corresponds to the current epoch.

theory. In quantum mechanics absolute vacuum as empty space does not exist. Quantum mechanics predicts fluctuations of energy in otherwise empty space whose average value yields total non-zero energy density always present in space called the Zero-Point Energy Density whose value for a scalar field with mass m can be expressed as [e.g., 5]

$$\rho_{\text{vac}} = \frac{m^4}{64\pi^2} \ln \left(\frac{m^2}{\mu^2} \right), \quad (1.33)$$

where μ is renormalization scale. The equation of state of the vacuum energy is the same as the equation of state for dark energy, Eq. (1.32), i.e. $p_{\text{vac}} = -\rho_{\text{vac}}$, which is what supports the assumption of the quantum vacuum as a possible candidate for dark energy. However, computation of the vacuum energy density predicts it to be in the range $\rho_{\text{vac}} \simeq 10^8 - 10^{72} \text{GeV}^4$ while $\rho_{\Lambda} \simeq 10^{-48} \text{GeV}^4$ is observed which deviates from the quantum vacuum prediction by 120 orders of magnitude! This inconsistency is known as the quantum vacuum

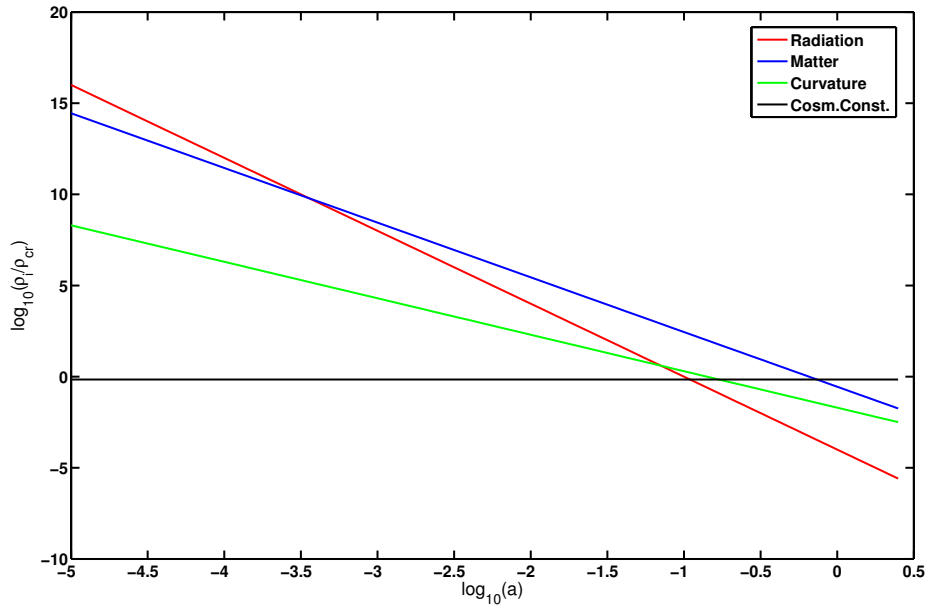


Figure 1.6: *The plot of $\log_{10}(\rho_i/\rho_{\text{cr}})$ vs the log of the scale factor $\log_{10}(a)$ for each component. One can see that the early universe was dominated by radiation, however since energy density of radiation dissipates as a^{-4} while energy density of ordinary matter decreases as a^{-3} , the radiation dominated epoch switches to matter dominated. Eventually, the universe becomes dominated by the cosmological constant, since its energy density does not evolve in time.*

problem in cosmology.

1.1.5 Standard Cosmological Model

According to general relativity (GR), any form of energy affects space-time dynamics and so cosmological evolution. This fact allows for a very simple phenomenological explanation of the observed accelerated expansion, attributing it to a cosmological constant Λ , homogeneously distributed in space and constant in time. This Λ CDM model [6] is now accepted as the standard cosmological model. At the current epoch Λ dominates the energy budget, with nonrelativistic cold dark matter (CDM) being the next largest contributor, followed by ordinary baryonic matter in third place. A widely discussed generalization of Λ CDM is

the ϕ CDM model in which Λ is replaced by a time-varying dark energy density modeled by a self-interacting scalar field ϕ [7]. For recent reviews see [8], [9], [10], and [11].

Observational data available [1] indicate that energy budget of the universe at the current epoch is largely dominated by dark energy contributing about 68.25%, with 26.86% for cold dark matter and 4.89% of baryonic matter. Curvature is constrained to less than 2.00% of the energy budget if the cosmological constant is dark energy. See Table 2 of [1] for the most recent and complete list of the parameters of the standard cosmological model or Λ CDM cosmology, where CDM stands for Cold Dark Matter and Λ refers to dark energy modeled by cosmological constant Λ . It is common in the field of physical cosmology to name alternative cosmological models of dark energy in a similar way by replacing only Λ with a symbol that refers to a particular alternative form of dark energy.

1.2 Observational Cosmology

In previous sections I have reviewed theoretical aspects of physical cosmology. In this section I provide a short overview of observational cosmology.

1.2.1 Redshift

The scale factor is a fundamental object in cosmology, although its absolute value does not have any useful physical meaning. What does have physical meaning and can be measured is the ratio of the scale factor taken between different epochs. It is a quantitative measurement to how much the universe has expanded between those two epochs. This ratio, as will be shown later, comes into many observable quantities. How can the ratio of scale factors at different epochs be measured? The physical meaning of expansion of space is that if one chooses any two arbitrary points in space with initial separation l_0 this physical distance will evolve in time approximately proportional to the scale factor i.e. $l(t) \sim l_0 a(t)$. In general relativity time-evolving spatial metrics causes a change in the wavelength of electromagnetic

radiation which can be expressed as

$$\lambda_{\text{em}} a_{\text{obs}} = \lambda_{\text{obs}} a_{\text{em}}, \quad (1.34)$$

where λ_{em} is the photon's wavelength when it was emitted by its source at epoch a_{em} and λ_{obs} is its wavelength when it was observed at epoch a_{obs} . This change in wavelength results in a so called, cosmological redshift. Redshift is when the wavelength of electromagnetic radiation increases. The cause of increase of wavelength determines the type of redshift. Thus there is a Doppler redshift, due to motion away from the source of radiation, gravitational redshift, due to radiation propagating away from the source of the gravity field, and cosmological redshift, due to the expansion of space. The word “redshift” originated from the optical effect when the wavelength of radiation increases towards the red part of the spectrum. The definition of redshift is

$$z = \frac{\lambda_{\text{obs}} - \lambda_{\text{em}}}{\lambda_{\text{em}}}, \quad (1.35)$$

which, after substituting cosmological wavelength change via scale factor given in Eq. (1.34) and recalling that $a_{\text{obs}} = 1$, yields the equation for cosmological redshift

$$z = \frac{1}{a} - 1. \quad (1.36)$$

Redshift is a directly measured quantity determined from analysis of spectral lines emitted by the observed source of radiation.

1.2.2 Hubble parameter

The name “Hubble parameter” originates from the Hubble law discovered by astronomer Edwin Hubble in 1928, which states that the velocity of recession v of a galaxy from an observer anywhere in the universe is proportional to the physical distance l between the

galaxy and observer, and the coefficient of proportionality is the Hubble constant H_0 . Thus, the Hubble law is

$$v = H_0 l, \tag{1.37}$$

where $v = \dot{l}$ and H_0 is the value of the Hubble parameter at the present epoch. Hubble law was first derived from the Einstein equations by George Lemaître in 1927 who independently derived the same equations of motion for the universe as Friedmann did. Recalling from the previous section $l(t) \sim l_0 a(t)$, which after differentiating yields $\dot{l} \sim l_0 \dot{a} = v$ and $v/l = \dot{a}/a$, therefore one has for the Hubble parameter the following

$$H = \frac{\dot{a}}{a}. \tag{1.38}$$

As we can see the Hubble parameter is not a constant.

Now we can rewrite the first Friedmann equation in terms of measurable quantities, which is used most of the time for practical purposes in physical cosmology. Below is an example for a universe filled with radiation, matter, cosmological constant, and non zero curvature

$$H^2(z) = H_0^2 [\Omega_{r0}(1+z)^4 + \Omega_{m0}(1+z)^3 + \Omega_{k0}(1+z)^2 + \Omega_\Lambda]. \tag{1.39}$$

1.2.3 Luminosity Distance

Distance measurement in astronomy is based on the parallax method and provides direct measurement up to about 100 pc; any distance beyond this limit has to be measured with the use of indirect techniques. Physical cosmology deals with intergalactic objects, thus distances involved are of order 10^6 pc. A major method widely used in cosmology is based on observations of Supernovae explosions of a specific type called Ia (reads as “one a”). Supernovae of type Ia are the only to be stars from binary systems where one of the stars is a white dwarf that is orbiting close enough to its partner so that it strips matter from it which accretes back to the white dwarf causing it to increase its mass until it reaches the so

called Chandrasekhar limit. At this point the white dwarf's internal electron pressure unable to resist against gravitational pull and the star collapses on itself triggering thermonuclear reactions in its interior which results in an explosion. Thus allowing for a determination of their absolute luminosity. Supernovae Ia are “standard candles” in determining distances on intergalactic scales. Measuring flux at a distance $r_L^{(\text{obs})}$ from a star can be used to figure out that distance via the relationship between absolute luminosity and observed flux

$$F_{\text{obs}} = \frac{L_{\text{em}}}{\pi \left(2r_L^{(\text{obs})}\right)^2}, \quad (1.40)$$

where F_{obs} is observed flux and L_{em} emitted absolute luminosity. This is closest method to what could be considered as a direct method of distance measurement. It is independent of the cosmological model, thus it can be used to study different cosmologies.

Theoretical prediction of distance traveled by photon between two points in space can be derived from the equation of the line element Eq. (1.1), or for our purposes we use the line element written in Friedmann metrics Eq. (1.5). For a photon $ds^2 = 0$, so one concludes that the distance traveled by a photon written in spherical coordinates is

$$dt = a(t) \frac{dr}{\sqrt{1 - kr^2}}, \quad (1.41)$$

where $dr/\sqrt{1 - kr^2}$ is the coordinate distance between two neighboring points that does not change as space expands or contracts. The physical distance however, does change as space expands or contracts. It is very easy to see from Eq. (1.41) that in case of flat space the coordinate distance between an object that emitted light at the time t_{em} and an observer receiving the signal at the current epoch t_0 is

$$r = \int_{t_{\text{em}}}^{t_0} \frac{dt}{a(t)}. \quad (1.42)$$

In the more general case with non-flat spatial geometry one can derive the expression

$$r = \frac{1}{\sqrt{-\Omega_{k0}}} \sin \left(\sqrt{-\Omega_{k0}} \int_{t_{\text{em}}}^{t_0} \frac{dt}{a(t)} \right), \quad (1.43)$$

here Ω_{k0} is the present value of the curvature energy density defined as $\Omega_{k0} = \rho_{k0}/\rho_{cr0}$. Let us rewrite Eq. (1.43) using redshift as a variable. Expressing $dt = da/\dot{a}$ and using Eq. (1.39) for \dot{a}/a Eq. (1.43) transforms to

$$r(z) = \frac{1}{\sqrt{-\Omega_{k0}}} \sin \left(\sqrt{-\Omega_{k0}} \int_0^z \frac{dz'}{H(z')} \right). \quad (1.44)$$

This determines the relation between coordinate distance and redshift. However, coordinate distance is not directly observable since observations done via measurements of the flux of radiation coming from distant which lose energy due to redshift, thus the physical distance $r_L^{(\text{obs})}$ in Eq. (1.40) is different from coordinate distance by a factor $(1+z)$ which accounts for the decrease in observable flux due to redshift. The distance $r_L^{(\text{obs})}$ called physical or photometric or luminosity distance and its physical meaning is it gives estimate of how much the flux from a star with redshift z decreased by the time it reached the observer. Therefore the appropriate theoretical physical distance suitable for comparison with observable physical distance is

$$r_L^{(\text{th})}(z) = \frac{1+z}{\sqrt{-\Omega_{k0}}} \sin \left(\sqrt{-\Omega_{k0}} \int_0^z \frac{dz'}{H(z')} \right). \quad (1.45)$$

Distance measurements are expressed using the distance modulus $\mu = m - M$, which is the difference between the apparent magnitude m and the absolute magnitude M of an astronomical object. It is related to the luminous distance r_L as

$$\mu = 5 \log_{10}(r_L) - 5. \quad (1.46)$$

In the Fig. (1.7) the collection of the most recent Supernovae Ia data of Union 2.1 compilation from Ref. [12] are shown.

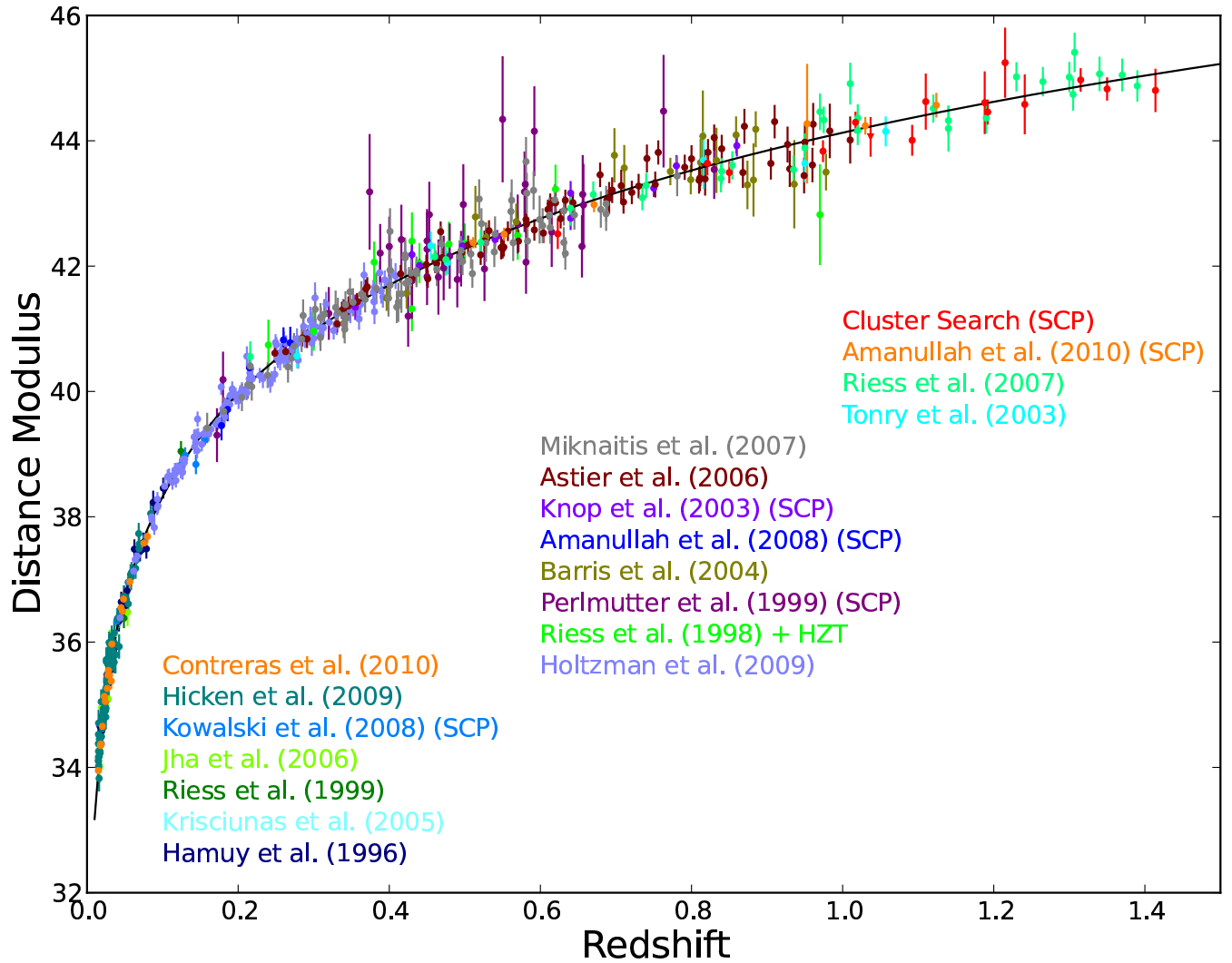


Figure 1.7: Hubble diagram for the Union2.1 compilation. The solid line represents the best-fit cosmology for a flat Λ CDM universe for supernovae alone. Source: Fig.(4) of [12]

Chapter 2

Forecasting cosmological parameter constraints from near-future space-based galaxy surveys

2.1 Introduction

Recent measurements of the apparent magnitude of Type Ia supernovae (SNeIa) continue to indicate, quite convincingly, that the cosmological expansion is currently accelerating [see, e.g., [12–15](#)].

There is good observational evidence that the large-scale radiation and matter distributions are statistically spatially isotropic. The (Copernican) cosmological principle, which is also consistent with current observations, then indicates that the Friedmann-Lemaître-Robertson-Walker (FLRW) models provide an adequate description of the spatially homogeneous background cosmological model.

In the FLRW models, the current accelerating cosmological expansion is a consequence of dark energy, the dominant, by far, term in the current cosmological energy budget. The dark energy density could be constant in time (and hence uniform in space) — Einstein’s

cosmological constant Λ [6] — or gradually decreasing in time and thus slowly varying in space [7].

The “standard” model of cosmology is the spatially-flat Λ CDM model in which the cosmological constant contributes around 68.25% of the current energy budget. Non-relativistic cold dark matter (CDM) is the next largest contributor, at around 26.86%, with non-relativistic baryons in third place with about 4.89%. For a review of the standard model see [16] and references therein.

Recent measurements of the anisotropies of the cosmic microwave background (CMB) radiation [e.g., 17, 18], in conjunction with significant observational support for a low density of non-relativistic matter [CDM and baryons together, e.g., 19], as well as measurements of the position of the baryon acoustic oscillation (BAO) peak in the matter power spectrum [e.g., 20–23], provide significant observational support to the spatially-flat Λ CDM model. Other data are also not inconsistent with the standard Λ CDM model. These include strong gravitational lensing measurements [e.g., 24–26], measurement of Hubble parameter as a function of redshift [e.g., 27–30], large-scale structure data [e.g., 31–34], and galaxy cluster gas mass fraction measurements [e.g., 35–37]. For recent reviews of the situation see, e.g., [38], [39], and [40].

While the predictions of the Λ CDM model are in reasonable accord with current observations, it is important to bear in mind that dark energy has not been directly detected (and neither has dark matter). Perhaps as a result of this, some feel that it is more reasonable to assume that the left hand side of Einstein’s Eq. (1.2) needs to be modified (instead of postulating a new, dark energy, component of the stress-energy tensor on the right hand side). While such modified gravity models are under active investigation, at present there is no compelling observational reason to prefer any of these over the standard Λ CDM cosmological model.

The Λ CDM model assumes that dark energy is a cosmological constant with equation

of state

$$p_\Lambda = -\rho_\Lambda, \tag{2.1}$$

where p_Λ and ρ_Λ are the pressure and energy density of the cosmological constant (fluid). This minimalistic model, despite being in good agreement with most observations available today, has some potential conceptual shortcomings that have prompted research into alternative explanations of the dark energy phenomenon.¹

To describe possible time-dependence of the dark energy density, it has become popular to consider a more general equation of state parametrization

$$p_\omega = \omega(z)\rho_\omega. \tag{2.2}$$

Here p_ω and ρ_ω are the pressure and energy density of the dark energy fluid with redshift z dependent equation of state parameter $\omega(z)$. The simplest such parametrization is the XCDM one for which the equation of state parameter is constant and results in accelerated expansion if $\omega(z) = \omega_X < -1/3$. In this case the dark energy density decreases with time and this allows for the possibility that the fundamental energy density scale for dark energy is set at high energy in the early Universe and the slow decrease of the energy density over the long age of the Universe ensures that the characteristic dark energy density scale now is small (a few meV). This also ensures that the dark energy density remains comparable to the matter energy density over a longer period of time (compared to that for the Λ CDM model).

When $\omega_X = -1$ the XCDM parametrization reduces to the consistent (and complete) Λ CDM model. For any other value of ω_X the XCDM parametrization cannot consistently describe spatial inhomogeneities without further assumptions and extension [see, e.g., 43, 44]. Models in which $\omega(z)$ varies in time, ω CDM models, are also unable to consistently describe spatial inhomogeneities without further assumptions and extension.

¹ Structure formation in the Λ CDM model is governed by the “standard” CDM structure formation model, which might be in some observational difficulty [see, e.g., 41, 42].

A physically and observationally viable alternative to the Λ CDM model, that consistently describes a slowly decreasing in time dark energy density, is the ϕ CDM model [7, 45]. This model, in which a dark energy scalar field, ϕ , slowly rolls down its potential, resulting in a slowly decreasing dark energy density, alleviates some of the conceptual problems, mentioned above, associated with the Λ CDM model. The slowly rolling scalar field, at a given instant of time, can be approximated by a dark energy fluid with an appropriately negative equation of state parameter.

More specifically, a ϕ CDM model with an inverse-power-law scalar field potential energy density $V(\phi) \propto \phi^{-\alpha}$, $\alpha > 0$, is a prototypical example that has been extensively studied. This model has a non-linear attractor or “tracker” scalar field solution that forces the initially sub-dominant dark energy density to come to dominate over the matter energy density, thus dominating the energy budget of the current Universe, and so resulting in the current accelerated cosmological expansion. In addition to therefore partially alleviating the “coincidence” problem of the Λ CDM model, the ϕ CDM model generates the current tiny dark energy scale of order an meV, measured by the SNeIa, through decrease, via cosmological expansion over the long age of the Universe, of a much larger energy scale.

The α parameter controls the steepness of the scalar field potential, with larger values resulting in a stronger time dependence of the approximate equation of state parameter and $\alpha = 0$ corresponds to the Λ CDM model limit. α has been constrained using currently available data [see e.g., 46–49, and references therein]. The strongest current limits are that α has to be less than ~ 0.7 at 2σ confidence [50].

In the ϕ CDM model, or in the XCDM or ω CDM parameterizations, the background evolution of the (spatially homogeneous) Universe differs from that in the Λ CDM case. This affects both the distance-redshift relation as well as the growth rate of large-scale structure. With precise measurements of distance and growth rate over a range of redshifts it will be possible to discriminate between cosmological models.²

² There are many other models under current discussion, besides the Λ CDM and ϕ CDM models and XCDM and ω CDM parameterizations we consider here for illustrative purposes. For a sample of the available

The BAO signature in the observed large-scale structure of the Universe allows for the measurements of radial and angular distances as functions of redshift [see, e.g., 20, 23, 59, 60]. In addition, the redshift-space distortion signal allows for inferences about the strength of gravitational interactions on very large scales [see, e.g., 61–66]. Currently available data sets have been used to measure distances and growth history up to a redshift $z \sim 0.8$ and the next generation of planned space-based galaxy redshift surveys of the whole extragalactic sky are expected to extend these measurements to a redshift $z \sim 2$. Possible candidates for such surveys include the Euclid satellite mission that has been approved by the European Space Agency [67] and the WFIRST satellite that was ranked high by the recent Decadal Survey [68]. These surveys have been shown to have the potential to measure angular distances, Hubble parameter $H(z)$, and growth rate as functions of redshift to a few percent precision over a wide range of redshifts [69–72].³

As mentioned above, an alternative potential explanation of the observed accelerated expansion of the Universe is to replace general relativity by a modified theory of gravity. For example, in the $f(R)$ -gravity models the Einstein-Hilbert gravitational action is modified to

$$S = \frac{1}{16\pi G} \int d^4x \sqrt{-g} f(R), \quad (2.3)$$

where the function $f(R)$ of the Ricci curvature R can in general be of any form. In the special case when $f(R) = R$ one recovers the Einstein-Hilbert action which yields the Einstein equations of general relativity, Eq. (1.2). For every dark energy model it is possible to find a function $f(R)$ that will result in exactly the same expansion history [see, e.g. 74–76] thus potentially eliminating the need for dark energy. However, nothing prevents the coexistence of modified gravity and dark energy, with both contributing to powering the current accelerated cosmological expansion. It is of significant importance to be able to determine which scenario best describes what is taking place in our Universe.

options see, e.g., [51], [52], [53], [54], [55], [56], [57], and [58].

³ For constraints on cosmological parameters from data from space missions proposed earlier, see [73] and references therein.

This chapter is based on [77]. We investigate how well anticipated data from the galaxy surveys mentioned above can constrain the time dependence of the dark energy. We will use the Fisher matrix formalism to obtain predictions for the ϕ CDM model and compare these with those made using the (model-dependent) XCDM and ω CDM parameterizations of dark energy. We will mostly assume that gravity is well described by general relativity, but will also look at some simple modified gravity cases. We find that the anticipated constraints on the parameter α of the ϕ CDM model are almost an order of magnitude better than the ones that are currently available.

Compared to the recent analysis of [70], here we use an updated characterization of planned next-generation space-based galaxy surveys, so our forecasts are a little more realistic. We also consider an additional dark energy parametrization, XCDM, a special case of ω CDM that was considered by [70], as well as the ϕ CDM model, forecasting for which has not previously been done.

The rest of the chapter is organized as follows. In Sec. 2.2 we briefly describe the observables and their relationship to basic cosmological parameters. In Sec. 2.3 we describe the models of dark energy that we study. Section 2.4 outlines the method we use for predicting parameter constraints, with some details given in the Appendix A. We present our results in Sec. 2.5 and provide conclusions in Chapter 5.

2.2 Measured power spectrum of galaxies

The large-scale structure of the Universe, which most likely originated as quantum-mechanical fluctuations of the scalar field that drove an early epoch of inflation [see, e.g., 78], became (electromagnetically) observable at $z \sim 10^3$ after the recombination epoch. Dark energy did not play a significant role at this early recombination epoch because of its low mass-density relative to the densities of ordinary and dark matter as well as that of radiation (neutrinos and photons). At $z \sim 5$ galaxy clusters began to form. Initially, in regions where

the matter density was a bit higher than the average, space expanded a bit slower than average. Eventually the dark and ordinary matter reached a minimum density and the regions contracted. If an over-dense region was sufficiently large its baryonic matter collapsed into its dark-matter halo. The baryonic matter continued to contract even more due to its ability to lose thermal energy through the emission of electromagnetic radiation. This can not happen with dark matter since it does not emit significant electromagnetic radiation nor does it interact significantly (non-gravitationally) with baryonic matter. As a result the dark matter remained in the form of a spherical halo around the rest of the baryonic part of a galaxy. At $z \sim 2$ the rich clusters of galaxies were formed by gravity, which gathered near-by galaxies together. Also by this time the dark energy's energy density had become relatively large enough to affect the growth of large-scale structure.

Different cosmological models with different sets of parameters can result in the same expansion history and so it is impossible to distinguish between such models by using only expansion history measurements. This is one place where measurements of the growth history of the large-scale structure of the Universe plays an important role. It is not possible to fix free parameters of two different cosmological models to give exactly the same expansion and growth histories simultaneously. It is therefore vital to observe both histories in order to obtain better constraints on parameters of a cosmological model.

In a cosmological model described by the FLRW metric, and to lowest order in dark matter over-density perturbations, the power-spectrum of observed galaxies is given by [79]

$$P_g(k, \mu) = P_m(k)(b\sigma_8 + f\sigma_8\mu^2)^2. \quad (2.4)$$

Here subscript g denotes galaxies, P_m is the underlying matter power spectrum, b is the bias of galaxies, f is the growth rate, μ is the cosine of the angle between wave-vector k and the line-of-sight direction, and σ_8 is the overall normalization of the power spectrum (σ_8 is the rms energy density perturbation smoothed over spheres of radius $8h^{-1}$ Mpc, where $h = H_0/(100\text{kms}^{-1}\text{Mpc}^{-1})$ and H_0 is the Hubble constant). Since, for a measured

power spectrum of galaxies on a single redshift slice, the bias and growth rate are perfectly degenerate with the overall amplitude, in the equations below we will refer to $b\sigma_8$ and $f\sigma_8$ simply as b and f .

The angular dependence of the power spectrum in Eq. (2.4) can be used to infer the growth rate factor $f(z)$ which is defined as the logarithmic derivative of the linear growth factor

$$f(z) = \frac{d \ln G}{d \ln a}, \quad (2.5)$$

where a is the cosmological scale factor, and the linear growth factor $G(t) = \delta(t)/\delta(t_{\text{in}})$ shows by how much the perturbations have grown since some initial time t_{in} .⁴

The numerical value of the $f(z)$ function depends both on the theory of gravity and on the expansion rate of the Universe. Since the growth rate depends very sensitively on the total amount of non-relativistic matter, it is often parametrized as [see, e.g., 80, and references therein]

$$f(z) \approx \Omega_m^\gamma(z), \quad (2.6)$$

where

$$\Omega_m(z) = \frac{\Omega_m(1+z)^3}{E^2(z)}, \quad (2.7)$$

and

$$E(z) = H(z)/H_0 = \sqrt{\Omega_m(1+z)^3 + \Omega_k(1+z)^2 + \Omega_{DE}(z)}. \quad (2.8)$$

Here $H(z)$ is the Hubble parameter and H_0 is its value at the present epoch (the Hubble constant), Ω_m is the value of the energy density parameter of non-relativistic matter at the present epoch ($z = 0$), Ω_k that of spatial curvature, and $\Omega_{DE}(z)$ is the energy density parameter which describes the evolution of the dark energy density and is different in different dark energy models.

⁴ Here we have expanded the energy density $\rho(t, \mathbf{x})$ in terms of a small spatially inhomogeneous fractional perturbation $\delta(t, \mathbf{x})$ about a spatially-homogeneous background $\rho_b(t)$: $\rho(t, \mathbf{x}) = \rho_b(t)[1 + \delta(t, \mathbf{x})]$.

The growth index, γ , depends on both a model of dark energy as well as a theory of gravity. When general relativity is assumed and the equation of state of dark energy is taken to be of the general form in Eq. (2.2) then [see, e.g., 80, and references therein]

$$\gamma \approx 0.55 + 0.05[1 + \omega(z = 1)] \quad (2.9)$$

to a few percent accuracy. In the Λ CDM cosmological model $\gamma \approx 0.55$. An observed significant deviation from this value of γ will present a serious challenge for the standard cosmological model.

The power spectrum is measured under the assumption of a fiducial cosmological model. If the angular and radial distances in the fiducial model differ from those in the real cosmology, the power spectrum will acquire an additional angular dependence via the Alcock-Paczyński (AP) [81] effect, as discussed in [70],

$$P_g(k, \mu) = \frac{1}{f_{\parallel} f_{\perp}^2} P_m \left(\frac{k}{f_{\perp} F} \sqrt{F^2 + \mu^2 (1 - F^2)} \right) \times \left\{ b + \frac{\mu^2 f}{F^2 + \mu^2 (1 - F^2)} \right\}^2, \quad (2.10)$$

where

$$f_{\parallel}(z) = R_r(z) / \hat{R}_r(z), \quad (2.11)$$

$$f_{\perp}(z) = D_A(z) / \hat{D}_A(z), \quad (2.12)$$

$$F = f_{\parallel} / f_{\perp}. \quad (2.13)$$

Here $R_r = dr/dz$ is the derivative of the radial distance, D_A is the angular diameter distance (both defined below), a hat indicates a quantity evaluated in the fiducial cosmological model, and a quantity without a hat is evaluated using the alternative cosmological model. The AP effect is an additional source of anisotropy in the measured power spectrum and allows for the derivation of stronger constraints on cosmological parameters.

2.3 Cosmological models

In an FLRW model with only non-relativistic matter and dark energy the distances $D_A(z)$ and $R_r(z)$ are

$$D_A(z) = \frac{1}{h\sqrt{\Omega_k}(1+z)} \sinh \left(\sqrt{\Omega_k} \int_0^z \frac{dz'}{E(z')} \right), \quad (2.14)$$

$$R_r(z) = \frac{1}{h(1+z)E(z)}. \quad (2.15)$$

Here $E(z)$ is defined in Eq. (2.8). The functional form of $E(z)$ depends on the model of dark energy.

2.3.1 Λ CDM, XCDM and ω CDM parameterizations

Here we describe the relevant features of the Λ CDM model and the dark energy parameterizations we consider.

If the dark energy is taken to be a fluid its equation of state can be written as $p = \omega(z)\rho$. For the Λ CDM model the equation of state parameter $\omega(z) = -1$ and the dark energy density is time independent.

In the XCDM parametrization $\omega(z) = \omega_X (< -1/3)$ is allowed to take any time-independent value, resulting in a time-dependent dark energy density.

In the ω CDM parametrization the time dependence of $\omega(z)$ is parametrized by introducing an additional parameter ω_a through [82, 83]

$$w(z) = w_0 + w_a \frac{z}{1+z}. \quad (2.16)$$

The XCDM parametrization is the limit of the ω CDM parametrization with $\omega_a = 0$. In the ω CDM parametrization the function $\Omega_{DE}(z)$ that describes the time evolution of the dark

energy density is

$$\Omega_{DE}(z) = (1 - \Omega_m - \Omega_k)(1+z)^{3(1+w_0+w_a)} \exp\left(-3w_a \frac{z}{1+z}\right), \quad (2.17)$$

and the corresponding expression for the XCDM case can be derived by setting $\omega_a = 0$ here.

2.3.2 ϕ CDM model

In the ϕ CDM model the energy density of the background, spatially homogeneous, scalar field ϕ can be found by solving the set of simultaneous ordinary differential equations of motion,

$$\ddot{\phi} + 3\frac{\dot{a}}{a}\dot{\phi} + V'(\phi) = 0, \quad (2.18)$$

$$\left(\frac{\dot{a}}{a}\right)^2 = \frac{8\pi G}{3}(\rho + \rho_\phi) - \frac{k}{a^2}, \quad (2.19)$$

$$\rho_\phi = \frac{1}{16\pi G} \left(\frac{1}{2}\dot{\phi}^2 + V(\phi) \right). \quad (2.20)$$

Here an over-dot denotes a derivative with respect to time, a prime denotes one with respect to ϕ , $V(\phi)$ is the potential energy density of the scalar field, ρ_ϕ is the energy density of the scalar field, and ρ that of the other constituents of the Universe.

Following [7] we consider a scalar field with inverse-power-law potential energy density

$$V(\phi) = \frac{\kappa}{2G}\phi^{-\alpha}. \quad (2.21)$$

Here α is a positive parameter of the model to be determined experimentally and κ is a positive constant. This choice of potential has the interesting property that the scalar field solution is an attractor with an energy density that slowly comes to dominate over the energy density of the non-relativistic matter (in the matter dominated epoch) and causes

the cosmological expansion to accelerate. The function $\Omega_{DE}(z)$ in the case of ϕ CDM is

$$\Omega_{DE}(z) = \frac{1}{12} \left(\dot{\phi}^2 + \frac{\kappa}{G} \phi^{-\alpha} \right). \quad (2.22)$$

2.4 Fisher matrix formalism

The precision of the galaxy power spectrum measured in redshift bins depends on the cosmological model, the volume of the survey, and the distribution of galaxies within the observed volume. See Appendix A for a summary of how to estimate the precision of measurements from survey parameters.

We assume that the power spectrum $P(k_i)^{\text{meas}}$ has been measured in N wave-number k_i bins ($i = 1 \dots N$) and each measurement has a Gaussian uncertainty σ_i . From these measurements a likelihood function

$$\mathcal{L} \propto \exp \left(-\frac{1}{2} \chi^2 \right) \quad (2.23)$$

can be constructed where

$$\chi^2 = \sum_{i=1}^N \frac{(P_i^{\text{meas}} - P_i(\mathbf{p}))^2}{\sigma_i^2}. \quad (2.24)$$

Here \mathbf{p} are the set of cosmological parameters on which the power spectrum depends.

The likelihood function in Eq. (2.23) can be transformed into the likelihood of theoretical parameters \mathbf{p} by Taylor expanding it around the maximum and keeping terms of only second order in $\delta\mathbf{p}$ as $\chi^2(\delta\mathbf{p}) = F_{jk} \delta p^j \delta p^k$, where F_{jk} is the Fisher matrix⁵ of the parameter set \mathbf{p} given by second derivatives of the likelihood function through

$$F_{jk} = - \left\langle \frac{\partial^2 \ln \mathcal{L}}{\partial p^j \partial p^k} \right\rangle. \quad (2.25)$$

⁵ For a review of the Fisher matrix formalism as applied to cosmological forecasting, see [84].

The Fisher matrix predictions are exact in the limit where initial measurements as well as derived parameters are realizations of a Gaussian random variable. This would be the case if the P_i^{meas} were perfectly Gaussian and the $P_i(\mathbf{p})$ were linear functions of \mathbf{p} , which would make the second order Taylor expansion of the likelihood around its best fit value exact. In reality, because of initial non-Gaussian contributions and nonlinear effects, the predictions of Fisher matrix analysis will be different (more optimistic) from what is achievable in practice. These differences are larger for strongly non-linear models and for the phase spaces in which the likelihood is non-negligible at some physical boundary ($\alpha = 0$ in case of ϕ CDM). A more realistic approach, that requires significantly more computational time and power, is to generate a large amount of mock data and perform a full Monte-Carlo Markov Chain (MCMC) analysis [see, e.g., 85, 86, where the authors find significant differences compared to the results of the Fisher matrix analysis].

We assume that the full-sky space-based survey will observe H α -emitter galaxies over 15000 deg² of the sky. For the density and bias of observed galaxies we use predictions from [87] and [88] respectively. We further assume that about half of the galaxies will be detected with a reliable redshift. These numbers roughly mirror what proposed space missions, such as the ESA Euclid satellite and the NASA WFIRST mission, are anticipated to achieve. For the fiducial cosmology we use a spatially-flat Λ CDM model with $\Omega_m = 0.25$, the baryonic matter density parameter $\Omega_b = 0.05$, $\sigma_8 = 0.8$, and the primordial density perturbation power spectral index $n_s = 1.0$, for convenience we summarize all the parameters of the fiducial model in Table 1.

We further assume that the shape of the power spectrum is known perfectly (for example from the results of the *Planck* satellite) and ignore derivatives of the real-space power spectrum with respect to cosmological parameters.

We predict the precision of the measured galaxy power spectrum and then transform it into correlated error bars on the derived cosmological parameters. At first we make predictions for the basic quantities b and f in the XCDM and ω CDM parameterizations

and in the ϕ CDM model. Then it allows us to predict constraints on deviations from general relativity and see how these results change with changing assumptions about dark energy. Finally, we forecast constraints on the basic cosmological parameters of dark energy models.

For the XCDM parametrization these basic cosmological parameters are $p_{\text{XCDM}} = (f, b, h, \Omega_m, \Omega_k, w_X)$. The ω CDM parametrization has one extra parameter describing the time evolution of the dark energy equation of state parameter, $p_{\omega\text{CDM}} = (f, b, h, \Omega_m, \Omega_k, w_0, w_a)$. For the ϕ CDM model the time dependence of the dark energy density depends only on one parameter α so we have $p_{\phi\text{CDM}} = (f, b, h, \Omega_m, \Omega_k, \alpha)$. In order to derive constraints on the parameters of the considered cosmological models while altering assumptions about the correctness of general relativity, we transform Fisher matrices of each model from the parameter set described above to the following parameter set (that now includes γ that parametrizes the growth rate) $p_{\text{model}} = (\gamma, \text{model})$, where by *model* we mean all the parameters of a particular model, for example, for ω CDM $\text{model} = p_{\omega\text{CDM}} = (f, b, h, \Omega_m, \Omega_k, w_0, w_a)$.

2.5 Results

2.5.1 Constraints on growth rate

Figure 3.1 shows predictions for the measurement of growth rate assuming different dark energy models. We find that in the most general case, when no assumption is made about the nature of dark energy, the growth rate can be constrained to a precision of better than 2% over a wide range of redshifts. This is in good agreement with previous similar studies [see, e.g., Fig. 1 of 70]. When we specify a dark energy model the constraints on growth rate improve by about a factor of two. There is very little difference between the results derived for different dark energy models: the precision is almost insensitive to the assumed model. Also, one can notice that the curves for the XCDM parametrization and for the ϕ CDM

model are almost identical. The likely explanation of this effect is that for a fixed redshift bin the ϕ CDM model is well described by the XCDM parametrization with the value of the parameter $\omega_X = p_\phi/\rho_\phi$, where the values of the scalar field pressure p_ϕ and energy density ρ_ϕ are evaluated at that redshift bin.

The measurements of growth rate can be remapped into constraints on parameters describing the deviation from general relativity. Figure 3.2 shows correlated constraints between the current re-normalized Hubble constant h and the γ parameter that describes the growth of structure. The ϕ CDM model constraints on both h and γ are tighter than those for the XCDM or ω CDM parameterizations. As expected, the most restrictive Λ CDM model results in the tightest constraints. In Table 2.2 we show the deviations of the parameter γ from its fiducial value for various dark energy models.

2.5.2 Constraints on dark energy model parameters

We use measurements of growth and distance to constrain parameters of the dark energy models.

Figure 3.3 shows constraints on parameters of the ω CDM parameterization [these should be compared to Figs. 4a and 5a of 70]. When no assumptions are made about the nature of gravity the constraints on ω_0 and ω_a are very weak and degenerate. When we assume general relativity the constraints tighten significantly, resulting in $\sim 10\%$ accuracy in the measurement of ω_0 and $\sim 25\%$ accuracy in the measurement of ω_a .

The upper panel of Fig. 3.4 shows constraints on the parameters ω_X and Ω_m of the XCDM parametrization. Similar to the previous case, the constraints tighten significantly when we assume general relativity as the model of gravity. About a 2% measurement of ω_X and a 5% measurement of Ω_m are possible in this case. The lower panel of Fig. 3.4 show the related constraints on Ω_k and Ω_m for the XCDM parametrization. The constraints are similar to, but somewhat tighter than, those for the ω CDM parametrization. This is because the XCDM parametrization has one less parameter than the ω CDM parametrization. Spatial

curvature can be constrained to about 15% precision in this case.

Figures 2.5 and 2.6 show constraints on parameters of the ϕ CDM model. In the most general case, when no assumption is made about the nature of gravity, the constraints are weak and the parameters α and Ω_m are strongly correlated, with larger values of α requiring larger values of Ω_m . When general relativity is assumed, the constraints become much stronger and parameter α can be constrained to be less than 0.1 at the 1- σ confidence level. This is significantly better than any constraint available at the moment.

Figure 2.7 shows constraints on the parameters of the Λ CDM model. From the clustering data alone the spatial curvature can be constrained with almost 1% precision, largely because this model has the least number of free parameters.

The exact numerical values for the forecast error bars and likelihood contours should be taken with caution and not be interpreted as predictions for the performance of any specific survey (such as *Euclid* or *WFIRST*). Our main objective in this work was first to investigate how the modified gravity constraints change with different models of dark energy and second to demonstrate the improvement in ϕ CDM model constraints achievable with future galaxy surveys. Because of this we were able to simplify our method by adopting a Fisher matrix formalism instead of a full MCMC approach and also use a simplified description of the survey baseline. For more realistic predictions of *Euclid* performance, see, e.g., [67, 70, 71].

Table 2.1: *Values of the parameters of the fiducial Λ CDM model and the survey.*

Ω_m	Ω_b	Ω_k	h	σ_8	n_s	Efficiency	Redshift span	Covered sky area in deg ²
0.25	0.05	0.0	0.7	0.8	1.0	0.45	$0.55 \leq z \leq 2.05$	15000

Table 2.2: *Predicted deviations of parameter γ from its fiducial value, at one standard deviation confidence level, for different assumptions about dark energy.*

DE model	Fiducial γ	deviation
ω CDM	0.55	0.035
ϕ CDM	0.55	0.023
XCDM	0.55	0.035
Λ CDM	0.55	0.016

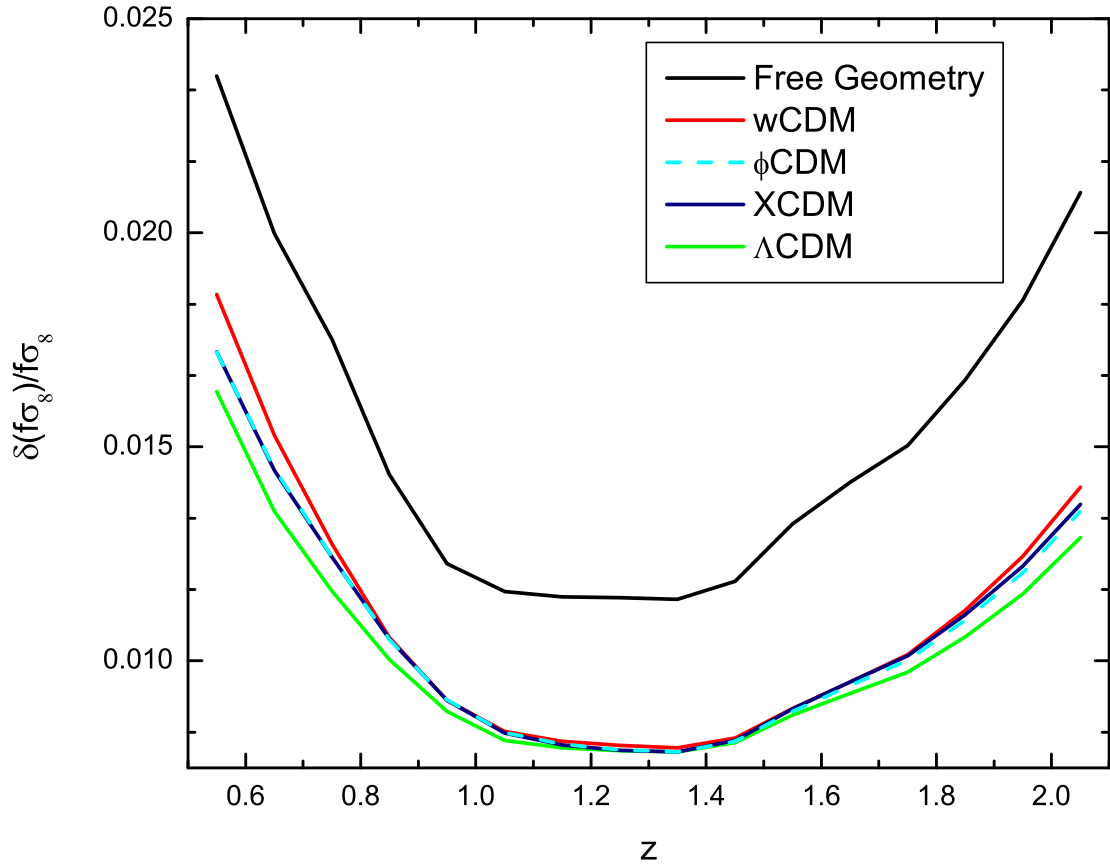


Figure 2.1: Predicted relative error on the measurements of growth rate as a function of redshift z in redshift bins of $\Delta z = 0.1$ for different models of dark energy. The upper solid black line shows predictions for the case when no assumption is made about the nature of dark energy.

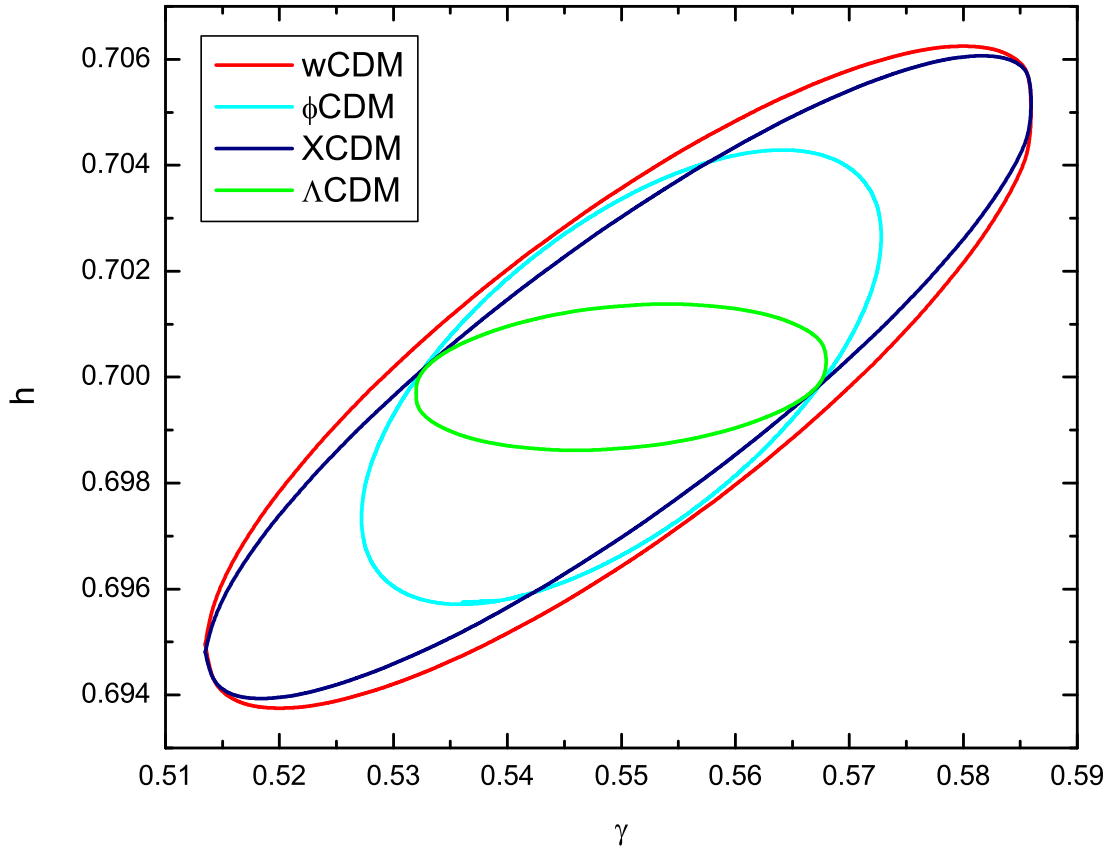


Figure 2.2: Predicted one standard deviation confidence level contour constraints on the current renormalized Hubble constant h and the parameter γ that describes deviations from general relativity for different dark energy models.

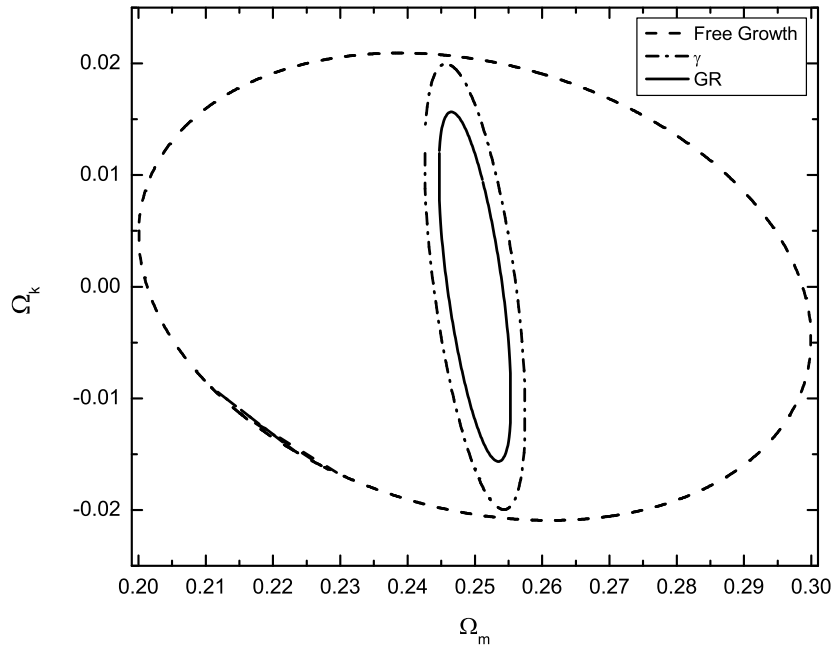
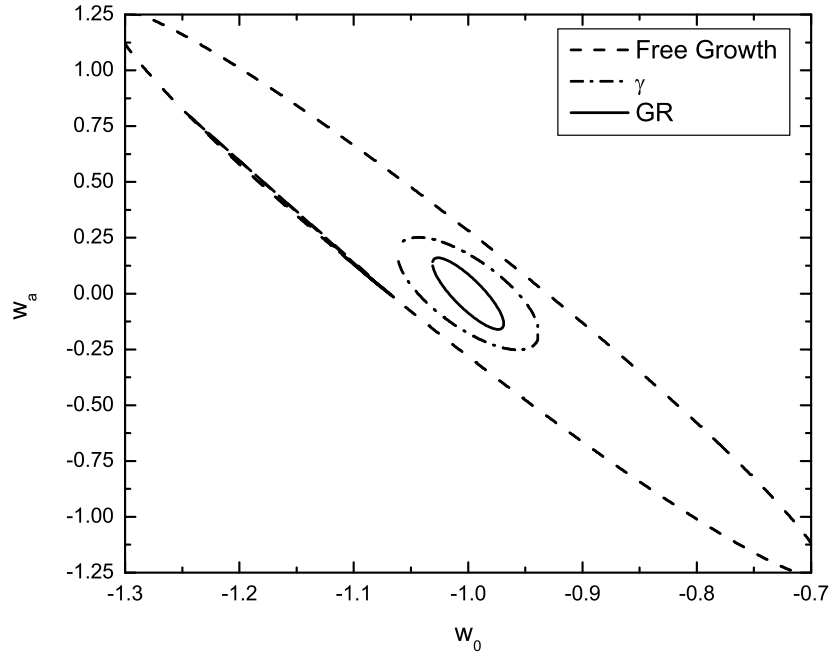


Figure 2.3: Upper panel shows one standard deviation confidence level contours constraints on parameters ω_a and ω_0 of the ω CDM parametrization, while lower panel shows these for parameters Ω_k and Ω_m .

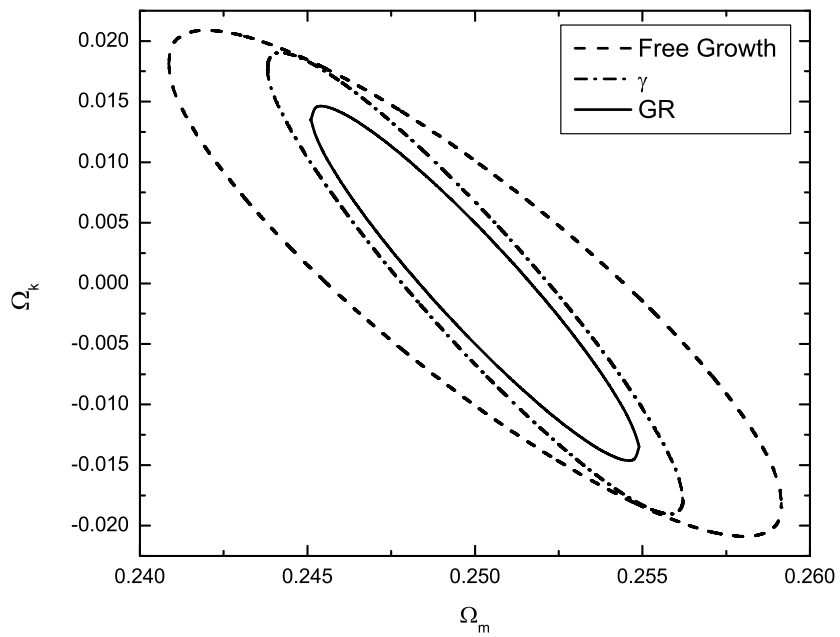
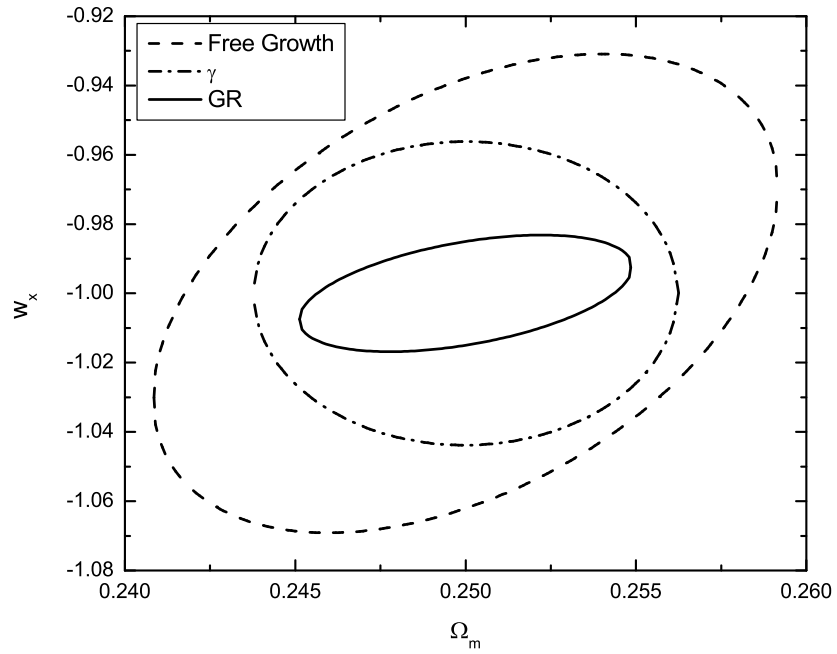


Figure 2.4: *One standard deviation confidence level contour constraints on parameters of the XCDM parametrization.*

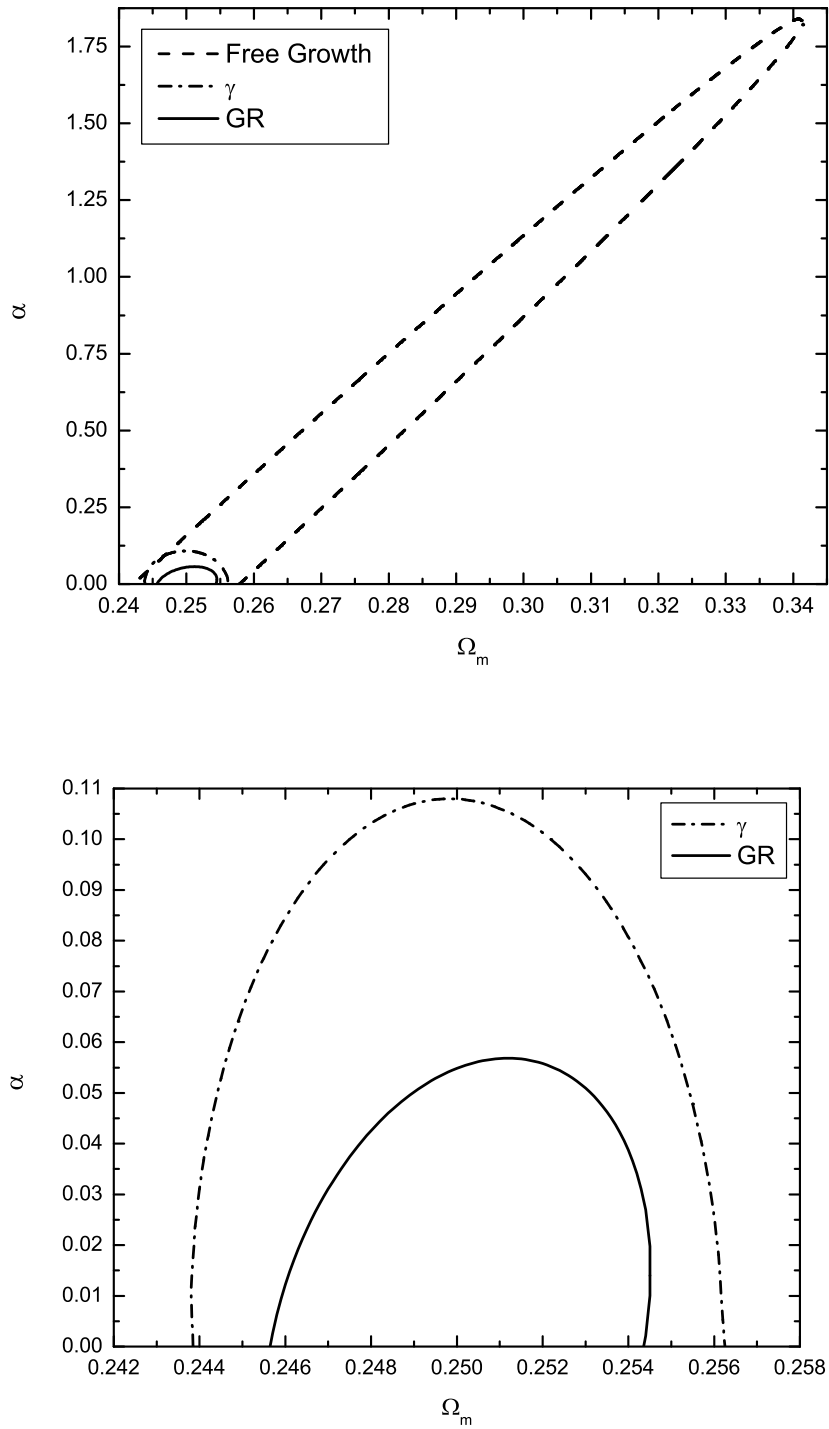


Figure 2.5: One standard deviation confidence level contour constraints on parameters α and Ω_m of the ϕ CDM model. Lower panel shows a magnification of the tightest two contours in the lower left corner of the upper panel.

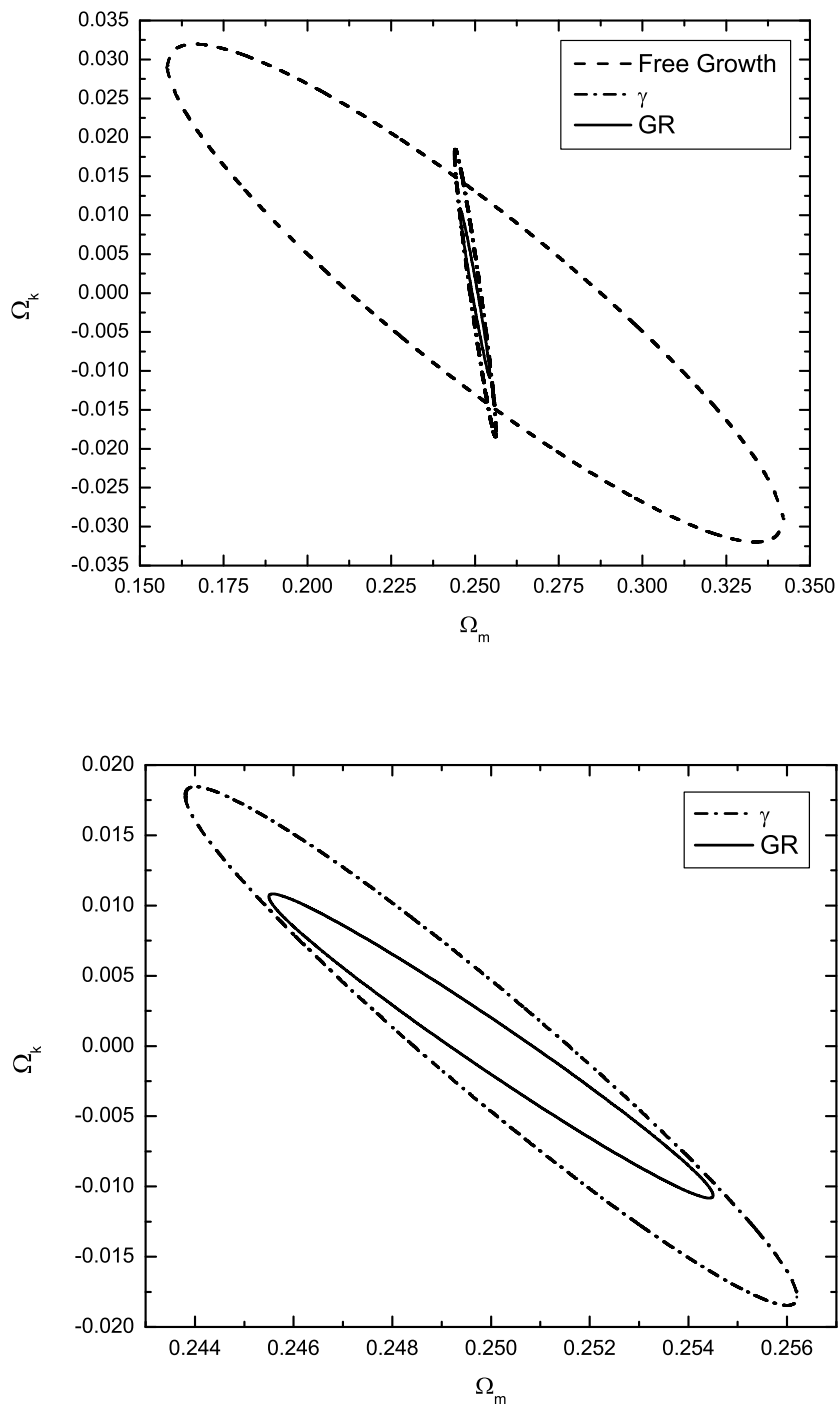


Figure 2.6: One standard deviation confidence level contour constraints on parameters Ω_k and Ω_m of the ϕ CDM model. The lower panel shows a magnification of the two tightest contours in the center of the upper panel.

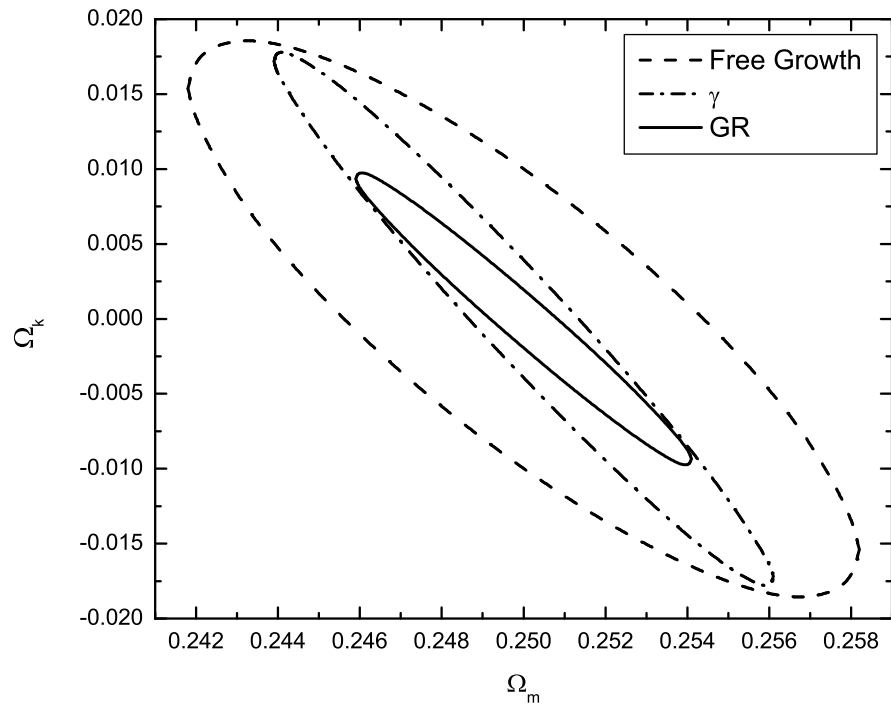


Figure 2.7: *One standard deviation confidence level contour constraints on parameters Ω_k and Ω_m of the Λ CDM model.*

Chapter 3

Nonflat time-variable dark energy cosmology

3.1 Introduction

When measurements of the cosmic microwave background (CMB) anisotropy are examined in the context of the current standard model of cosmology, the Λ CDM model¹, they indicate that the cosmological spatial hypersurfaces are close to flat, see [1, 92, 93]. On the other hand, under the assumption of flat spatial geometry the data favor time-independent dark energy (DE). However, it has been known for a while now that if a spatially curved time-variable DE model is used to analyze the CMB anisotropy measurements there is a degeneracy between spatial curvature and the parameter that governs the DE time variability, and this results in significantly weaker constraints on both parameters compared to the cases when only either non-zero spatial curvature or DE time variability is assumed, early

¹In this model [6], the current cosmological energy budget is dominated by a cosmological constant Λ , with non-relativistic cold dark matter (CDM) being the next largest contributor. For some time now most observations have been reasonably consistent with the predictions of the spatially-flat Λ CDM model; For early indications, see e.g., [35, 47, 89, 90]. Note that there are tentative observational indications that the standard CDM structure formation model, assumed in the Λ CDM cosmological model, might need to be improved upon [91].

work includes [94–107].

Most of these analyses are based on the Λ CDM parametrization or generalizations thereof. In the Λ CDM parametrization time-evolving DE is taken to be an X -fluid with equation of state $p_X = w_X \rho_X$ where ρ_X and p_X are the X fluid energy density and pressure and the equation of state parameter $w_X < -1/3$ is a constant. This is an incomplete model of time-variable DE since, unless extended, it cannot consistently describe the evolution of spatial inhomogeneities [43] and [44].

The Φ CDM model [7, 45] is the simplest consistent model of time-variable DE. In this model a scalar field Φ with potential energy density $V(\Phi)$ is the DE; $V(\Phi) \propto \Phi^{-\alpha}$, where constant $\alpha > 0$, is a widely used example². The original Φ CDM model assumed flat spatial sections. In this paper we develop the curved space extension of the Φ CDM model. Related models have been previously considered, see Ref. [94–96, 109–111]. However, as far as we are aware, we are the first to establish that the scalar field solution in the curvature-dominated epoch is a time-dependent fixed point or attractor, and that in the curvature-dominated epoch the scalar field energy density grows relative to that of space curvature, generalizing the results of [7, 45] to curved space.

This chapter is based on [112]. In the next section we describe the curved-space Φ CDM model we study. In this section and in the Appendix B we show that this model has a time-dependent fixed point scalar field solution in the curvature-dominated epoch. In Sec. 3.3 we compute some observable cosmological-test predictions for this model as a function of the three cosmological parameters of the model. Then we discuss these results by comparing those for flat and nonflat geometries as well as for open and closed geometries. In Chapter 5 we provide conclusions.

²See Ref. [108] for more general examples.

3.2 The Model

The original Φ CDM model of [7] was designed to describe the late-time consequences of an inflationary scalar field Φ model in which the scalar field potential energy density $V(\Phi)$ has an inverse power-law tail at large Φ . This form of $V(\Phi)$ was chosen because it provides a self-consistent phenomenological description of DE whose density decreases as the Universe expands, but decreases less rapidly than the nonrelativistic (cold dark and baryonic) matter density in a spatially flat universe. This eventually results in the expansion reaching a point at which the densities of nonrelativistic matter and DE have the same value and the decelerating cosmological expansion of the matter-dominated epoch switches to the accelerating expansion of the DE-dominated epoch that is currently observed [113–115].

In spacetime coordinates x^μ ($\mu = 0, 1, 2, 3$), with units chosen so that $\hbar = c = 1$, the late-time action of the model we consider is

$$S = \int d^4x \sqrt{-g} \left[\frac{m_p^2}{16\pi} \left(-R + \frac{1}{2} g^{\mu\nu} \partial_\mu \Phi \partial_\nu \Phi - \frac{\kappa}{2} m_p^2 \Phi^{-\alpha} \right) + \mathcal{L} \right]. \quad (3.1)$$

Here the Planck mass $m_p = G^{-1/2}$ where G is the gravitational constant and \mathcal{L} is the Lagrangian density of ordinary matter. The constants κ and α are positive real numbers and we adopt

$$\kappa = \frac{8}{3} \left(\frac{\alpha + 4}{\alpha + 2} \right) \left[\frac{2}{3} \alpha (\alpha + 2) \right]^{\alpha/2}. \quad (3.2)$$

With this choice for κ , our results in the limit of zero space curvature reduce to those of Ref. [7].

Applying the variational principle with respect to the metric to the action (3.1) gives

the Einstein equations,

$$R_{\mu\nu} - \frac{1}{2}Rg_{\mu\nu} = \frac{8\pi}{m_p^2} (T_{\mu\nu} + Q_{\mu\nu}). \quad (3.3)$$

Here $R_{\mu\nu}$ and R are the Ricci tensor and scalar and $T_{\mu\nu}$ is the stress-energy tensor of ordinary matter while $Q_{\mu\nu}$ is the stress-energy tensor of the Φ field and has the form

$$Q_{\mu\nu} = \frac{m_p^2}{32\pi} [2\partial_\mu\Phi\partial_\nu\Phi - (g^{\zeta\xi}\partial_\zeta\Phi\partial_\xi\Phi - \kappa\Phi^{-\alpha})g_{\mu\nu}]. \quad (3.4)$$

Assuming the cosmological principle of large-scale spatial homogeneity, the Friedmann metrics in coordinates (t, r, θ, φ) are

$$ds^2 = dt^2 - a^2 \left(\frac{dr^2}{1 - kr^2} + r^2 d\theta^2 + r^2 \sin^2\theta d\varphi^2 \right). \quad (3.5)$$

Here a is the scale factor and k is the curvature parameter that takes values $-1, 0, 1$ for open, flat, and closed spatial geometry. References [7, 45] consider only the $k = 0$ case.

The equation of motion for the scale factor a can be obtained by substituting the metric of Eq. (3.5) into the Einstein equations (3.3). The equation of motion for the scalar field Φ can be derived by either applying the variational principle with respect to the Φ field to the scalar field part of the action (3.1), or from the continuity conditions on the scalar field stress-energy tensor $Q_{\mu\nu}$ given in Eq. (3.4), and then using the metrics of Eq. (3.5).

The complete system of equations of motion is

$$\begin{aligned} \ddot{\Phi} + 3\frac{\dot{a}}{a}\dot{\Phi} - \frac{\kappa\alpha}{2}m_p^2\Phi^{-(\alpha+1)} &= 0, \\ \left(\frac{\dot{a}}{a}\right)^2 &= \frac{8\pi}{3m_p^2}(\rho + \rho_\Phi) - \frac{k}{a^2}, \\ \rho_\Phi &= \frac{m_p^2}{32\pi} \left(\dot{\Phi}^2 + \kappa m_p^2 \Phi^{-\alpha} \right). \end{aligned} \quad (3.6)$$

Here an overdot denotes a derivative with respect to time, and ρ is the energy density of ordinary matter while ρ_Φ is that of the dark energy scalar field Φ . It is also useful to introduce the density of spatial curvature,

$$\rho_k = -\frac{3m_p^2}{8\pi} \frac{k}{a^2}. \quad (3.7)$$

In this convention the spatially open model has $\rho_k > 0$.

DE cannot have a significant effect at early times, so we assume $\rho_\Phi \ll \rho$ at $a(t) \ll a_0$, where a_0 is the current value of the scale factor. Neither can space curvature play a significant role in the early nonrelativistic matter-dominated epoch, so $\rho_k \ll \rho$ for $a(t) \ll a_0$. Under these assumptions the Einstein–de Sitter model provides an accurate description of the nonrelativistic matter-dominated epoch and so can be used to derive initial conditions for the scalar field Φ identical to these in the original flat-space case of Ref. [7]. Of course, since the solution is a time-dependent fixed point or attractor, as shown here and in Refs. [7, 45], it is not sensitive to the precise initial conditions adopted: a large range of initial conditions results in the same scalar field fixed point or attractor solution.

3.2.1 Solution for the curvature-dominated epoch

In order to find whether the system (3.6) has an attractor solution in a certain epoch (i.e. matter dominated, radiation dominated or curvature dominated) we use a perturbation theory approach in which we treat the energy density of the scalar field Φ as a perturbation. Therefore, we neglect all terms in the right-hand side of the second equation of the system (3.6) (i.e. the Friedmann equation) except the energy density which dominates at the epoch of interest. When the energy budget of the Universe is dominated by radiation, ordinary matter or curvature, the solution of the Friedmann equation for the scale factor a varies as a power of time, $a \propto t^n$ (which in general is not true in a quintessence-dominated epoch), where the index n is determined for each epoch (as discussed in more detail later in this

section). By substituting this power-law solution for the scale factor $a \propto t^n$ into the system (3.6), the equation of motion for the scalar field is

$$\ddot{\Phi} + \frac{3n}{t}\dot{\Phi} - \frac{\kappa\alpha}{2}m_p^2\Phi^{-(\alpha+1)} = 0. \quad (3.8)$$

Equation (3.8) has a special power-law solution

$$\Phi_e(t) = At^{2/(\alpha+2)} \quad (3.9)$$

where the label e denotes that this is an unperturbed, exact, spatially homogeneous solution. The value of the constant A is

$$A = \left(\frac{\kappa\alpha m_p^2(\alpha+2)^2}{4[3n(\alpha+2) - \alpha]} \right)^{1/(\alpha+2)}. \quad (3.10)$$

We now show that, for the range of α and n values that we are interested in, the special solution (3.9) is an inwardly spiraling attractor in the phase space of solutions to (3.8). This means, for example, that in a curvature-dominated epoch (which has $n = 1$), the scalar field will approach the special solution (3.9) for a wide range of initial conditions. In order to show this we follow the methods of Sec. V of Ref. [45], and make the change of variables $(\Phi, t) \mapsto (u, \tau)$ where

$$\Phi(t) = \Phi_e(t)u(t), \quad t = e^\tau. \quad (3.11)$$

Substituting (3.11) into (3.8) and using (3.9) for $\Phi_e(t)$ we derive the equation for perturbation $u(t)$ of the scalar field $\Phi(t)$,

$$u'' - \left(1 - 3n - \frac{4}{\alpha+2}\right)u' + \left(\frac{6n(\alpha+2) - 2\alpha}{(\alpha+2)^2}\right)(u - u^{-(\alpha+1)}) = 0. \quad (3.12)$$

Here primes denote derivatives with respect to τ . Finally we switch to the phase space of

solutions of the system (3.8) by rewriting (3.12) as the system

$$\begin{aligned} u' &= p, \\ p' &= \left(1 - 3n - \frac{4}{\alpha + 2}\right)p - \left(\frac{6n(\alpha + 2) - 2\alpha}{(\alpha + 2)^2}\right)(u - u^{-(\alpha+1)}). \end{aligned} \quad (3.13)$$

The critical point $(u_0, p_0) = (1, 0)$ corresponds to the special solution (3.9). Although there exist, in general, other critical points at $p = 0$, these involve complex roots of unity for u , which are not physically relevant in this case.

Taking the linearization of (3.13) about the critical point, one obtains the eigenvalues

$$\lambda_{1,2} = f(\alpha, n) \pm i\sqrt{g(\alpha, n)} \quad (3.14)$$

where

$$\begin{aligned} f(\alpha, n) &= \frac{\alpha - 2 - 3n(\alpha + 2)}{2(\alpha + 2)}, \\ g(\alpha, n) &= \frac{6n(\alpha + 2)(5\alpha + 6) - 9n^2(\alpha + 2)^2 - (3\alpha + 2)^2}{4(2 + \alpha)^2}. \end{aligned} \quad (3.15)$$

For $f(\alpha, n) < 0$ and $g(\alpha, n) > 0$, the eigenvalues λ_1 and λ_2 show that the critical point is an inwardly spiraling attractor in the phase space. The cases $n = 1/2$ (radiation-dominated epoch) and $n = 2/3$ (matter-dominated epoch) were previously studied in Ref. [45]. Note that for the case $n = 1$ (curvature-dominated epoch) our critical point is an inwardly spiraling attractor if $\alpha > -2 + 2/\sqrt{3}$ or if $\alpha < -4$. In the Φ CDM model we are specifically interested in the range $\alpha > 0$. So the critical point is an attractor for all α values of interest.

The above analysis ignores spatial inhomogeneities in the gravitational field. In the Appendix we show that the time-dependent fixed point solution found above remains stable in the presence of gravitational field inhomogeneities.

We can use our results to show how this model partially resolves the ‘‘coincidence’’ puzzle.

From the last equation of the system (3.6) it follows that in the curvature-dominated epoch

$$\rho_{\Phi}(t) \propto t^{-2\alpha/(\alpha+2)}, \quad (3.16)$$

while $\rho_k(t) \propto 1/t^2$ and $\rho_m(t) \propto 1/t^3$. The exponent in Eq. (3.16) varies from -2 to 0 as α varies from ∞ to 0 , thus for $\alpha < \infty$ $\rho_{\Phi}(t)$ decays at a slower rate than ρ_k in the curvature-dominated epoch and eventually comes to dominate. This is consistent with the results of similar analyses in the radiation-dominated and matter-dominated epochs given in Ref. [45].

3.3 Some observational predictions

To gain some insight into the effects space curvature has on the Φ CDM model, we compute predictions for some cosmological tests in this section. To make these predictions we first numerically integrate the equations of motion (3.6) with initial condition of the form (3.9) taken in the matter-dominated epoch, where $n = 2/3$ with the usual expression for the scale factor in the matter-dominated epoch, see Ref. [7]. Instead of ρ , ρ_{Φ} and ρ_k we use dimensionless density parameters such as

$$\Omega_m = \frac{8\pi\rho}{3m_p^2 H^2} = \frac{\rho}{\rho + \rho_k + \rho_{\Phi}}, \quad (3.17)$$

where $H = \dot{a}/a$ is the Hubble parameter. We present the predictions as isocontours in the space of model parameters (Ω_{m0}, α) for a number of different values of the spatial curvature density parameter Ω_{k0} . (Here the subscript 0 refers to the value at the current epoch. For the open model $\Omega_{k0} > 0$.) For our illustrative purposes here we consider the same four cosmological tests studied in Ref. [7]. For a discussion of these and other cosmological tests see Ref. [41]. While it is of great interest to determine constraints on the three cosmological parameters of the model — Ω_{m0} , Ω_{k0} , and α — using various cosmological observables, in this paper we restrict ourselves to some qualitative remarks; a detailed quantitative comparison

between the predictions of the model and observations is given in Ref. [116], where it is found that observational data less tightly constrains space curvature in a dynamical dark energy matter of the type we study here.

3.3.1 The time parameter $H_0 t_0$

The dimensionless time parameter is

$$H_0 t_0 = H_0 \int_0^{a_0} \frac{da}{\dot{a}(t)}, \quad (3.18)$$

where t_0 is the age of the Universe and H_0 and a_0 are the present values of the Hubble parameter and scale factor. Figure 3.1 shows contours of constant $H_0 t_0$ as a function of Ω_{m0} and α for a series of fixed values of Ω_{k0} . A recent summary estimate of $H_0 = 68 \pm 2.8 \text{ km s}^{-1} \text{ Mpc}^{-1}$ [117] and the Planck (with WMAP polarization) estimate of $t_0 = 13.824 \pm_{0.055}^{0.041} \text{ Gyr}$ [1, 92, 93] gives, for the 2σ range, $0.88 \leq H_0 t_0 \leq 1.04$, where we have added the 1σ errors in quadrature and doubled to get the 2σ range. From Fig. 3.1 we see that $\Omega_{m0} = 0.27$ and $\alpha = 3$ is reasonably consistent with these constraints for a range of Ω_{k0} .

In the limit $\alpha \rightarrow 0$ this model reduces to the constant Λ one (but not necessarily with zero space curvature), while the limit $\alpha \rightarrow \infty$ corresponds to the open, closed, or flat (Einstein–de Sitter) model with $\Lambda = 0$, depending on the value of space curvature. At fixed Ω_{m0} (and Ω_{k0}), or in the flat-space case [7], the effect of increasing α is to reduce the value of $H_0 t_0$, making the Universe younger at fixed H_0 , since $\alpha = 0$ corresponds to a constant Λ and so the oldest Universe for given Ω_{m0} and Ω_{k0} . However, nonzero space curvature brings interesting new effects. At $\alpha = 0$ the Φ CDM model reduces to the Λ CDM one and here it is well known that to hold $H_0 t_0$ constant in the open case as Ω_{m0} is reduced and Ω_{k0} is increased requires a decrease in Ω_Λ (to compensate for the increase of t_0 at constant H_0 as Ω_{m0} is reduced and Ω_{k0} is increased). The converse is true in the closed case. Studying the $\alpha = 0$ intercepts of the $H_0 t_0$ isocontours in both panels of Fig. 3.1 confirms these arguments.

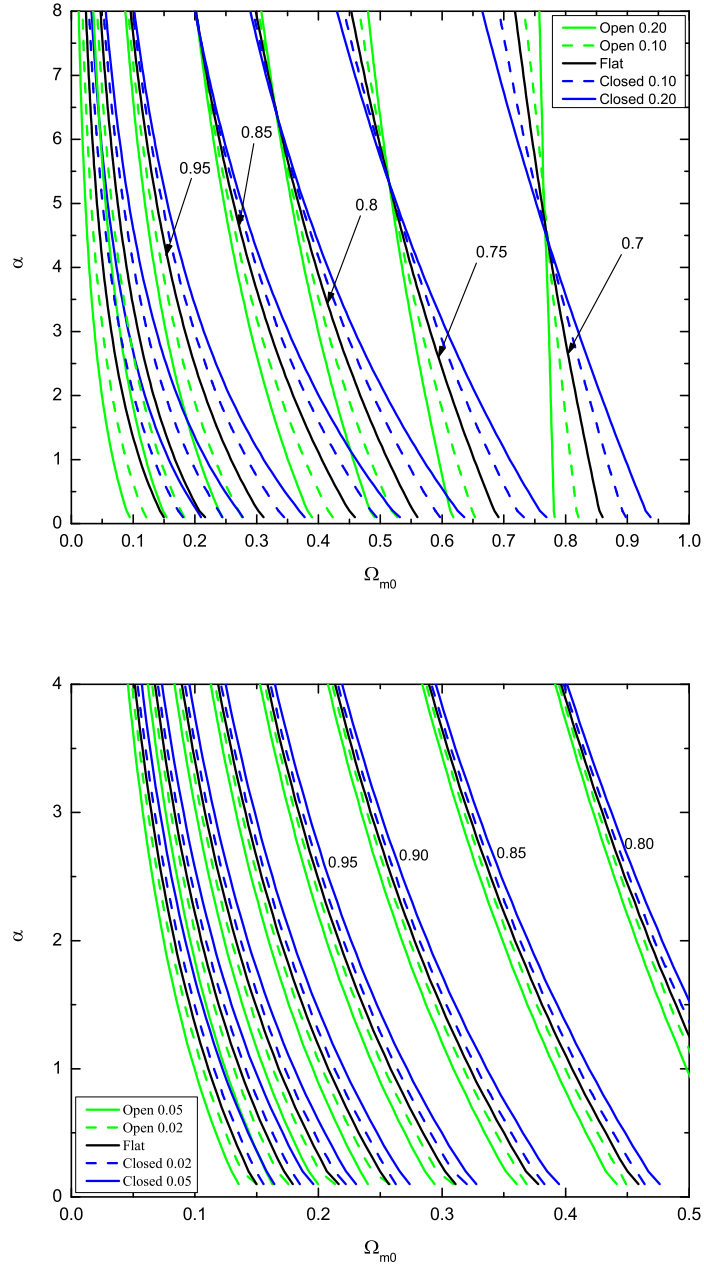


Figure 3.1: Contours of fixed time parameter $H_0 t_0$, as a function of the present value of the nonrelativistic matter density parameter Ω_{m0} and scalar field potential power-law index α , at various values of the current value of the space-curvature density parameter Ω_{k0} (as listed in the inset legend boxes). The upper panel shows a larger part of (Ω_{m0}, α) space for a larger range of Ω_{k0} values [for $H_0 t_0 = 0.7, 0.75, 0.8, 0.85, 0.95, 1.05$ and 1.15 , from right to left], while the lower panel focuses on a smaller range of the three parameters [for $H_0 t_0$ from 0.8 to 1.15 in steps of 0.05 , from right to left].

That is, for a fixed value of $H_0 t_0$ at smaller α (i.e. $\alpha \lesssim 4$) the contours corresponding to open geometry shift to the left of the flat geometry, i.e., to lower Ω_{m0} , while the contours corresponding to closed geometry shift to the right of the flat case.

At higher α the DE density decreases more rapidly with the expansion (unlike the $\alpha = 0$ case where Λ remains constant), and the contours switch around. Here to hold $H_0 t_0$ constant in the open case as Ω_{k0} is increased requires that Ω_{m0} increase and $\Omega_{\Phi0}$ decrease to compensate. In the closed case as Ω_{k0} is increased, Ω_{m0} must decrease and $\Omega_{\Phi0}$ must also decrease. Thus, as evident from Fig. 3.1, for a given $H_0 t_0$ value there is a point in (Ω_{m0}, α) space at which contours corresponding to different space curvatures cross. The intersection point moves to larger α as Ω_{m0} is decreased. This is because the Universe is older (at fixed H_0) at smaller Ω_{m0} so even DE with larger α now has more time to come to dominate the energy budget (and so behave more like DE with a constant DE density).

3.3.2 The distance modulus difference $\Delta m(z)$

We next consider the difference in bolometric distance moduli, at redshift $z = 1.5$, of the Φ CDM model and the Einstein–de Sitter model. The coordinate distance r is

$$r = \frac{1}{\sqrt{-\Omega_{k0}}} \sin \left(\sqrt{-\Omega_{k0}} \int_{t_{\text{em}}}^{t_0} \frac{dt}{a(t)} \right). \quad (3.19)$$

Here t_{em} and t_0 are the times when the signal was emitted and received. Thus the difference in the distance moduli of the two models is

$$\Delta m(z) = 5 \log_{10} \left(\frac{r}{r_{\text{EdS}}} \right) \quad (3.20)$$

where r_{EdS} is the coordinate distance in the Einstein–de Sitter model.

Figure 3.2 shows contours of constant $\Delta m(z = 1.5)$ as a function of Ω_{m0} and α for some values of Ω_{k0} . Comparing Figs. 3.1 and 3.2, we see that near $\alpha = 0$, where the DE behaves

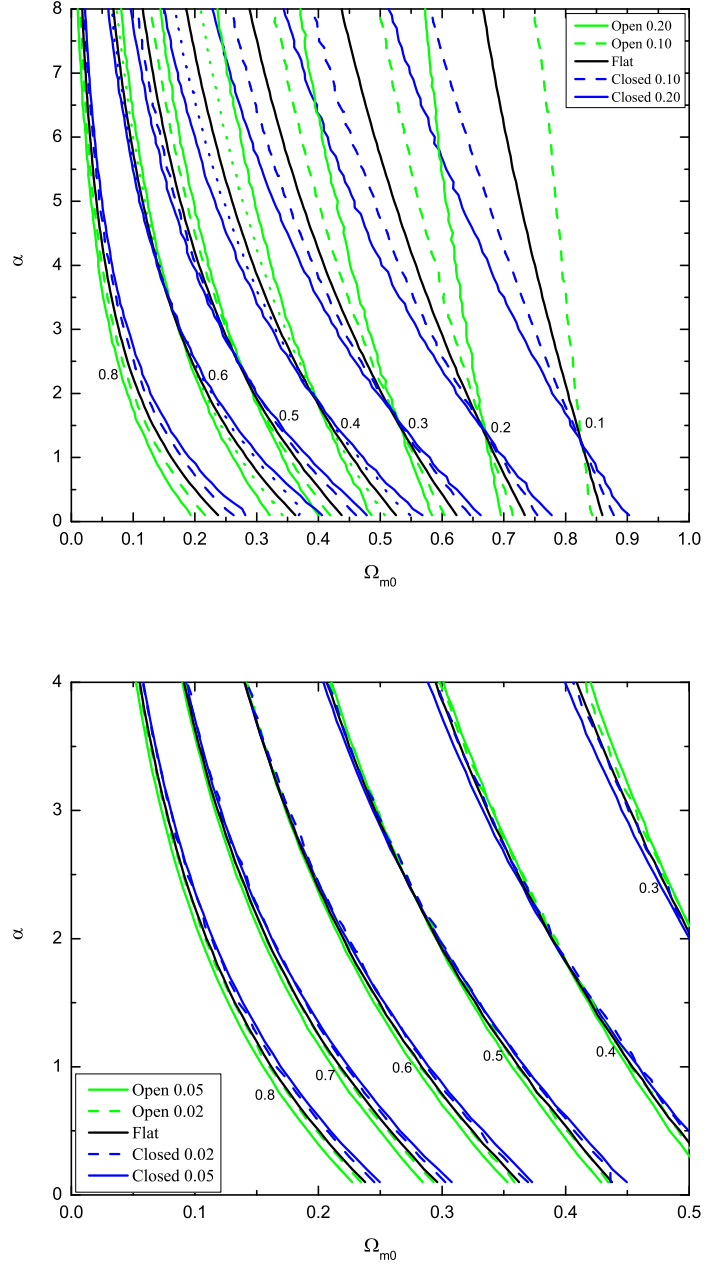


Figure 3.2: Contours of fixed bolometric distance modulus relative to the Einstein–de Sitter model, $\Delta m(z = 1.5)$, as a function of the matter density parameter Ω_{m0} and scalar field potential power-law index α , and various values of the space curvature density parameter Ω_{k0} (as listed in the inset legend boxes). The upper panel shows a larger part of (Ω_{m0}, α) space for a larger range of Ω_{k0} values [for $\Delta m(z = 1.5) = 0.1, 0.2, 0.3, 0.4, 0.5, 0.6$, and 0.8 from right to left], while the lower panel focuses on a smaller range of the three parameters [for $\Delta m(z = 1.5)$ from 0.3 to 0.8 in steps of 0.1 , from right to left]. In the upper panel there is no $\Omega_{k0} = 0.2$ contour for $\Delta m(z = 1.5) = 0.1$ since in this case the model is too open for such a small distance modulus difference. 58

like constant Λ , $\Delta m(z = 1.5)$ is less sensitive to the value of Ω_{k0} than is $H_0 t_0$. However at larger α $\Delta m(z = 1.5)$ is more sensitive to spatial curvature than is $H_0 t_0$. Clearly, extending the Φ CDM model to include space curvature as a free parameter broadens the range of allowed parameter values. As in the $H_0 t_0$ case, for a given value of $\Delta m(z = 1.5)$ there is a point in (Ω_{m0}, α) space at which all contours intersect.

3.3.3 Number counts

The count per unit increment of redshift for conserved objects is³

$$\frac{dN}{dz} \propto z^2 A(z), \quad A(z) = \frac{H_0^3 a_0^2 r^2 a}{z^2 \dot{a}}. \quad (3.21)$$

Isocontours of fixed $A(z = 0.7)$ are shown in Fig. 3.3. The general features are similar to those shown in Figs. 3.1 and 3.2 for $H_0 t_0$ and $\Delta m(z = 1.5)$.

3.3.4 The growth of structure

Finally, we consider the growth of large-scale structure of the Universe which started as small primordial density inhomogeneities in the early Universe, see [78, 121], and references therein. Within the framework of linear perturbation theory the scalar field stays homogeneous as we show in the Appendix B on the scales of matter perturbations and the density contrast in ordinary matter, $\delta = \delta\rho/\rho$, satisfies

$$\ddot{\delta} + 2\frac{\dot{a}}{a}\dot{\delta} - \frac{4\pi}{m_p}\rho\delta = 0. \quad (3.22)$$

Following Ref. [7] the cosmological test parameter we consider is

$$\Delta(\Omega_{m0}, \Omega_{k0}, \alpha) = \frac{\delta(t_0)}{(1 + z_i)\delta(t_i)} \quad (3.23)$$

³See Sec. IV.B.5 of Ref. [41] and Refs. [118–120] for discussions of this test.

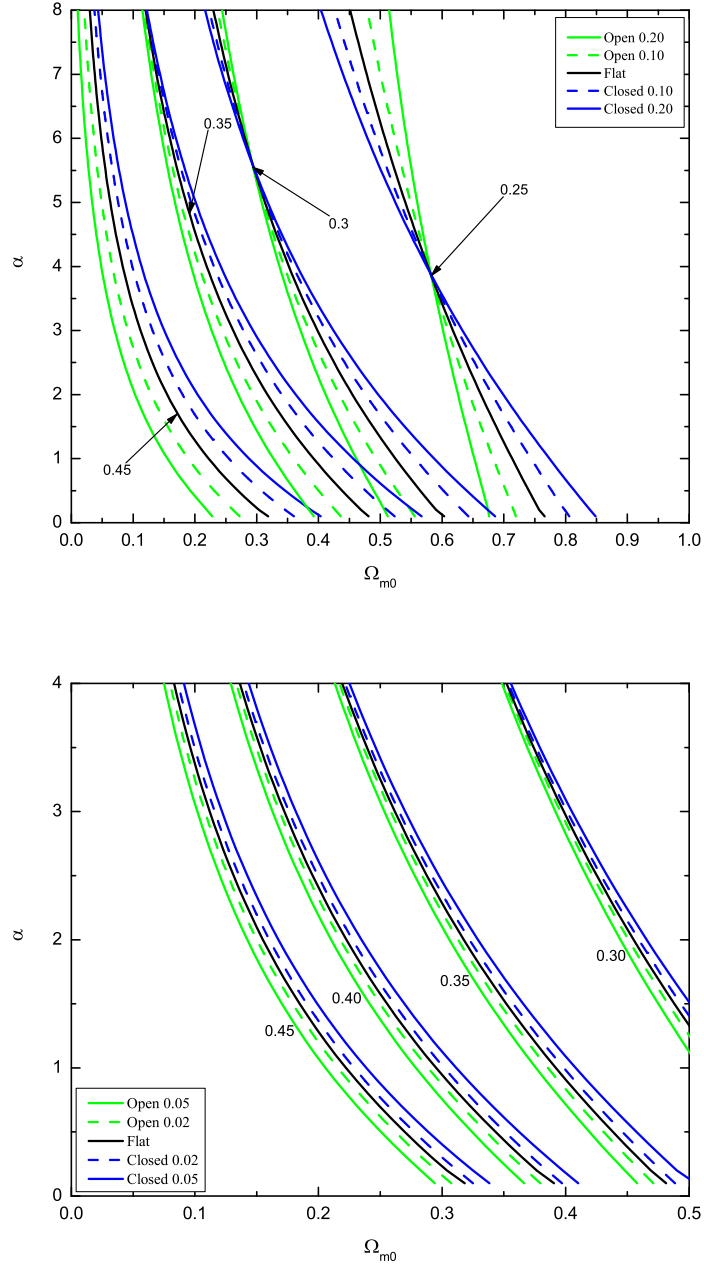


Figure 3.3: Contours of fixed $A(z = 0.7)$ as a function of Ω_{m0} and α at various values of Ω_{k0} (as listed in the inset legend boxes). The upper panel shows a larger part of the parameter space for $A(z = 0.7) = 0.25, 0.3, 0.35$ and 0.45 from right to left. The lower panel shows a smaller range of the three parameters for $A(z = 0.7) = 0.3, 0.35, 0.4$ and 0.45 from right to left.

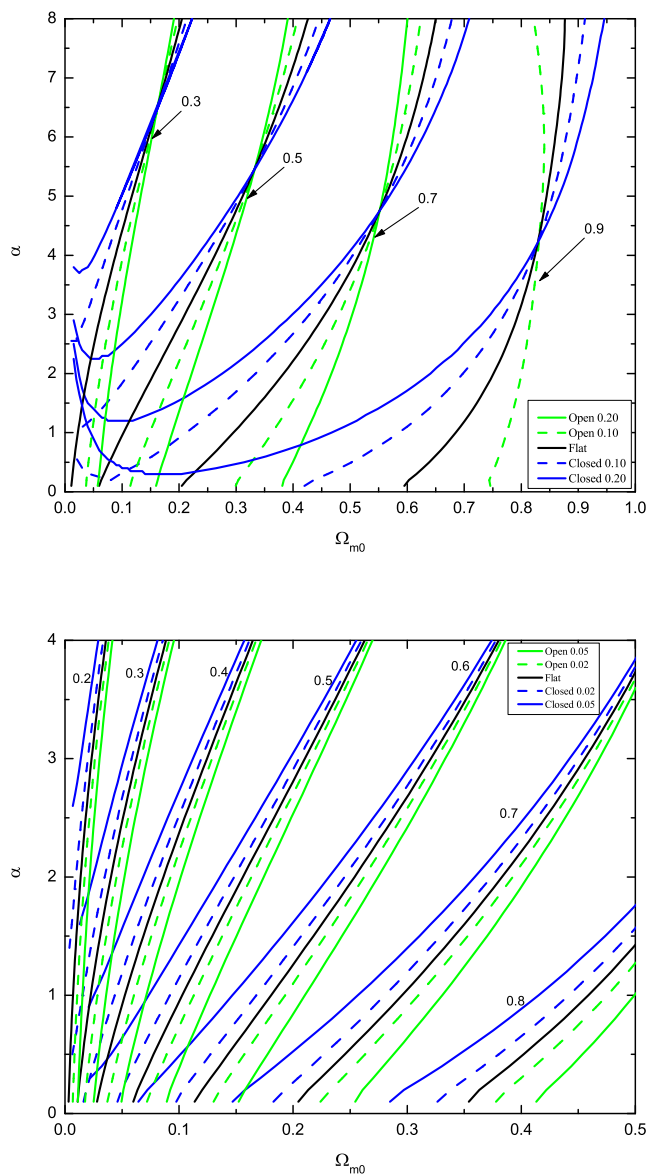


Figure 3.4: Contours of the factor by which the growth of ordinary matter perturbations falls below that of the Einstein–de Sitter model, $\Delta(\Omega_{m0}, \Omega_{k0}, \alpha)$, as a function of the matter density parameter Ω_{m0} and scalar field potential power-law index α , and various values of the space curvature density parameter Ω_{k0} (as listed in the inset legend boxes). The upper panel shows a larger part of (Ω_{m0}, α) space for a larger range of Ω_{k0} values [for $\Delta(\Omega_{m0}, \Omega_{k0}, \alpha) = 0.3, 0.5, 0.7$ and 0.9 from left to right], while the right panel focuses on a smaller range of the three parameters [for $\Delta(\Omega_{m0}, \Omega_{k0}, \alpha)$ from 0.2 to 0.8 in steps of 0.1 , from left to right]. In the lower panel there is no $\Omega_{k0} = 0.2$ contour for $\Delta = 0.9$ since in this case the model is too open to allow such a large growth factor.

where t_0 denotes the current epoch while t_i is the time when the scale factor $a_i \ll a_0$, well within the matter-dominated epoch when the Einstein–de Sitter model was a good approximation. Thus the factor Δ is the ratio by which the growth of linear fluctuations in density have declined below that of the Einstein–de Sitter model prediction. We graph contours of Δ in Fig. 3.4.

There are two interesting facts about the Δ contours shown in Fig. 3.4. First, the growth rate is quite sensitive to the value of Ω_{k0} , much more so than any of the other parameters we have considered. (This is not unexpected, as it is well known in more conventional models that the growth factor is much more sensitive to Ω_{m0} when Ω_{k0} is nonzero.) Second, the curvature dependence of the isocontours is the opposite of that for the other three parameters. So a joint analysis of growth factor and geometry measurements would seem to be a very good way to constrain Ω_{k0} .

Chapter 4

Cosmological constraints from large-scale structure growth rate measurements

4.1 Introduction

The following chapter is based on [122]. We assume that GR provides an adequate model for cosmological gravity and we test various models of dark energy (DE) as a possible explanation of the observed accelerated cosmological expansion. In particular, we consider three models of DE. The first one is the standard Λ CDM cosmology in which the energy density of DE does not evolve in time and its equation of state (EoS) is $p_\Lambda = -\rho_\Lambda$, where p_Λ is the pressure and ρ_Λ the energy density of DE. Space sections are not assumed to be flat in this case and the cosmological parameters that characterize the model are $\mathbf{p} = (\Omega_{m0}, \Omega_\Lambda)$ where Ω_{m0} is the current value of the nonrelativistic CDM and baryonic matter density parameter and Ω_Λ is that of Λ . The second model we consider is the simplest modification of Λ CDM cosmology in which the energy density of DE is time dependent and its EoS is parametrized as $p_X = w_X \rho_X$, where w_X is constant and $< -1/3$. The upper limit of $-1/3$ is a consequence

of the requirement that DE provide positive acceleration. This spatially-flat XCDM model is the simplest parametrization of dynamical DE, with parameters $\mathbf{p} = (\Omega_{m0}, w_X)$. However, it is incomplete as it cannot describe density inhomogeneities [see, e.g., 44]. The last model we study is the consistent quintessence model of DE in which DE is a scalar field. In particular we consider the much studied spatially-flat ϕ CDM model [7, 45] whose equations of motion in units where $\hbar = c = 1$ are

$$\begin{aligned} \ddot{\phi} + 3\frac{\dot{a}}{a}\dot{\phi} - \frac{\kappa\alpha}{2}m_p^2\phi^{-(\alpha+1)} &= 0, \\ \left(\frac{\dot{a}}{a}\right)^2 &= \frac{8\pi}{3m_p^2}(\rho_m + \rho_\phi), \\ \rho_\phi &= \frac{m_p^2}{32\pi}\left(\dot{\phi}^2 + \kappa m_p^2\phi^{-\alpha}\right). \end{aligned} \tag{4.1}$$

Here an over-dot denotes a derivative with respect to time, a is the scale factor, ρ_m is the energy density of nonrelativistic (cold dark and baryonic) matter, ρ_ϕ is that of the dark energy scalar field ϕ , $m_p = G^{-1/2}$ is the Planck mass where G is the gravitational constant, and $\alpha > 0$ is a free parameter of the potential energy density of ϕ and determines κ which is [see 7, 45]

$$\kappa = \frac{8}{3} \left(\frac{\alpha + 4}{\alpha + 2} \right) \left[\frac{2}{3} \alpha (\alpha + 2) \right]^{\alpha/2}. \tag{4.2}$$

In the limit $\alpha \mapsto 0$ the ϕ CDM model reproduces the spatially-flat Λ CDM cosmology while in the limit $\alpha \mapsto \infty$ it reduces to the Einstein–De Sitter model with no DE but only CDM and baryonic matter. The value of α determines the rapidity of the time-evolution of the DE density, with a larger α corresponding to more rapidly decreasing DE density. The cosmological parameters of the ϕ CDM model are $\mathbf{p} = (\Omega_{m0}, \alpha)$.

Many different data sets have been used to derive constraints on the parameters of the three models we consider here.¹ In this paper we use growth-factor measurements to

¹See, e.g., [123], [49], [115], [124], [125], [126], [127], and [128]; also see [129]. For constraints on these

constrain cosmological parameters,² under the assumption that GR is the correct model of gravity. Growth factor data have previously been used to test GR. Here we find that if we assume GR then growth-factor measurements provide tight constraints on cosmological parameters.

This chapter is organized as follows. In the next section we discuss the data and the analysis techniques that we use to derive cosmological parameter constraints. In Sec. 4.3, we present and discuss our results. Chapter 5 contains our conclusions.

4.2 Data and analysis

We use three different types of data to constrain cosmological parameters: the growth rate of large-scale structure (LSS) measurements; supernova type Ia (SNIa) distance-modulus measurements as a function of redshift; and Hubble parameter measurements.

4.2.1 Growth rate of LSS

In linear perturbation theory the nonrelativistic (cold dark and baryonic) matter density perturbation $\delta_m = \delta\rho_m/\rho_m$ obeys

$$\ddot{\delta}_m + 2\frac{\dot{a}}{a}\dot{\delta}_m - \frac{4\pi}{m_p}\rho_m\delta_m = 0, \quad (4.3)$$

where the scale factor a , with current value a_0 , is related to redshift z through $1+z = a_0/a$.

The analytic growing solution of (4.3) is

$$\delta_m(t) \propto D(z) = \frac{5\Omega_{m0}E(z)}{2} \int_z^\infty \frac{1+z'}{E^3(z')} dz', \quad (4.4)$$

and related models from near-future data see [77], [130], [131], and references therein.

²For related work with growth factor data, see [132].

z	$A(z)$	σ	Reference
0.067	0.4230	0.0550	1
0.150	0.3900	0.0800	2
0.170	0.5100	0.0600	3
0.220	0.4200	0.0700	4
0.250	0.3512	0.0583	5
0.350	0.4400	0.0500	3
0.370	0.4602	0.0378	5
0.410	0.4500	0.0400	4
0.550	0.5000	0.0700	6
0.570	0.4150	0.0340	7
0.600	0.4300	0.0400	4
0.770	0.4900	0.1800	8
0.780	0.3800	0.0400	4
0.800	0.4700	0.0800	9

Table 4.1: Growth parameter measurements and 1σ uncertainties. Reference number shown in the last column: 1. [133], 2. [134], 3. [135], 4. [64], 5. [65], 6. [136], 7. [66], 8. [63], 9. [137].

where $E(z) = H(z)/H_0$ and $H(z)$ is the Hubble parameter whose current value is the Hubble constant H_0 . $D(z)$ is normalized such that $D(z = 0) = 1$. Note, that the analytic solution (4.4) is valid only for, in general spatially non-flat, Λ CDM cosmology. In cosmological models where dark energy density is allowed to evolve in time, Eq. (4.3) has to be solved numerically, which we do, in order to compute growth factor $D(z)$ for XCDM and ϕ CDM cosmological models.

The observable we use in our analysis is constructed from the linear theory, redshift-dependent rms mass fluctuations in $8h^{-1}$ Mpc spheres (where h is H_0 in units of $100 \text{ km s}^{-1} \text{ Mpc}^{-1}$), $\sigma_8(z) = \sigma_8^0 D(z)$, where σ_8^0 is the current value of $\sigma_8(z)$. We shall also need $f(z)$, the logarithmic derivative of the matter density perturbation $D(z)$ with respect to the scale factor a , $f(z) = d \ln D / d \ln a$. Using (4.4) we find an analytic expression for $f(z)$ that we use to compute growth factor in the Λ CDM cosmological model

$$f(z) = \frac{\ddot{a}a}{\dot{a}^2} - 1 + \frac{5\Omega_{m0}}{2} \frac{(1+z)^2}{E^2(z)D(z)}. \quad (4.5)$$

For Λ CDM and ϕ CDM cosmological models we compute $f(z)$ numerically. The observable we use is the growth parameter $A_{\text{obs}}(z) = f(z)\sigma_8(z)$ that also accounts for the Alcock-Paczynski effect in redshift-space distortions. The model prediction at redshift z is $A_{\text{th}}(z, \sigma_8^0, \mathbf{p}) = f(z, \mathbf{p})\sigma_8(z, \sigma_8^0, \mathbf{p})$ where \mathbf{p} is the vector of cosmological parameters.

We use a χ^2 analysis to derive constraints on cosmological parameters from growth factor data. χ^2 depends on the cosmological parameters \mathbf{p} and σ_8^0 ,

$$\chi_G^2(\sigma_8^0, \mathbf{p}) = \sum_{i=1}^N \frac{[A_{\text{th}}(z_i, \sigma_8^0, \mathbf{p}) - A_{\text{obs}}(z_i)]^2}{\sigma_i^2}. \quad (4.6)$$

Here N is the number of data points and σ_i is the 1σ uncertainty on measurement $A_{\text{obs}}(z_i)$ at redshift z_i , see Table 4.1.³ For our purposes, σ_8^0 is a nuisance parameter that we marginalize over. To do so we assume a Gaussian prior for σ_8^0 determined from cluster observations by [138], for spatially-flat Λ CDM, with mean $\overline{\sigma_8^0(\Omega_{m0})} = 0.813(\Omega_{m0}/0.25)^{-0.47}$ and 1σ uncertainty $\sigma_{\overline{\sigma_8^0}(\Omega_{m0})} = (\sigma_{\sigma_8^0}^2 + b^2)^{1/2}(\Omega_{m0}/0.25)^{-0.47}$, where the statistical uncertainty $\sigma_{\sigma_8^0} = 0.012$ and the systematic uncertainty $b = 0.02$ are added in quadrature. [138] note that this relation is also adequate in the non-flat Λ CDM model and for alternative background cosmologies.⁴ Then the posterior probability density function that depends only on the cosmological parameters \mathbf{p} is given by

$$\mathcal{L}_G(\mathbf{p}) = \frac{1}{\sigma_{\overline{\sigma_8^0}(\Omega_{m0})}\sqrt{2\pi}} \int_0^\infty \exp \left\{ -\frac{\chi_G^2(\sigma_8^0, \mathbf{p})}{2} - \frac{[\sigma_8^0 - \overline{\sigma_8^0(\Omega_{m0})}]^2}{2\sigma_{\overline{\sigma_8^0}(\Omega_{m0})}^2} \right\} d\sigma_8^0. \quad (4.7)$$

Finally, we compute the marginalized $\chi_G^2(\mathbf{p}) = -2 \ln(\mathcal{L}_G(\mathbf{p}))$, and minimize this with respect to parameters \mathbf{p} to find the best-fit parameter values \mathbf{p}_0 . We also compute 1σ , 2σ , and 3σ

³For the redshift $z = 0.57$ bin we use the value for model 2 from Table 1 of [66] and an average of the upper and lower 1σ uncertainties given for that model.

⁴In this preliminary analysis we use this approximate, empirical expression for illustrative purposes. However, σ_8^0 does (weakly) depend on the full set of cosmological parameters \mathbf{p} in its own way for every cosmological model, so our analyses are approximate. Given that our results, described below, are encouraging, a more careful analysis that accounts for this effect is warranted and will be discussed elsewhere.

cosmological parameter confidence contours bounded by $\chi_G^2(\mathbf{p}) = \chi_G^2(\mathbf{p}_0) + 2.3$, $\chi_G^2(\mathbf{p}) = \chi_G^2(\mathbf{p}_0) + 6.17$, and $\chi_G^2(\mathbf{p}) = \chi_G^2(\mathbf{p}_0) + 11.8$, respectively.

4.2.2 SNIa distance modulus

The largest set of data we use are the 580 Type Ia supernova distance modulus $\mu_{\text{obs}}(z)$ measurements from the [12] Union 2.1 compilation (covering the redshift range of $0.015 \leq z \leq 1.414$). The predicted distance-modulus is

$$\mu_{\text{th}}(z) = 5 \log_{10}[3000y(z)(1+z)] + 25 - 5 \log_{10}(h), \quad (4.8)$$

where $y(z)$ is the dimensionless coordinate distance

$$y(z) = \frac{1}{\sqrt{-\Omega_k}} \sin \left(\sqrt{-\Omega_k} \int_0^z \frac{dz'}{E(z')} \right), \quad (4.9)$$

and Ω_k is the spatial curvature density parameter. Since the SNIa distance modulus measurements μ_{obs} are correlated we use χ^2 defined through the inverse covariance matrix $\chi_{SN}^2(h, \mathbf{p}) = \Delta \boldsymbol{\mu}^T C^{-1} \Delta \boldsymbol{\mu}$. Here the vector of differences $\Delta \mu_i = \mu_{\text{th}}(z_i, H_0, \mathbf{p}) - \mu_{\text{obs}}(z_i)$, and C^{-1} is the inverse of the 580 by 580 Union 2.1 compilation covariance matrix.

4.2.3 Hubble parameter

We use 20 Hubble parameter measurements $H_{\text{obs}}(z)$ and 1σ uncertainties covering redshift range $0.09 \leq z \leq 2.3$ [113, 139–141], as listed in Table 1 of [114]. We only include independent measurements of the Hubble parameter, i.e., we exclude $H_{\text{obs}}(z)$ points that are possibly correlated with growth factor measurements in Table 4.1 above.

Theoretical expressions for the Hubble parameter follow directly from the Friedmann

equation in each model. In the case of the Λ CDM model,

$$H_{\text{th}}^2(z, \mathbf{p}) = H_0^2 \left[\Omega_{m0}(1+z)^3 + (1 - \Omega_{m0} - \Omega_\Lambda)(1+z)^2 + \Omega_\Lambda \right], \quad (4.10)$$

while for the spatially-flat XCDM parameterization,

$$H_{\text{th}}^2(z, \mathbf{p}) = H_0^2 \left[\Omega_{m0}(1+z)^3 + (1 - \Omega_{m0})(1+z)^{3(1+w_X)} \right], \quad (4.11)$$

and for the spatially-flat ϕ CDM model,

$$H_{\text{th}}^2(z, \mathbf{p}) = H_0^2 \Omega_{m0}(1+z)^3 + \frac{1}{12} \left(\dot{\phi}^2 + \kappa m_p^2 \phi^{-\alpha} \right). \quad (4.12)$$

We use the same technique to constrain cosmological parameters from $H(z)$ measurements as we used in Sec. 4.2.1 for the growth factor data analysis. First, we define $\chi_H^2(H_0, \mathbf{p})$ in accordance with Eq. (4.6) where instead of the growth factor $A(z)$ we insert the Hubble parameter $H(z)$.

4.2.4 Computation of joint $\chi^2(\mathbf{p})$

We perform two joint analyses, one for the combination of SNIa and $H(z)$ data, the other for all three data sets. For the SNIa+ $H(z)$ analysis we multiply likelihood functions from the SNIa data and the $H(z)$ data and then marginalize this over the nuisance parameter H_0 with a Gaussian prior with mean value $\overline{H_0} = 68.0 \text{ km s}^{-1} \text{ Mpc}^{-1}$ and 1σ uncertainty $\sigma_{H_0} = 2.8 \text{ km s}^{-1} \text{ Mpc}^{-1}$ ([117], also see [142], [143], [144]) to finally determine the joint $\chi_{\text{SNIa}+H}^2(\mathbf{p})$ function, which depends only on cosmological parameters \mathbf{p} . This is then used to find the best-fit values of \mathbf{p}_0 and corresponding cosmological parameter constraints. The second joint analysis, of the SNIa+ $H(z)$ data with the growth factor data, is based on adding their χ^2 -functions, $\chi_{\text{Jnt}}^2(\mathbf{p}) = \chi_{\text{SNIa}+H}^2(\mathbf{p}) + \chi_G^2(\mathbf{p})$.

4.3 Results and discussion

We derived cosmological parameter constraints from combination of SNIa+ $H(z)$ data sets as well as from a joint analysis of all three data sets.⁵ Our results, presented in the form of isocontours in cosmological parameter space, are shown in Figs. 4.1, 4.2, and 4.3 for the Λ CDM, XCDM and ϕ CDM models, respectively.

In the Λ CDM model the growth factor data favor higher best-fit value of a negative spatial curvature parameter $\Omega_{k0} = 1 - \Omega_{m0} - \Omega_{\Lambda}$ (which corresponds to a closed, spherical spatial geometry) along with a higher best-fit value of Ω_{m0} compared to what other cosmological tests favor, such as SNIa, Hubble parameter measurements, BAO and CMB (see for example [123]-[129] and references therein). In the case of the XCDM parameterization the growth factor data favor a steeper time dependence of dark energy density and also a higher value of ordinary matter energy density parameter (i.e. equation of state parameter w_X has a lower best-fit value and Ω_{m0} has a higher best-fit value) in comparison with constraints derived from the above-mentioned data sets. However, for the ϕ CDM model one observes consistent results for the best-fit values of cosmological parameters (Ω_{m0} , α) with those previously obtained using the data sets mentioned above.

Also, our results for the Λ CDM model differ from constraints obtained for this model from other analyses of growth factor data (see [133], [66]). We suspect that the reason for this and the reason that the constraining power of growth rate data has not previously been recognized is because these data have almost always been used to constrain cosmological parameters in the context of modified gravity models. These modified gravity models have more free parameters than the models we have considered here, because we have assumed that general relativity provides an adequate description of gravitation on cosmological scales.

The other striking feature of the growth rate data constraints is that for all three models they align well with those of the SNIa+ $H(z)$ joint constraints.

⁵We have not used all the $H(z)$ measurements in this paper, excluding points from Table 1 of [114] that are possibly correlated with some of the growth rate data we use in this paper.

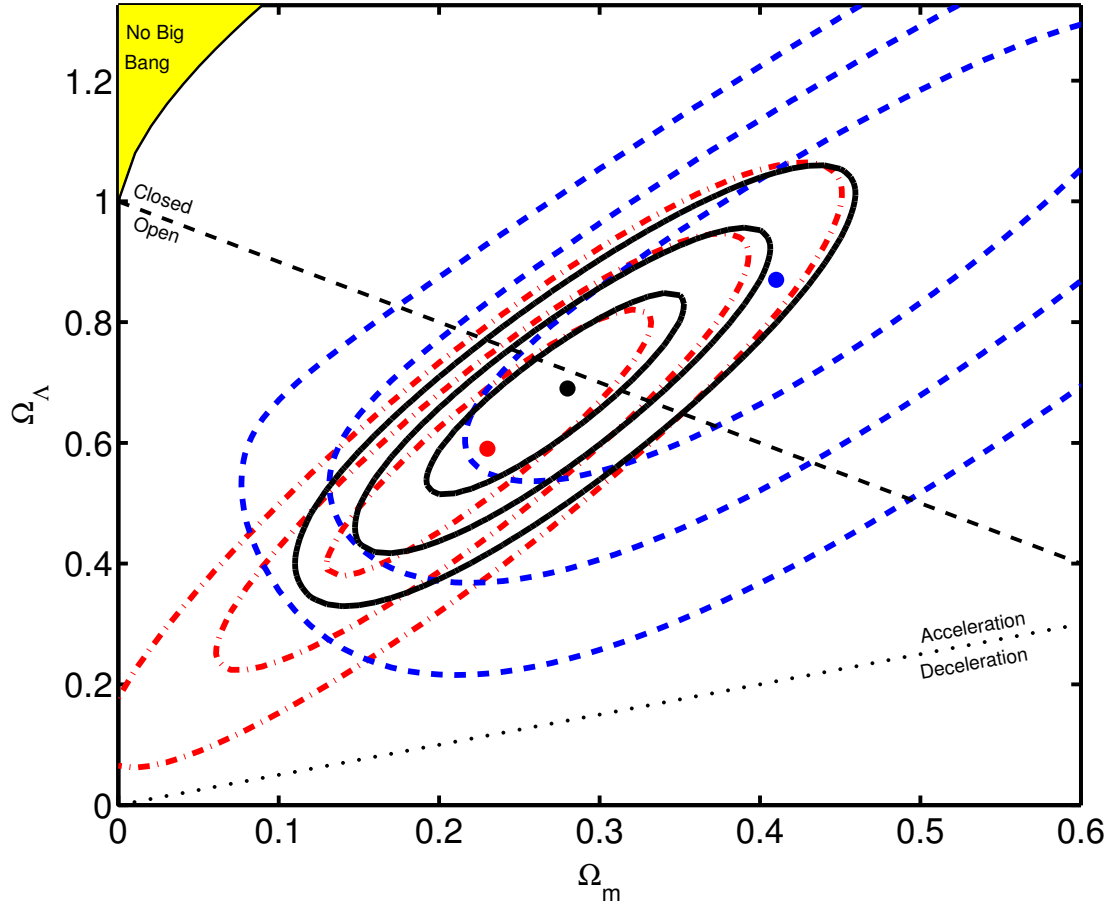


Figure 4.1: 1 , 2 , and 3σ constraint contours for the Λ CDM model from: growth factor measurements [blue dashed lines with blue filled circle at best-fit $(\Omega_m, \Omega_\Lambda) = (0.41, 0.87)$ with $\chi^2_{\min}/\text{dof} = 7.65/12$]; SNIa+ $H(z)$ apparent magnitude data [red dot-dashed lines with red filled circle at best-fit $(\Omega_m, \Omega_\Lambda) = (0.23, 0.59)$ with $\chi^2_{\min}/\text{dof} = 562/598$]; and a combination of all data sets [black solid lines and black filled circle at best-fit $(\Omega_m, \Omega_\Lambda) = (0.28, 0.69)$ with $\chi^2_{\min}/\text{dof} = 571/612$]. The dashed straight line corresponds to spatially-flat models, the dotted line demarcates zero acceleration models, and the area in the upper left-hand corner is the region for which there is no big bang.

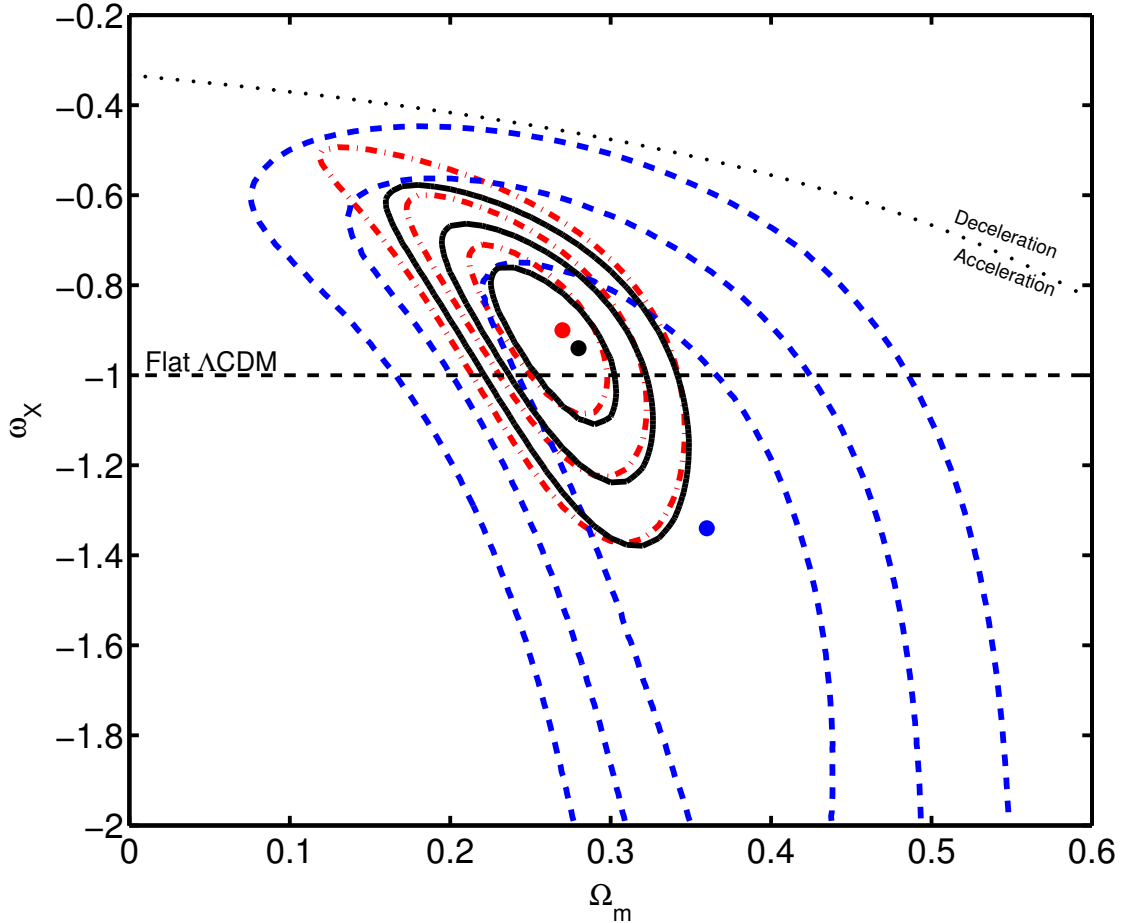


Figure 4.2: 1 , 2 , and 3σ constraint contours for the Λ CDM model from: growth factor measurements [blue dashed lines with blue filled circle at best-fit $(\Omega_m, w_X) = (0.36, -1.34)$ with $\chi_{\min}^2/\text{dof} = 7.70/12$]; SNIa+ $H(z)$ apparent magnitude data [red dot-dashed lines with red filled circle at best-fit $(\Omega_m, w_X) = (0.27, -0.90)$ with $\chi_{\min}^2/\text{dof} = 562/598$]; and a combination of all data sets [black solid lines and black filled circle at best-fit $(\Omega_m, w_X) = (0.28, -0.94)$ with $\chi_{\min}^2/\text{dof} = 571/612$]. The dashed straight line corresponds to spatially-flat Λ CDM models and the dotted curved line demarcates zero acceleration models.

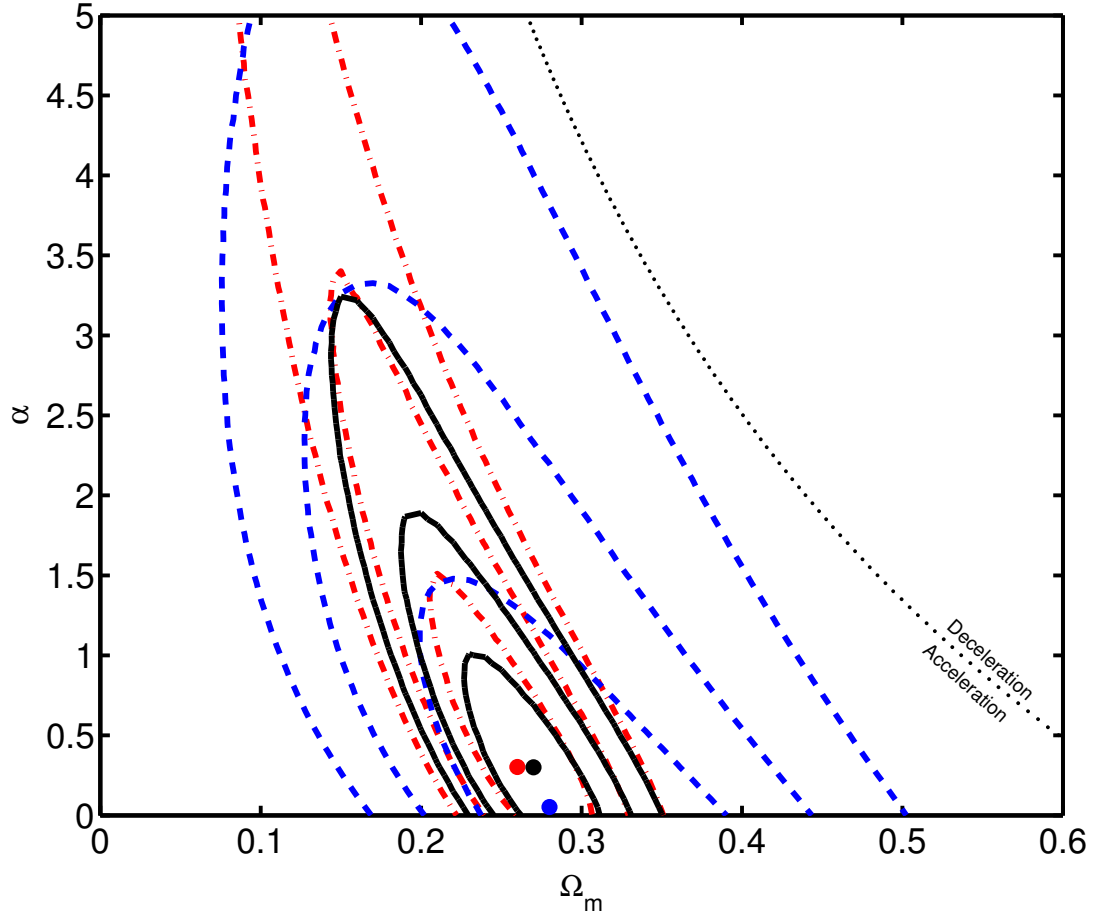


Figure 4.3: 1, 2, and 3 σ constraint contours for the ϕ CDM model from: growth factor measurements [blue dashed lines with blue filled circle at best-fit $(\Omega_m, \alpha) = (0.28, 0.052)$ with $\chi_{\min}^2/\text{dof} = 8.62/12$]; SNIa+ $H(z)$ apparent magnitude data [red dot-dashed lines with red filled circle at best-fit $(\Omega_m, \alpha) = (0.26, 0.302)$ with $\chi_{\min}^2/\text{dof} = 562/598$]; and a combination of all data sets [black solid lines and black filled circle at best-fit $(\Omega_m, \alpha) = (0.27, 0.300)$ with $\chi_{\min}^2/\text{dof} = 570/612$]. The dotted curved line demarcates zero acceleration models and the horizontal $\alpha = 0$ axis corresponds to spatially-flat Λ CDM models.

Chapter 5

Conclusion

Chapter 2 presents a forecast of the precision at which planned near-future space-based spectroscopic galaxy surveys should be able to constrain the time dependence of dark energy density. For the first time, was used a consistent physical model of time-evolving dark energy, ϕ CDM, in which a minimally-coupled scalar field slowly rolls down its self-interaction potential energy density. It has been shown that if general relativity is assumed, the deviation of the parameter α of the ϕ CDM model can be constrained to better than 0.05; this is almost an order of magnitude better than the best currently available result.

The constraints on basic cosmological parameters, such as the relative energy densities of non-relativistic matter and spatial curvature, depend on the adopted dark energy model. However, in the ϕ CDM model the expected constraints are more restrictive than those derived using the XCDM or wCDM parameterizations. This is due to the fact that the ϕ CDM model has fewer parameters. Also, the XCDM and wCDM parameterizations assign equal weight to all possible values of w , while in the ϕ CDM model there is an implicit theoretical prior on which equation of state parameter values are more likely, based on how easy it is to produce such a value within the model.

Since the observational consequences of dark energy and modified gravity are partially degenerate, constraints on modified gravity parameters will depend on the assumptions

made about dark energy. The constraints on γ are most restrictive in the Λ CDM model. For the ϕ CDM model the constraints on γ are about a third tighter than those for the ω CDM and XCDM parameterizations.

These results are very encouraging: data from an experiment of the type we have modeled will be able to provide very good, and probably revolutionary, constraints on the time evolution of dark energy.

In Chapter 3 the original ϕ CDM model was extended to nonflat geometries and it was shown that in the curvature-dominated epoch the solution is also an attractor or time-dependent fixed point (see Sec. 3.2.1 and the Appendix B). Predictions of the model for an illustrative set of cosmological tests were computed and shown that the presence of space curvature will broaden the allowed range of model parameters. Spatial curvature should be considered as a free parameter when observational data are analyzed. The nonflat ϕ CDM model we have developed here is the only consistent nonflat time-variable DE model to date and can be used as a fiducial model for such analyses.

The computations have shown that for a single cosmological test there is a degeneracy point in parameter space for each fixed value of the cosmological observable of the test. At this point one cannot differentiate between contours corresponding to different values of spatial curvature. However, these points of degeneracy do not coincide in (Ω_{m0}, α) parameter space for the different cosmological tests. Hence it is important to use multiple cosmological tests in order to determine spatial curvature from observations.

A joint analysis of geometry and growth factor measurements appears to be a fruitful way to constrain space curvature. CMB anisotropy data will also likely provide useful constraints on space curvature. This will first require accounting for spatial curvature effects on the quantum-mechanical zero-point fluctuations generated during inflation, which will affect the primordial density perturbations power spectrum [145–153]. While the curved-space computation is more involved than the corresponding flat-space one, the resulting constraints from CMB anisotropy data on space curvature in the presence of dynamical

dark energy are likely to prove quite interesting.

In Chapter 4 three general-relativistic DE cosmological models were used to analyze the largest collection of growth factor measurements to date. It was shown that growth factor data constraints on cosmological parameters are quite restrictive, roughly close to those from joint SNIa+ $H(z)$ and baryon acoustic oscillations (BAO) peak length-scale measurements, and less restrictive than those from cosmic microwave background (CMB) anisotropy observations.

These growth factor results must be viewed as tentative, given that this is an area of research that is still under active development. It is important to continue to study possible sources of systematic uncertainty – and given the differences we have found between growth rate data constraints and these from SNIa and $H(z)$ measurements, it is not unreasonable to suspect that there might be an as yet hidden source of systematic uncertainty.

It is, however, clear that growth factor measurements will soon be able to provide cosmological constraints as restrictive and as reliable as those from CMB anisotropy, BAO, $H(z)$, and SNIa measurements.

Bibliography

- [1] P. A. R. Ade, et al., arXiv:1303.5076 (2013).
- [2] S. Dodelson, *MODERN COSMOLOGY*, ACADEMIC PRESS, 2003.
- [3] S. Capozziello and M. D. Laurentis, arXiv:1307.4523 (2013).
- [4] M. Sami and R. Myrzakulov, arXiv:1309.4188 (2013).
- [5] J. Martin, *Comptes Rendus Physique* **13**, 566 (2012).
- [6] P. J. E. Peebles, *Astrophys. J.* **284**, 439 (1984).
- [7] P. J. E. Peebles and B. Ratra, *Astrophys. J. Lett.* **325**, L17 (1988).
- [8] S. Tsujikawa, *Class. Quant. Grav.* **30**, 214003 (2013).
- [9] J. Solà, *J. Phys. Conf. Ser.* **453**, 012015 (2013).
- [10] R. Jimenez, arXiv:1307.2452 (2013).
- [11] C. P. Burgess, arXiv:1309.4133 (2013).
- [12] N. Suzuki, et al., *Astrophys. J.* **746**, 85 (2012).
- [13] A. Conley, et al., *Astrophys. J. Suppl.* **192**, 1 (2011).
- [14] X.-D. Li, et al., *JCAP* **1107**, 011 (2011).
- [15] A. Barreira and P. P. Avelino, *Phys. Rev.* **D84**, 083521 (2011).
- [16] B. Ratra and M. S. Vogeley, *Publ. Astron. Soc. Pac.* **120**, 235 (2008).

- [17] E. Komatsu, et al., *Astrophys. J. Suppl.* **192**, 18 (2011).
- [18] C. L. Reichardt, et al., *Astrophys. J.* **749**, L9 (2012).
- [19] G. Chen and B. Ratra, *Publ. Astron. Soc. Pac.* **115**, 1143 (2003).
- [20] W. J. Percival, et al., *Mon. Not. Roy. Astron. Soc.* **401**, 2148 (2010).
- [21] M. A. Dantas, et al., *Phys. Lett.* **B699**, 239 (2011).
- [22] A. Carnero, et al., *Mon. Not. Roy. Astron. Soc.* **419**, 1689 (2012).
- [23] L. Anderson, et al., arXiv:1203.6594 (2012).
- [24] K.-H. Chae, et al., *Astrophys. J.* **607**, L71 (2004).
- [25] S. Lee and K.-W. Ng, *Phys. Rev.* **D76**, 043518 (2007).
- [26] M. Biesiada, et al., *Mon. Not. Roy. Astron. Soc.* **406**, 1055 (2010).
- [27] L. Samushia and B. Ratra, *Astrophys. J.* **650**, L5 (2006).
- [28] A. A. Sen and R. J. Scherrer, *Phys. Lett.* **B659**, 457 (2008).
- [29] N. Pan, et al., *Class. Quantum Grav.* **27**, 155015 (2010).
- [30] Y. Chen and B. Ratra, *Phys. Lett.* **B703**, 406 (2011).
- [31] M. Baldi and V. Pettrino, *Mon. Not. Roy. Astron. Soc.* **412**, L1 (2011).
- [32] C. D. Boni, et al., *Mon. Not. Roy. Astron. Soc.* **415**, 2758 (2011).
- [33] N. Brouzakis, et al., *JCAP* **03**, 049 (2011).
- [34] L. Campanelli, et al., arXiv:1110.2310 (2011).
- [35] S. W. Allen, et al., *Mon. Not. Roy. Astron. Soc.* **383**, 879 (2008).

- [36] L. Samushia and B. Ratra, *Astrophys. J.* **680**, L1 (2008).
- [37] M. Tong and H. Noh, *Eur. Phys. J.* **C71**, 1586 (2011).
- [38] A. Blanchard, *A&AR* **18**, 595 (2010).
- [39] D. Sapone, *Int. J. Mod. Phys.* **A25**, 5253 (2010).
- [40] R. Jimenez, *Fortschr. Phys.* **59**, 602 (2011).
- [41] P. J. E. Peebles and B. Ratra, *Rev. Mod. Phys.* **75**, 559 (2003).
- [42] L. Perivolaropoulos, *J. Phys. Conf. Ser.* **222**, 012024 (2010).
- [43] B. Ratra, *Phys. Rev.* **D43**, 3802 (1991).
- [44] S. Podariu and B. Ratra, *Astrophys. J.* **532**, 109 (2000).
- [45] B. Ratra and P. J. E. Peebles, *Phys. Rev.* **D37**, 3406 (1988).
- [46] G. Chen and B. Ratra, *Astrophys. J.* **612**, L1 (2004).
- [47] K. M. Wilson, et al., *Mod. Phys. Lett.* **A21**, 2197 (2006).
- [48] Y. Chen and B. Ratra, *A&A* **543**, A104 (2012).
- [49] D. Mania and B. Ratra, *Phys. Lett.* **B715**, 9 (2012).
- [50] L. Samushia, *CONSTRAINING SCALAR FIELD DARK ENERGY WITH COSMOLOGICAL OBSERVATIONS*, PhD thesis, Kansas State University, 2009.
- [51] R.-J. Yang, et al., *Int. J. Mod. Phys.* **A26**, 317 (2011).
- [52] A. V. Frolov and J.-Q. Guo, arXiv:1101.4995 (2011).
- [53] N. J. Nunes, et al., *Phys. Rev.* **D83**, 083523 (2011).
- [54] J. Grande, et al., *JCAP* **1108**, 007 (2011).

- [55] R. Saitou and S. Nojiri, *Eur. Phys. J.* **C71**, 1712 (2011).
- [56] R. Silva, et al., *A&A* **537**, A11 (2012).
- [57] A. Y. Kamenshchik, et al., *Phys. Lett.* **B702**, 191 (2011).
- [58] M. Maggiore, et al., *Phys. Lett.* **B704**, 102 (2011).
- [59] C. Blake, et al., *Mon. Not. Roy. Astron. Soc.* **418**, 1707 (2011).
- [60] F. Beutler, et al., *Mon. Not. Roy. Astron. Soc.* **416**, 3017 (2011).
- [61] W. J. Percival, et al., *Mon. Not. Roy. Astron. Soc.* **385**, L78 (2004).
- [62] R. E. Angulo, et al., *Mon. Not. Roy. Astron. Soc.* **387**, 921 (2008).
- [63] L. Guzzo, et al., *Nature* **451**, 541 (2008).
- [64] C. Blake, et al., *Mon. Not. Roy. Astron. Soc.* **415**, 2876 (2011).
- [65] L. Samushia, et al., *Mon. Not. Roy. Astron. Soc.* **420**, 2102 (2012).
- [66] B. A. Reid, et al., arXiv:1203.6641 (2012).
- [67] R. Laureijs, et al., arXiv:1110.3193 (2011).
- [68] J. Green, et al., arXiv:1108.1374 (2011).
- [69] Y. Wang, et al., *Mon. Not. Roy. Astron. Soc.* **409**, 737 (2010).
- [70] L. Samushia, et al., *Mon. Not. Roy. Astron. Soc.* **410**, 1993 (2010).
- [71] E. Majerotto, et al., *Mon. Not. Roy. Astron. Soc.* **424**, 1392 (2012).
- [72] T. Basse, et al., arXiv:1205.0548 (2012).
- [73] S. Podariu, et al., *Astrophys. J.* **553**, 39 (2001).

- [74] T. P. Sotiriou and V. Faraoni, *Rev. Mod. Phys.* **82**, 451 (2010).
- [75] S. Tsujikawa, *Lectures on Cosmology Accelerated Expansion of the Universe by Georg Wolschin*, volume 800, Berlin: Springer, 1999.
- [76] S. Capazziello and M. D. Laurentis, *Phys. Rept.* **509**, 167 (2011).
- [77] A. Pavlov, et al., *Astrophys. J.* **760**, 19 (2012).
- [78] W. Fischler, *Nucl. Phys.* **B259**, 730 (1985).
- [79] N. Kaiser, *Mon. Not. Roy. Astron. Soc.* **227**, 1 (1987).
- [80] E. V. Linder, *Phys. Rev.* **D72**, 043529 (2005).
- [81] C. Alcock and B. Paczyński, *Nature* **281**, 358 (1979).
- [82] M. Chevallier and D. Polarski, *Int. J. Mod. Phys.* **D10**, 213 (2001).
- [83] E. V. Linder, *Phys. Rev. Lett.* **90**, 091301 (2003).
- [84] A. Albrecht, et al., arXiv:0901.0721 (2009).
- [85] L. Perotto, et al., *JCAP* **0610**, 013 (2006).
- [86] M. Martinelli, et al., *Phys. Rev.* **D83**, 023012 (2011).
- [87] A. Orsi, et al., *Mon. Not. Roy. Astron. Soc.* **405**, 1006 (2010).
- [88] J. E. Geach, et al., *Mon. Not. Roy. Astron. Soc.* **402**, 1330 (2010).
- [89] H. K. Jassal, et al., *Mon. Not. Roy. Astron. Soc.* **405**, 2639 (2010).
- [90] T. M. Davis, et al., *Astrophys. J.* **666**, 716 (2007).
- [91] D. H. Weinberg, et al., arXiv:1306.0913 (2013).
- [92] G. Hinshaw, et al., *Astrophys. J. Suppl.* **208**, 19 (2013).

- [93] S. Podariu, et al., *Astrophys. J.* **559**, 9 (2001).
- [94] R. Aurich and F. Steiner, *Mon. Not. Roy. Astron. Soc.* **334**, 735 (2002).
- [95] R. Aurich and F. Steiner, *Int. J. Mod. Phys.* **13**, 123 (2004).
- [96] R. Aurich and F. Steiner, *Phys. Rev.* **D67**, 123511 (2003).
- [97] J. L. Crooks, *Astropart. Phys.* **20**, 361 (2003).
- [98] K. Ichikawa and T. Takahashi, *Phys. Rev.* **D73**, 083526 (2006).
- [99] K. Ichikawa and T. Takahashi, *JCAP* **02**, 001 (2007).
- [100] K. Ichikawa and T. Takahashi, *JCAP* **04**, 027 (2008).
- [101] E. L. Wright, et al., *arXiv:astro-ph/0603750* (2006).
- [102] K. Ichikawa, et al., *JCAP* **12**, 005 (2006).
- [103] G.-B. Zhao, et al., *Phys. Lett.* **B648**, 8 (2007).
- [104] Y. Wang and P. Mukherjee, *Phys. Rev.* **D76**, 103533 (2007).
- [105] Y. Gong, et al., *Astrophys. J.* **681**, 27 (2008).
- [106] J.-M. Virey, et al., *JCAP* **12**, 008 (2008).
- [107] Y. Wang and P. Mukherjee, *Phys. Rev.* **D80**, 123504 (2009).
- [108] J. Martin, *Mod. Phys. Lett.* **A23**, 1252 (2008).
- [109] K. Thepsuriya and B. Gumjudpai, *arXiv:0904.2743* (2009).
- [110] Z.-Q. Chen and D.-H. Guo, *Int. J. Theor. Phys.* **51**, 3856 (2012).
- [111] B. Gumjudpai and K. Thepsuriya, *Astrophys. Space Sci.* **342**, 537 (2012).

- [112] A. Pavlov, et al., Phys. Rev. **D88**, 123513 (2013).
- [113] N. G. Busca, et al., Astron. Astrophys. **552**, A96 (2013).
- [114] O. Farooq and B. Ratra, Astrophys. J. Lett. **766**, L7 (2013).
- [115] O. Farooq, et al., Phys. Lett. **B726**, 72 (2013).
- [116] O. Farooq, et al., Astrophys.Space Sci. **357**, 11 (2015).
- [117] G. Chen and B. Ratra, Publ. Astron. Soc. Pac. **123**, 1127 (2011).
- [118] J. A. Newman and M. Davis, Astrophys. J. Lett. **534**, L11 (2000).
- [119] D. Huterer and M. S. Turner, Phys. Rev. **D64**, 123527 (2001).
- [120] S. Podariu and B. Ratra, Astrophys. J. **563**, 28 (2001).
- [121] B. Ratra, Phys. Rev. **D45**, 1913 (1992).
- [122] A. Pavlov, et al., Phys. Rev. **D90**, 023006 (2014).
- [123] L. Samushia, et al., arXiv:0706.1963 (2007).
- [124] A. Piloyan, et al., JCAP **1307**, 042 (2013).
- [125] O. Akarsu, et al., Eur. Phys. J. Plus **129**, 22 (2014).
- [126] M. Li, et al., JCAP **1309**, 021 (2013).
- [127] E. L. D. Perico, et al., Phys. Rev. **D88**, 063531 (2013).
- [128] V. H. Cárdenas, et al., arXiv:1306.0779 (2013).
- [129] S. Crandall and B. Ratra, arXiv:1311.0840 (2013).
- [130] S. A. Appleby and E. V. Linder, Phys. Rev. **D87**, 023532 (2013).

- [131] M. Arabsalmani, et al., Phys. Rev. **D87**, 083001 (2013).
- [132] N. A. Arkhipova, et al., arXiv:1406.0407 (2014).
- [133] F. Beutler, et al., Mon. Not. Roy. Astron. Soc. **423**, 3430 (2012).
- [134] C. Hawkins, et al., Mon. Not. Roy. Astron. Soc. **346**, 78 (2003).
- [135] Y.-S. Song and W. J. Percival, JCAP **0910**, 004 (2009).
- [136] N. P. Ross, et al., Mon. Not. Roy. Astron. Soc. **381**, 573 (2007).
- [137] A. Torre, et al., arXiv:1303.2622 (2013).
- [138] A. Vikhlinin, et al., Astrophys. J. **692**, 1060 (2009).
- [139] L. V. J. Simon and R. Jimenez, Phys. Rev. **D71**, 123001 (2005).
- [140] D. Stern, et al., JCAP **1002**, 008 (2010).
- [141] M. Moresco, et al., JCAP **1208**, 006 (2012).
- [142] J. R. Gott, et al., JCAP **549**, 1 (2001).
- [143] G. Chen, et al., Publ. Astron. Soc. Pac. **115**, 1269 (2003).
- [144] E. Calabrese, et al., Phys. Rev. **D86**, 043520 (2012).
- [145] J. R. Gott, Nature **295**, 304 (1982).
- [146] B. Ratra and P. J. E. Peebles, Astrophys. J. Lett. **432**, L5 (1994).
- [147] B. Ratra and P. J. E. Peebles, Phys. Rev. **D52**, 1837 (1995).
- [148] M. Kamionkowski, et al., Astrophys. J. **434**, L1 (1994).
- [149] M. Bucher, et al., Phys. Rev. **D52**, 3314 (1995).

- [150] D. H. Lyth and A. Woszczyna, Phys. Rev. **D52**, 3338 (1995).
- [151] K. Yamamoto, et al., Astrophys. J. **455**, 412 (1995).
- [152] K. Ganga, et al., Astrophys. J. **484**, 517 (1997).
- [153] M. Górski, et al., Astrophys. J. Suppl. **114**, 1 (1998).
- [154] M. Tegmark, Phys. Rev. Lett. **79**, 3806 (1997).
- [155] D. J. Eisenstein and W. Hu, Astrophys. J. **496**, 605 (1998).
- [156] B. Ratra, Phys. Rev. **D50**, 5252 (1994).

Appendix A

Appendix for Chapter 2

In this Appendix we summarize how to estimate the precision of measurements from the survey parameters.

The Fisher matrix coefficients are given by

$$F_{ij} = \frac{1}{2} \int_{k_{\min}}^{k_{\max}} \left(\frac{\partial \ln P}{\partial p^i} \right) \left(\frac{\partial \ln P}{\partial p^j} \right) V_{\text{eff}}(k, \mu) \frac{d^3 k}{(2\pi)^3}, \quad (\text{A.1})$$

where the effective volume is

$$V_{\text{eff}} = V_0 \frac{nP(k, \mu)}{1 + nP(k, \mu)}, \quad (\text{A.2})$$

and V_0 is the total survey volume and n is the number density. Also, following [154], we multiply the integrand in Eq. (A.1) by a Gaussian factor $\exp\left(-k^2 \sigma_z \frac{dr(z)}{dz}\right)$, where $r(z)$ is the co-moving distance, in order to account for the errors in distance induced by the errors of redshift measurements, $\sigma_z = 0.001$. We model the theoretical power spectrum using an analytic approximation of [155]. We integrate in k from $k_{\min} = 0$ to k_{\max} , where the k_{\max} values depend on redshift and are chosen in such a way that the small scales that are dominated by non-linear effects are excluded. The range of scales that will be fitted to the future surveys will depend on how well the theoretical templates are able to describe small-scale clustering and is difficult to predict. The k_{\max} values along with the expected

bias and number density of galaxies are listed in Table A.1.

In order to derive the Fisher matrix of a specific cosmological model we have to go from our initial parameter space to the parameter space of the cosmological model whose Fisher matrix we want. The transformation formula for the Fisher matrix is given by [see, e.g., 84, for a review]

$$F'_{lm} = \frac{\partial p_i}{\partial p'_l} \frac{\partial p_j}{\partial p'_m} F_{ij}, \quad (\text{A.3})$$

where the primes denote the “new” Fisher matrix and parameters.

We now list the derivatives of the transformation coefficients of the ϕ CDM model in the limit $\alpha \rightarrow 0$ and $\Omega_k \rightarrow 0$ (which corresponds to the fiducial spatially-flat Λ CDM model). The transformation coefficients relating $f_{\parallel}(z)$ and the parameters $(h, \Omega_m, \Omega_k, \alpha)$ are

$$\frac{\partial f_{\parallel}(z)}{\partial h} = -\frac{1}{h}, \quad (\text{A.4})$$

$$\frac{\partial f_{\parallel}(z)}{\partial \Omega_m} = \frac{1}{2E(z)^2} [1 - (1+z)^3], \quad (\text{A.5})$$

$$\frac{\partial f_{\parallel}(z)}{\partial \Omega_k} = \frac{1}{2E(z)^2} [1 - (1+z)^2], \quad (\text{A.6})$$

$$\frac{\partial f_{\parallel}(z)}{\partial \alpha} = -\frac{(1 - \Omega_m)}{8E(z)^2}. \quad (\text{A.7})$$

For the other transformation coefficients, it is convenient to introduce the integral

$$D(z) = \int_0^z \frac{dz'}{E(z')}. \quad (\text{A.8})$$

Then the transformation coefficients between $f_{\perp}(z)$ and the parameters $(h, \Omega_m, \Omega_k, \alpha)$ are

$$\frac{\partial f_{\perp}(z)}{\partial h} = -\frac{1}{h}, \quad (\text{A.9})$$

$$\frac{\partial f_{\perp}(z)}{\partial \Omega_m} = \frac{1}{2D(z)} \int_0^z \frac{dz'}{E(z')^3} [1 - (1+z')^3], \quad (\text{A.10})$$

$$\frac{\partial f_{\perp}(z)}{\partial \Omega_k} = \frac{D(z)^2}{6} + \frac{1}{2D(z)} \int_0^z \frac{dz'}{E(z')^3} [1 - (1 + z')^2], \quad (\text{A.11})$$

$$\frac{\partial f_{\perp}(z)}{\partial \alpha} = -\frac{(1 - \Omega_m)}{8D(z)} \int_0^z \frac{dz'}{E(z')^3}. \quad (\text{A.12})$$

Finally, the transformation coefficients between the growth factor $f(z)$ and the parameters $(\gamma, h, \Omega_m, \Omega_k, \alpha)$ are

$$\frac{\partial f(z)}{\partial \gamma} = \frac{f(z)}{\gamma} \ln f(z), \quad (\text{A.13})$$

$$\frac{\partial f(z)}{\partial \Omega_m} = \frac{\gamma f(z)}{\Omega_m E(z)^2} \{E(z)^2 - \Omega_m [(1 + z)^3 - 1]\}, \quad (\text{A.14})$$

$$\frac{\partial f(z)}{\partial \Omega_k} = -\frac{\gamma f(z)}{E(z)^2} [(1 + z)^2 - 1], \quad (\text{A.15})$$

$$\frac{\partial f(z)}{\partial \alpha} = -\frac{\gamma f(z)}{4E(z)^2} [1 - \Omega_m]. \quad (\text{A.16})$$

Table A.1: Values of the k_{max} , bias $b(z)$ from [87], and the number densities $n(z)$ taken from [88].

z	k_{max}	$b(z)$	$n(z)$
0.55	0.144	1.0423	3220
0.65	0.153	1.0668	3821
0.75	0.163	1.1084	4364
0.85	0.174	1.1145	4835
0.95	0.185	1.1107	5255
1.05	0.197	1.1652	5631
1.15	0.2	1.2262	5972
1.25	0.2	1.2769	6290
1.35	0.2	1.2960	6054
1.45	0.2	1.3159	4985
1.55	0.2	1.4416	4119
1.65	0.2	1.4915	3343
1.75	0.2	1.4873	2666
1.85	0.2	1.5332	2090
1.95	0.2	1.5705	1613
2.05	0.2	1.6277	1224

Appendix B

Appendix for Chapter 3

In Sec. 3.2.1 we showed that the special time-dependent fixed point solution for the scalar field in the curvature-dominated epoch is stable if we ignore spatial inhomogeneities in the gravitational field. In this Appendix we show that gravitational spatial inhomogeneities do not spoil this property of the solution, thus preserving the inclination of the scalar field DE density to always want to try to dominate over the dominant energy density source [7, 45].

Inhomogeneities in the scalar field will induce inhomogeneities in the metric, and vice versa. We show that, in the curvature-dominated epoch, any slight inhomogeneities will die out. (This generalizes the flat-space results of Sec. IX of Ref. [45].)

We linearize the disturbances in the metric about a curved Friedmann background metric in synchronous gauge. To this end, we write the line element as

$$ds^2 = \tilde{g}_{\mu\nu} dx^\mu dx^\nu = (g_{\mu\nu} + \delta g_{\mu\nu}) dx^\mu dx^\nu. \quad (\text{B.1})$$

We work in time-orthogonal coordinates (t, r, θ, φ) with $g_{\mu\nu}$ given in Eq. (3.5) and the

perturbations

$$\delta g_{\mu\nu} = a(t)^2 \begin{pmatrix} 0 & 0 & 0 & 0 \\ 0 & f(r)h_{rr} & h_{r\theta} & h_{r\varphi} \\ 0 & h_{r\theta} & r^2 h_{\theta\theta} & h_{\theta\varphi} \\ 0 & h_{r\varphi} & h_{\theta\varphi} & r^2 \sin^2(\theta) h_{\varphi\varphi} \end{pmatrix}, \quad (\text{B.2})$$

where $f(r) = 1/(1 - kr^2)$, $|h_{ij}| \ll 1$, and each h_{ij} is a function of t, r, θ , and φ .

The scalar field equation of motion in a space-time with cometric $\tilde{g}^{\mu\nu}$ reads

$$\tilde{\nabla}_\mu (\tilde{g}^{\mu\nu} \partial_\nu \Phi) + V'(\Phi) = 0. \quad (\text{B.3})$$

The perturbed scalar field is written

$$\Phi(x^\mu) = \Phi_0(t) + \phi(x^\mu) \quad (\text{B.4})$$

where ϕ is a small perturbation, $|\phi| \ll |\Phi_0|$, and Φ_0 is a solution to the scalar field equation of motion in the unperturbed homogeneous Friedmann background,

$$\ddot{\Phi}_0 + 3\frac{\dot{a}}{a}\dot{\Phi}_0 - \frac{\kappa\alpha m_p^2}{2}\Phi_0^{-(\alpha+1)} = 0. \quad (\text{B.5})$$

Plugging (B.4) into (B.5) gives, to first order in ϕ ,

$$\ddot{\phi} + \frac{3\dot{a}}{a}\dot{\phi} - \frac{1}{a^2}\nabla^2\phi + V''(\Phi_0)\phi - \frac{1}{2}\dot{h}\dot{\Phi}_0 = 0, \quad (\text{B.6})$$

where $h = h_{rr} + h_{\theta\theta} + h_{\varphi\varphi} = -g^{\mu\nu}\delta g_{\mu\nu}$, and ∇^2 is the Laplacian for the three-dimensional

spacelike hypersurface of constant t in the unperturbed Friedman geometry,

$$\begin{aligned}\nabla^2 &= \frac{1}{r^2} \frac{\partial}{\partial r} \left((r^2 - kr^4) \frac{\partial}{\partial r} \right) + kr \frac{\partial}{\partial r} \\ &+ \frac{1}{r^2 \sin(\theta)} \frac{\partial}{\partial \theta} \left(\sin(\theta) \frac{\partial}{\partial \theta} \right) + \frac{1}{r^2 \sin^2(\theta)} \frac{\partial^2}{\partial \varphi^2}.\end{aligned}\tag{B.7}$$

When $k = 0$, ∇^2 is the usual three-dimensional flat-space Laplacian in spherical coordinates.

The tt component of the stress-energy tensor $Q_{\mu\nu}$ for $\Phi = \Phi_0 + \phi$, to first order in ϕ , is

$$Q_{tt} = \frac{m_p^2}{32\pi} \left[\dot{\Phi}_0^2 + 2V(\Phi_0) \right] + \frac{m_p^2}{16\pi} \left[\dot{\Phi}_0 \dot{\phi} + V'(\Phi_0) \phi \right],\tag{B.8}$$

and the trace $Q = \tilde{g}^{\mu\nu} Q_{\mu\nu}$ is, to first order,

$$Q = \frac{m_p^2}{16\pi} \left[4V(\Phi_0) - \dot{\Phi}_0^2 \right] + \frac{m_p^2}{8\pi} \left[2\phi V'(\Phi_0) - \dot{\Phi}_0 \dot{\phi} \right].\tag{B.9}$$

As for the Ricci tensor $R_{\mu\nu}$, we will also only require the tt component. To first order it is

$$R_{tt} = -\frac{3\ddot{a}}{a} + \left[\frac{\dot{a}}{a} \dot{h} + \frac{1}{2} \ddot{h} \right].\tag{B.10}$$

By the Einstein field equations (3.3) we therefore get the first-order perturbation equation,

$$\ddot{h} + \frac{2\dot{a}}{a} \dot{h} = 2\dot{\Phi}_0 \dot{\phi} - V'(\Phi_0) \phi.\tag{B.11}$$

This corresponds to Eq. (3.14) of Ref. [147].

We now take $a = a_0 t$ for the curvature-dominated epoch, where a_0 is a constant of integration and we consider times $t > 0$. Thus, the system we need to analyze is

$$\ddot{\phi} + \frac{3}{t} \dot{\phi} - \frac{L^2}{a_0^2 t^2} \phi + V''(\Phi_0) \phi = \frac{1}{2} \dot{h} \dot{\Phi}_0,\tag{B.12}$$

$$\ddot{h} + \frac{2}{t}\dot{h} = 2\dot{\Phi}_0\dot{\phi} - V'(\Phi_0)\phi. \quad (\text{B.13})$$

Here we have made a hyperspherical harmonic transformation, the variables ϕ and h are now harmonic mode amplitudes, and L^2 is the eigenvalue of the Laplacian operator (B.8) (see Ref. [147] and Sec. II of Ref. [156]). One has $L^2 \rightarrow -1$ (respectively $L^2 \rightarrow -\infty$) in the limit of long wavelength (short wavelength) modes for the negative curvature case.

The field Φ_0 is the special solution obtained in Sec. 3.2.1, Eq. (3.9). We here write it as

$$\Phi_0 = At^m, \quad (\text{B.14})$$

where

$$m = \frac{2}{\alpha + 2}, \quad (\text{B.15})$$

and A is, by (3.10) with $n = 1$,

$$A = \left(\frac{\kappa\alpha m_p^2(\alpha + 2)}{8\alpha + 24} \right)^{1/(\alpha+2)}. \quad (\text{B.16})$$

Defining

$$B = \frac{\kappa\alpha}{2}m_p^2, \quad (\text{B.17})$$

Eqs. (B.12) and (B.13) can be rewritten as

$$\ddot{\phi} + \frac{3}{t}\dot{\phi} + \frac{J}{t^2}\phi = \frac{mA}{2}\dot{h}t^{m-1}, \quad (\text{B.18})$$

$$\ddot{h} + \frac{2}{t}\dot{h} = 2mA t^{m-1}\dot{\phi} + BA^{-(\alpha+1)}t^{m-2}\phi, \quad (\text{B.19})$$

where $J = (\alpha + 1)(m^2 + 2m) - L^2/a_0^2$. As mentioned previously, $L^2 \rightarrow -1$ in the case that we are presently interested in (long-wavelength perturbations and negative curvature), so the constant J is a positive real number > 3 .

For the curvature-dominated case $\rho_k \propto t^{-2}$ and so

$$C^2 \frac{\rho_\Phi}{\rho_k} = t^{2m}, \quad (\text{B.20})$$

where C is a constant of integration. Thus, Eqs. (B.18) and (B.19) can be written as

$$\ddot{\phi} + \frac{3}{t}\dot{\phi} + \frac{J}{t^2}\phi = \frac{mAC}{2} \frac{\dot{h}}{t} \sqrt{\frac{\rho_\Phi}{\rho_k}}, \quad (\text{B.21})$$

$$\ddot{h} + \frac{2}{t}\dot{h} = \frac{2mBC}{t} \sqrt{\frac{\rho_\Phi}{\rho_k}} \dot{\phi} + \frac{BA^{-(\alpha+1)}C}{t^2} \sqrt{\frac{\rho_\Phi}{\rho_k}} \phi. \quad (\text{B.22})$$

Following Ref. [45] we solve these equations by using a linear perturbation technique. Since we are in the curvature-dominated epoch and $\sqrt{\rho_\Phi/\rho_k}$ is small, we begin by searching for approximate solutions to (B.21) and (B.22) where the source terms on the right-hand side are neglected. That is, we first solve the homogeneous equations (to get zeroth order solutions for ϕ and \dot{h}),

$$\ddot{\phi}_0 + \frac{3}{t}\dot{\phi}_0 + \frac{J}{t^2}\phi_0 = 0, \quad (\text{B.23})$$

$$\ddot{h}_0 + \frac{2}{t}\dot{h}_0 = 0, \quad (\text{B.24})$$

where subscript 0 now denotes solutions in zeroth order of the perturbation approach. Once we have these zeroth order solutions, we will plug them into the right-hand side of Eqs.

(B.18) and (B.19) in order to obtain new differential equations which can then be used to derive correction terms of order $\sqrt{\rho_\Phi/\rho_k}$. If our solutions with order $\sqrt{\rho_\Phi/\rho_k}$ corrections are still decaying then it means that the stability result is established at least in the first-order perturbation analysis.

The zeroth order solution to (B.23) is

$$\phi_0(t) = \frac{C_1}{t} \cos \left[\sqrt{J-1} \ln(t) \right] + \frac{C_2}{t} \sin \left[\sqrt{J-1} \ln(t) \right], \quad (\text{B.25})$$

where C_1 and C_2 are constants of integration, and the zeroth order solution to (B.24) is

$$h_0(t) = \frac{C_3}{t} + C_4, \quad (\text{B.26})$$

where C_3 and C_4 are constants of integration. Note that, up to oscillatory bounded functions of time, $\phi_0/\Phi_0 \propto t^{-(\alpha+4)/(\alpha+2)} \in (t^{-2}, t^{-1})$, so we confirm the result of Sec. 3.2.1 that if we ignore the effect of metric perturbations the time-dependent fixed-point solution is stable.

Writing $\phi = \phi_0 + \phi_1$ and $h = h_0 + h_1$, and plugging (B.26) into Eq. (B.18), we get for the first order ϕ_1 equation

$$\ddot{\phi}_1 + \frac{3}{t} \dot{\phi}_1 + \frac{J}{t^2} \phi_1 = \frac{mA}{2} \dot{h}_0 t^{m-1}. \quad (\text{B.27})$$

(We shall not need the h_1 differential equation.) Solving this differential equation for ϕ_1 we find

$$\phi_1(t) = -\frac{mAC_3 t^{m-1}}{2(m^2 - 1 + J)}. \quad (\text{B.28})$$

From this solution and that in (B.25), we find, up to oscillatory bounded functions of time, $\phi_1(t)/\phi_0(t) \propto \sqrt{\rho_\Phi/\rho_k}$, so in the curvature-dominated epoch, where $\rho_\Phi \ll \rho_k$, the correction to the scalar field solution from the metric inhomogeneity is small.